AFM investigations of cellular response to environmental and local chemo-mechanical stimulus.

By

Fernando Suárez Sánchez

Centre for the Physics of Materials
Department of Physics
McGill University, Montréal
June, 2011.

A thesis submitted to McGill University in partial fulfillment of the requirements for the degree of Doctor of Philosophy

Abstract

Several cell types are found in organisms. Each type displays specific characteristics such as morphology, proliferation rate, genetic expression, mechanical properties, etc. Many investigations have been performed to study the effect of chemical cues on these cell properties. This is in contrast to the present work, which investigates the effect of mechanical properties of the global or local surroundings. Here, we have studied the effect of the matrix stiffness on the mechanical properties of airway smooth muscle cells using Atomic Force Microscopy (AFM). Our results show that the elastic modulus (G') of these cells increases to 820 ± 360 Pa when cultured on stiff gels when compared to the elastic modulus of 340 ± 160 Pa for cells cultured on soft polyacrylamide gels. We notice no significant difference in elastic modulus for cells plated on a glass substrate when compared to the stiffer gels. There is no evident effect of substrate stiffness on the loss modulus. The variability of the measured elastic modulus is attributed to cellular variability. This variability is smaller for cells cultured on the soft gel. When the cell cultures were labeled with Red-phalloidin, we observed an increase in the organization of the actin fibers at the cell cortex for stiffer substrates. We thus hypothesize that the increase in cellular stiffness is the consequence of the actin organization beneath the cell membrane.

Proliferation rate was significantly diminished when the cells were cultured on the softer polyacrylamide gels. Matrix stiffness also had an effect on genetic expression as demonstrated by gene arrays. We observed a significant difference of genetic expression when cells were cultured on a glass substrate. All these results indicate that smooth muscle cells respond structurally and genetrically to the mechanical properties of the environment.

Neurons are mechanically much more fragile and responsive than smooth muscle cells. We locally changed the mechano-chemical environment of axons and observed that this was sufficient to induce major structural changes such as synapse formation and even the extraction of proteins containing membrane strings. We developed a new approach to induce and study the creation of presynaptic site formation in axons through a combination of local modification to

the mechano-chemical environment using a combination of AFM and fluorescence microscopy. First, we use a poly-D-lysine coated bead attached to an AFM tip to induce a synapse. We used transfection techniques and fluorescence microscopy to study the recruitment of two synaptic proteins, bassoon and synaptophysin, and measure their absolute arrival times to the presynaptic site. We find that bassoon arrives after 23 ± 10 minutes and that synaptophysin arrives after 43 ± 9 minutes. Finally, we observed the formation of long (several 10s of μm) membrane strings as the AFM tip was withdrawn from the axon. These membrane strings seemed functionally intact. It is conceivable that these strings might be a mechanism by which new neurites and branch points along existing neurites can be generated *in situ*.

Résumé

Plusieurs types de cellules se retrouvent dans les organismes. Chaque type présente des caractéristiques spécifiques telles que la morphologie, le taux de prolifération, l'expression génétique, les propriétés mécaniques, etc. De nombreuses enquêtes ont été réalisées afin d'étudier l'effet des signaux chimiques dans la cellule. Ceci contraste avec les travaux actuels qui étudie l'effet des propriétés mécaniques sur l'environnement global et local. Ici, nous avons étudié l'influence de la rigidité du substrat sur les propriétés mécaniques et l'expression génétique des cellules musculaires lisses des voies aériennes. Nos résultats démontrent que le module d'élasticité (G') des cellules augmente à 820 ± 360 Pa lorsqu'elles sont cultivées sur les gels rigides par rapport à 340 ± 160 Pa aux cellules cultivées sur les gels polyacrylamides doux. Nous n'avons pas remarqué de différence significative dans le module d'élasticité pour les cellules étalées sur un substrat de verre en comparaison aux gels rigides. L'effet de rigidité sur le module de perte n'est donc pas observé. La variabilité du module d'élasticité mesuré est attribuée à la variabilité cellulaire. Cette variabilité cellulaire est moins effective pour les cellules cultivées sur les gels doux. Lorsque les cultures de cellules ont été marquées avec Red-phalloïdine, nous observons une augmentation dans l'organisation des fibres d'actine au niveau du cortex cellulaire. Ainsi, nous émettons l'hypothèse que l'augmentation de la rigidité cellulaire est une conséquence de l'organisation d'actine sous la membrane cellulaire.

Le taux de prolifération a significativement diminué lorsque les cellules ont été cultivées dans les gels de polyacrylamide plus doux. La rigidité du substrat a également une influence sur l'expression génétique comme démontrée dans les réseaux de gènes. D'un autre côté, une variation significative sur l'expression génétique a été observée dans les cellules cultivées sur du verre. Tous ces résultats suggèrent que les cellules musculaires lisses répondent aux propriétés fournis par l'environment.

Les neurones sont mécaniquement beaucoup plus fragiles et sensibles que les cellules musculaires lisses. Nous avons localement changé l'environment

mécanochimique des axones et avons observé que cela suffisait pour induire des changements structurels significatifs tels que la formation des synapses et même l'extraction de protéines contenant des chaînes membranaires. Nous avons développé une nouvelle approche pour inciter et étudier la formation des sites présynaptiques dans les axones par une combinaison de modifications locales de l'environnement mécano-chimique en utilisant une combinaison de l'AFM et de la microscopie à fluorescence. Tout d'abord, nous utilisons une bille enrobée de poly-D-lysine pour attacher sur une pointe d'AFM dans le but d'induire une synapse. Nous avons utilisé des techniques de transfection et la microscopie à fluorescence pour étudier le recrutement de deux protéines synaptiques, basson et synaptophysine, et de mesurer leur temps d'arrivée absolue aux sites présynaptiques. Nous constatons que le basson arrive après 23 ± 10 minutes et que la synaptophysine arrive après 43 ± 9 minutes. Finalement, nous avons observé la formation de longues chaînes membranaires contenant des protéines de l'ordre de 10µm quand la pointe d'AFM a été retirée de l'axone. Ces chaînes membranaires semblent être fonctionnellement intactes. Il est concevable que ces chaînes pourraient être un mécanisme rénovateur par lequel les nouvelles neurites et les nouveaux points de branchement au long des neurites existants peuvent être générés *in situ*.

.

Acknowledgments

I want to thanks the institutions and people that make possible the development of the present study. First, I thank the the Natural Science and Engineering Research Council of Canada and the Canadian Institute for Health Research and the Consejo Nacional de Ciencia y Tecnologia for their financial assistance, both through scholarship awards and the research funding provided.

I am deeply grateful to my supervisor, Dr. Peter Grütter, who has been very supportive through the development of this study. His insight and advices have contributed importantly to improve my research skills.

I thank Dr. Barbara Tolloczko and Dr. James Martin. Both have helped me to increase my biological knowledge and have guided me through many of the the biological methods employed in this thesis.

Dr. David Colman has been a supportive figure in the neuro-physics study described in this thesis. He facilitated the access to neuronal cultures by providing us access to the installations in his laboratory.

My colleges Peter Thostrup and Jeff LeDue at the physics department, Paul Andre, Taisuke Jo and technician Jamilah Saeed at the Meakins-Christie Laboratories as well as Anna Lisa Lucido at the Montreal Neurological Institute deserve my appreciation and credit. Talks with them were very helpful to organize the ideas and discuss the results.

Especial thanks to Helene Bourque at the physics department for her friendship and encourage during the first days of my time Canada. She taught me much of the AFM methodologies employed in this thesis.

I thank my lab-mates for their partnership and to all my friends that helped me in different manners and circumstances.

I want to thank my parents for their love and support during all this years and thanks to Lizbel, who has been supportive and has been with me since the first days of my doctoral studies.

Table of Content

J

Statement of Originality

The author claims the following aspects of this thesis as original contributions to the field of biophysics.

1. Cellular response to matrix stiffness study.

• The first study where the viscoelastic properties of airway smooth muscle cells cultured on different matrix stiffnesses were measured.

• The study sheds light on the influence of the substrate mechanics in the proliferative and genetic expression of airway smooth muscle cells.

• Description of a methodology to determine the the Hertzian best fit on force distance curves adquired with the AFM

• The first study where the mechanical properties, the proliferation, morphology and the genetic expression of ASMC are determined as a function of the matrix stiffness.

2. Time-lapse presynaptic formation study.

• The first study where the formation of presynaptic buttons is induced in a controlled fashion. The process is initiated by the contact of a poly-lysin coated bead and the axon membrane.

• The formation of long strings (potentially functional neurites) was formed after bead pulling. Movement of vesicles in the strings was observed.

• Determination of the presence of important structural molecules for protein and vesicle transport (tubulin) as well as actin in the strings. Synaptophysin and bassoon proteins normally found moving along the axon shaft or stationed on the presynaptic sites were also observed.

Essential procedures in this thesis not performed by the author are the following.

• Gene arrays were performed by Genome Quebec Innovation Center, McGill University with total RNA provided by our laboratory.

• Neuron culture preparation. Procedure explained in brief in material and methods. Prepared by Dr. Peter Thostrup, Physics department, McGill University.

1 Introduction

In his book “Imagined Worlds” Freeman Dayson, a notable US theoretical physicist and mathematician wrote:

“The effect of concept-driven revolution is to explain old things in new ways. The effect of tool-driven revolution is to discover new things that have yet to be explained.”

Freeman Dyson, Imagined Worlds

This is to say that the use of tools, especially when new ones are used in science, have the potential to generate numerous new findings that can lead to a search of its basics principles, understanding of previous unsolved questions or originate new ones that have to be explored.

In this logic, the aim of the use of the Atomic Force Microscope (AFM) tool in this thesis is to explore two biological questions and make new discoveries that then stimulate a more systematic examination in more detail by biologists. This will lead to a deeper understanding of cell behavior. Here, we are motivated in how mechanical cues affect cell response and properties. We will explore the effect of the global substrate stiffness on cell mechanical properties. We will also use a local mechano-chemical cue to investigate the formation of synapses in neurites. We will demonstrate that this technique can be used to understand the dynamics of proteins known to be involved in the formation of synapses. In particular, we determined the arrival time of two different proteins to the AFM induced newly formed presynaptic sites.

However, before going deeper in the uses of the AFM in biology, it is worth to give some examples of its use to explore questions in physics and the type of information that can be obtained. Above all, after its introduction by Binnig et al., (1986), the AFM was first employed by physicists. For instance, the AFM has been used to detect atomic interactions, something that requires very sensitive techniques due to the small forces involved. To achieve that, two approaches that have been used include the utilization of a cantilever oscillating at its resonance frequency above the sample while keeping track of small shifts

in the resonance frequency. Any change in the resonance frequency is associated to the interactions that occur between the cantilever tip and the closest atom on the sample. In the other case, atomic force spectroscopy at low temperature was exploited (Lantz et al., 2001) for a similar purpose. In this case, the AFM was used to detect and directly measure the formation of a chemical bond. A silicon tip was approached to a silicon (111) 7×7 surface and quantitative and atomic-scale information about the interaction forces was acquired by the frequency shift methodology. The short-range forces measured and depicted in the force-distance plot shown in Figure 1 were compared to the chemical bond interaction calculated by basic principles (Perez et al., 1998). This study showed that there is a very good agreement between the two values and thus the sensitivity of the AFM to measure atomic interactions was evidenced.

Atomic manipulation is another area where AFM has shown is value and flexibility. Sugimoto et al., (2007) demonstrated that vacancy-mediated lateral manipulations of the Si atoms in the same type of surface used in the previous work is possible. It was achieved as a result of structural relaxations that weaken the adatom[1] surface bonds when the tip is in close proximity to the surface. This, in turn, enables the hopping of atoms to new locations by lowering the energetic barriers that keep the atoms still. Similarly, atomic manipulation was achieved by Oyabu et al., (2003) that demonstrated that repulsive short-range interaction forces during soft nanoindentation allows the removal of a silicon atom. Atom deposition was also achieved and both spatial manipulation processes were purely mechanical.

Another study where the ability of the AFM to precisely control the spatial movement of the probe has been exploited is in the deposition of molecules on surfaces. For instance, Moldovan et al., (2006) designed and fabricated a nanoprobe system that consist of an ultrasharp volcano-like tip with microfluidic capabilities. The tip is connected to an on-chip reservoir through a channel inside

[1] Contraction of "adsorbed atom". An adatom is an atom that lies on a crystal surface, and can be thought of as the opposite of a surface vacancy.

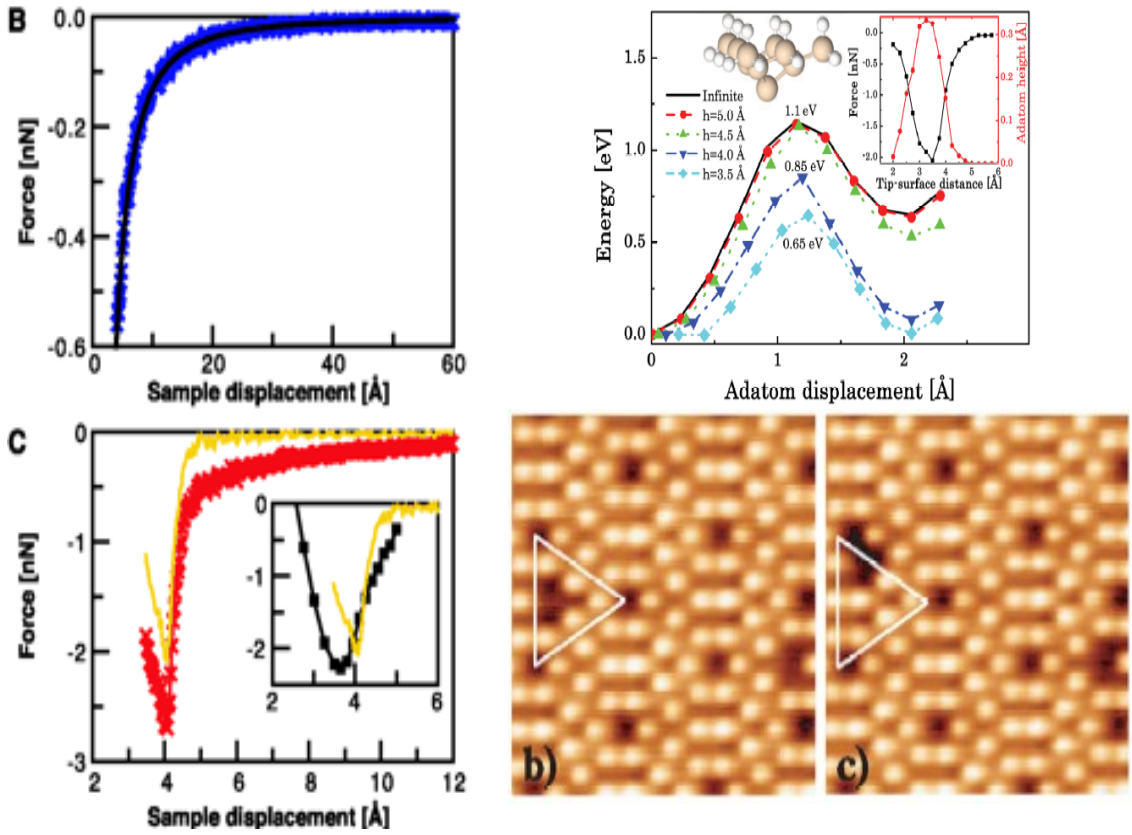

Figure 1: Force-distance curve above the Si surface and a fit to the data using a sphere-plane model for the Van der Waals interaction force (upper left image). Total force (red line) and short-range force (yellow line) determined above an atom (lower left image, Lantz et al., 2001) In the inset, a comparison between the measured short range force and the calculated bonding interaction by first-principles is shown. Calculated diffusion barriers for adatoms on a lattice when the tip is at different height above the surface (upper right image). Topographic images from a series of vacancy-mediated manipulations mediated by the AFM tip (lower right images, Sugimoto et al., 2007)

the cantilever. This system is an upgrade of the dip-pen nanolithography where the “ink” is only deposited on the surface of the cantilever tip (Piner et al., 1999) and used for writing. The potential uses of the volcano-like tip system in biology include localized drug delivery at specific sites of the cells or close to membrane receptors and biofluid sampling applications. This potentially allows the detection of cells that are different of the rest by sampling the secreted molecules for individual cells at specific locations.

Combination of AFM with volcano-like tips and fluorescence microscopy could be very valuable. Detection of spatial distribution of single molecules can be performed with fluorescence imaging (Eckel et al., 2006). Force spectroscopy by atomic force microscopy allows addressing, manipulation and quantitative probing of the nanomechanical properties of individual macromolecules thus allow the investigation of optical and mechanical properties at the single molecule level. In Eckel et al., (2006) study, they report the distance-controlled quenching of semiconductor quantum dot clusters with an AFM tip.

In biology, the AFM as been used more often in recent years. A traditional applications is the collection of topographic data to reveal cellular structures. Prior to the AFM introduction, such information was to the best scarce or difficult to obtain. However, nowadays, contact and dynamic modes have been employed with success. It is evidenced by AFM images of cells (Le Grimellec et al., 1998, Espenel et al., 2008) but also other biological molecules such as RNA and DNA (Hamon et al., 2007), DNA-protein complexes (Muller et al., 1997; Kopp-Marsaudon et al., 2000), sole proteins (Möller et al., 1999; San Paulo and García, 2000), polymers (Reiter et al., 2000) are other biological structures. Tip radius is still a limiting factor to obtain good lateral resolution (Sun et al., 2002; Kienberger et al., 2004).

Conformational changes in the DNA-protein complexes are central for many cellular processes and high resolution visualization of such interactions might provide some clues about their biology (see Figure 2). The association of proteins to the cytoskeleton has been explored by Afrin and Ikai, (2006) by force spectroscopy where differences in the force-distances profiles got after pulling proteins were used to determine whether or not they were connected to the cytoskeleton.

Recent investigations (Lopez M., personal communication) have used the AFM as a tool to study Ca^{2+} signalization cascades that are triggered by mechanical stimulus in osteoblasts. In those studies, the cantilever tip is positioned on a defined region on a cell and after the mechanical stimulus was

delivered, the force needed to trigger the signalization as well as the extent and propagation of the stimulus to nearby cells were measured.

Force spectroscopy has been used to study the intermolecular interactions of proteins as well. Here, a layer of the protein of interest is deposited on a solid surface and a linker is used to connect the tip to the protein. Pulling results in the break of intermolecular interactions and a portrait of the unfolding event is visible at the force-distance curves as successive peaks in the retraction curve (see Figure 2; Meadows et al., 2003).

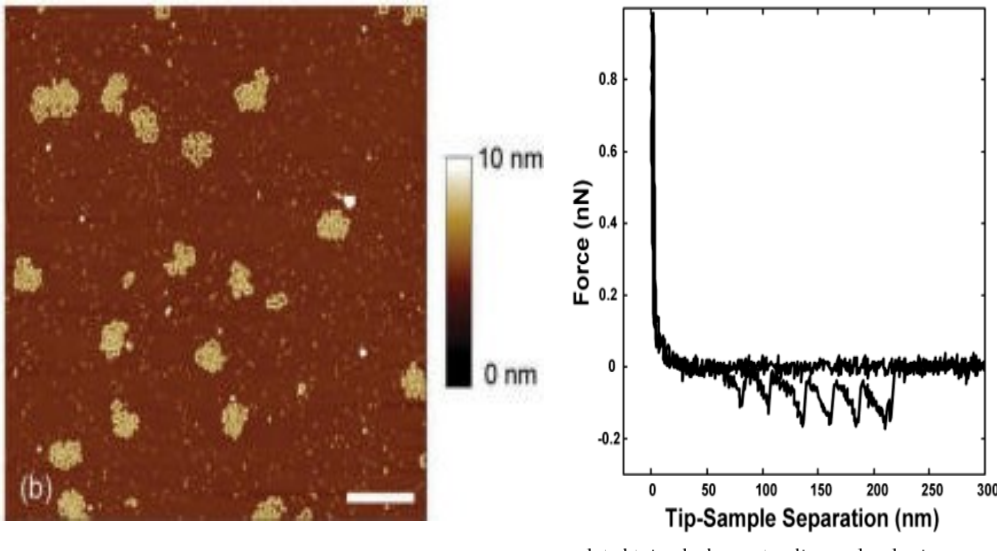

Figure 2: AFM topographic image of DNA on mica (left image, Hamon et al., 2007). Force plot obtained when extending single molecules of fibronectin away from a mica surface in water (right image). The successive picks in the retraction curve evidence unfolding events. Meadows et al., 2003.

The mechanical response of endothelial cells to a shear flow was investigated by AFM by Sato et al., 2000. In this study, the cells were exposed for several hours to a shear flow at the end of which the AFM was used to asses changes in cell rigidity. Large Young's modulus was found at the upstream side of the cells after 6 h exposure although this stiffness polarity was not permanent and disappeared after long exposure times. Changes in stiffness during the cell cycle have been found with marked but transient decrease in stiffness in the mitotic spindle region during anaphase. (Dvorak and Nagao, 1998).

Measurements of the stiffness of cells in response to contractile agonist were published by our lab (Smith et al., 2005). In those experiments, it was shown that inhibition of myosin with 1-(5-iodonaphthalene-1-sulfonyl)-1H-hexahydro-1,4-diazepine hydrochloride (ML-7) as well as treatment of cell cultures with cytochalasin-D (which induces actin depolymerization) cause a decrease in cell stiffness. A major contribution of this study is the evidence that presented implicating cortical actin polymerization as the dominant mechanism actuating the stiffening response of smooth muscle cells.

In sections 5.1 and 5.4, we exploit the ability of the AFM to measure mechanical properties and we combine this capacity with other well established biological techniques to generate data that put together can provide a more comprehensive idea of the processes that the cells undergo when cultured on non-rigid substrates. In this thesis, the mechanical properties of the cells are determined and correlated with other cellular characteristics such as substrate mechanics, actin fibers, cell proliferation rate, and genetic expression.

It was mentioned at the beginning of the introduction that AFM was used to manipulate atoms on a Si surface (Sugimoto et al., 2007). This AFM manipulation capability has been exploited in biology as well. For example, Han et al., (2005) developed an AFM based methodology for gene or molecule transfer. A nanoneedle covered with the molecule of interest was attached to the AFM cantilever and inserted into the cell body. Some of the material was transferred to the cell cytoplasm. Similar experiments have demonstrated that it is possible to manipulate needles and insert them in the cell body to extract mRNA from the cell (Kim et al., 2008). In these experiments, the needle with the mRNA attached was used later to do Polymerase Chain Reaction (PCR) and determine the gene expression on individual cells. This demonstrates that combination of AFM and other established biological techniques can produce valuable information. Other studies led by Afrin et al., 2009, used a beaded cantilever coated with phospholipase A (this enzyme hydrolyzes phospholipids on the cell membrane into fatty acids and other lipophilic substances) to produce holes at specific locations in the membrane and study the viability of such cells.

Transfer of DNA through the holes was achieved as well and the success evaluated by observing fluorescence. Manipulation of proteins in the membrane as also been achieved with the AFM (Afrin et al., 2003). On these studies, it was possible to bind surface proteins and even pull them from their initial transmembranal location.

From the atomic to nanometric and micrometric levels, the AFM has demonstrated to be a valuable tool to manipulate objects in both physics and biology. Its unique capability to allow the manipulation of mechano-chemical cues in space with nm precision and in time with ms resolution was utilized in this thesis. Here, the AFM probe was used to explore its usefulness to investigate the presynaptic formation and in particular the recruitment times of presynaptic proteins (refer to section 8). It was done by controlled manipulating in space and time a polystyrene bead attached to the AFM tip contacting a neuronal cell

1.1 Why study mechanics in biological systems?

Traditionally, cells cultured in plastic or glass Petri dishes have been widely used in biological studies. There are practical advantages in using this type of culture; the conditions in which the cells grow can be well controlled (i.e. temperature and pH), the density of plated cells per unit area can be easily manipulated, the physical access to the cells in order to challenge them with drugs is easy and optical observation of the cell cultures facilitated. However, probably the most important factors that determined this tendency are the unawareness (until recent years) or shortage of studies that strongly establish the importance of the elastic properties of the matrix on the cell behavior. The effect of the substrate stiffness on cell behavior was usually ignored and only lately efforts are been made to determine the extent of the influence of the substrate stiffness on cell behavior (Engler et al., 2006a; Saha et al., 2008a; Discher et al., 2009).

Early studies aimed to investigate cell differentiation have focused on chemical signals as the main cause of cell differentiation. However, new and recent studies have shown that chemical cues are not the only cause of

differentiation but the structure and mechanical properties of the microenvironment also influences cell differentiation. Lineage specification, a determinant process in embryology as well as in adult organisms is in part modulated by substrate stiffness as shown by Engler et al., (2006a); Saha et al., (2008a); Discher et al., (2009). In these experiments, naive mesenchymal stem cells were plated on polyacrylamide matrices and cell differentiation was evaluated by morphological changes, immunostaining (it uses antibodies to detect specific proteins in a sample), and western blot (a method to detect proteins in a sample through electrophoresis and subsequent antibody detection).

The molecular mechanism involved in the mechanically mediated regulation is still unknown but new and increasing numbers of investigations are under way to answer these questions (Paszek et al., 2005; Discher et al., 2009; Tamara and et al., 2005; Lo et al., 2000; Cheng et al., 2009a). Recently, Cheng et al., (2009b) have shown that mechanical stress, in addition to molecular cues (*i.e.* growth factors) and other environmental cues (Ashkenazi and Dixit, 1998), suppress proliferation and trigger apoptosis via the mitochondrial pathway. Cell migration is also influenced by the stiffness of the substrate as Lo et al., (2000); Cheng et al., (2009a) demonstrated. In these experiments, polyacrylamide sheets were prepared such that the opposite extremes had different stiffness. When cells were seeded, those that initially adhered onto the soft region of the substrate migrated towards the stiffer region. This migration was solely a response to the substrate stiffness (“durotaxis”).

In response to the matrix stiffness, mesenchymal stem cells plated on soft matrices (mimicking the mechanical properties of the brain) turned neurogenic, on stiffer matrices (that mimic muscle) they turned myogenic, and on comparatively rigid matrices (that mimic collagenous bone) they evolved to an osteogenic phenotype. Saha et al., (2008a) showed that neural stem cells differentiate into neurons when the matrix stiffness was in a range between 100-500 Pa which resembles the stiffness of the brain tissue. Analysis of protein markers in those cells also showed a peak level of the neuronal marker, *β*-tubulin

III. Harder matrixes (> 500 Pa) promoted glial cultures but when the stiffness of the matrix was lower than 100 Pa, differentiation was inhibited. This data demonstrates the strong interconnection between cell differentiation and the mechanics of the microenvironment in which the cells grow.

1.2 Synaptic formation in Neurons.

In addition to cell mechanics, the AFM was also used to study presynaptic formation in this thesis by applying localized mechano-chemical cues. Synapse formation, maturation and functioning is determinant not only in memory and learning as broadly recognized but it is also important in several other automatic and unconscious processes that take place in the mammalian organism such as breathing, heart contraction, muscle movement and homeostasis. Usually, synapses are formed between an axon and a dendrite (synapsis between axons and non-neuronal cells occur too) but an important difference in the number of connections that they can maintain exists. While the axons only form a single synapse with a dendrite, the dendrites can form several synapses with many axons.

Synapse formation is a complex process that involves, at the beginning, the apparently random movement of highly dynamic filopodia. These “fingers” move constantly searching for locations along the nearby axons to form synapses. The resultant dendritic spines are more mechanically stable than their precursors. In fact, spines associated with axons appear stiffer than non-associated spines (Smith et al., 2007a). Many important issues are not understood, such as how does this stabilization happen what are the signaling pathways, what proteins are involved and how fast does it happen?

Although neuroscientist have studied synapses for several years many of these questions remain or the answer is known to be incomplete. Such a question is in what order do the different known components of the presynaptic site arrive? In the second part of this thesis we will develop a new methodology to answer this question. A good description of the arrival sequence of proteins

would provide new clues to understand the signaling cascades and steps that occur starting from the first contact to the establishment of a mature synapse.

Although there are reports that have quantified the arrival times of presynaptic proteins (Friedman et al., 2000), the procedure that was followed relies on the random formation of a synapse between the neurons in the culture dish. The observation of one of such events can take a considerable amount of time. Here, we explore a more direct approach in which the formation of a presynaptic site is induced by the contact between the axon and a poly-D-lysin coated bead on an AFM tip.

In this proof-of-principle study we limit ourselves to determining the recruitment times for synaptophysin and piccolo-bassoon proteins. This new and original approach has the potential to be used to measure recruitment times of many other protein that are located at the mature presynaptic site. Fundamentally, the only change that has to be made to the technique is in the neuronal culture transfection step. A vector carrying the right sequence for the protein of interest has to be employed. All the other steps remain the same.

,An interesting observation, not persued further in this thesis, is the use of the AFM to pull threads from the axon shaft. These threads have the potential to be used to artificially make connections between neurites. If its functionality is proved, this would become a remarkable way to induce the creation of synapses at will. Initial examination of the proteins present in the threads suggest that they contain and transport some of the important and characteristic proteins found in axons.

2 Material and Methods (Atomic Force Microscope)

2.1 AFM and inverted optical microscope setup

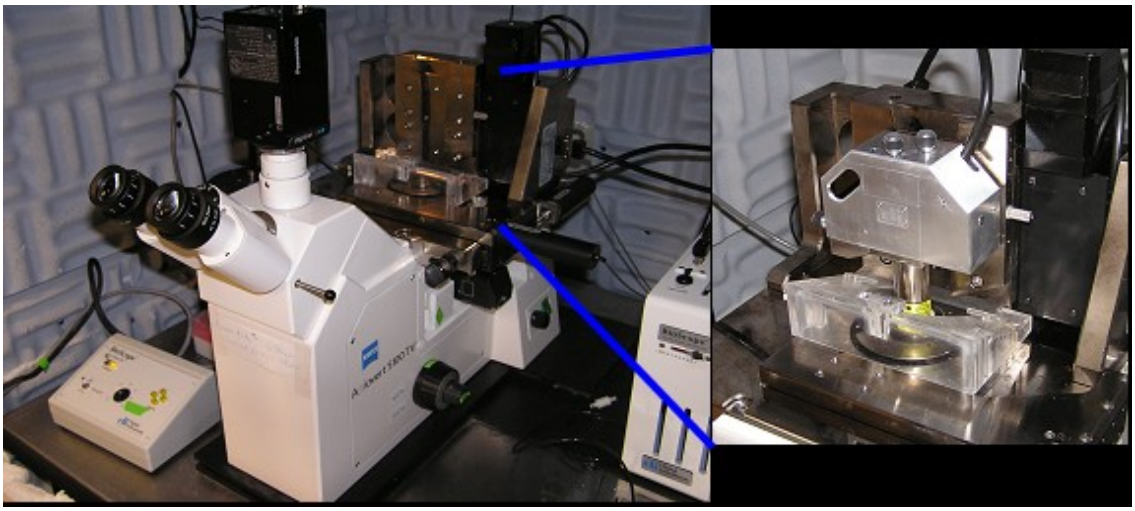

Figure 3: The equipment used in this work consists of an inverted optical microscope and an AFM mounted on a damping table. A heavy metal stage placed on the inverted microscope support the heated stage that keeps the cell cultures at 37 C during the course of the experiments (circular element observed under the AFM head, inset). A plexiglass box is then positioned above the heater and the AFM head placed into position (see inset). The space between the box and the cylinder that encloses the piezo tube in the AFM is sealed with a rubber sheet. The complete setup can keep cultures at a controlled temperature and gas environment. We inject 5 % CO_2 into the plastic box to keep the pH of the medium at 7.2. Note that water condensation on the piezo has to be avoided and dried carefully to avoid electrical shorts or shocks.

An inverted optical microscope (Axiovert S100 TV, Carl Zeiss Canada Ltd., Toronto, Ontario) was used for optical observation of the samples and identification of the region of interest (live cells for the purpose of this thesis). The microscope is equipped with 10X, 40X no-oil objectives as well as 40X, 60X and 100X oil immersion objectives. An short arc mercury lamp (HBO 50 W, Osram, Munich, Germany) and an argon laser (Model, 35 LAP 431-220, Melles Griot, Albuquerque, New Mexico) allows the detection of a wide range of fluorescent proteins and dyes. The argon laser also serves as an illumination source for a home built Total Internal Reflection Fluorescence (TIRF) (Durisic et al., 2009).

For fluorescence microscopy as well as bright field, a CCD camera (Cascade:1k camera, Photometrics; Tucson, AZ) is employed to collect images of the samples (see Figure 3).

The design of the Bioscope permits the acquisition of optical images simultaneously with AFM images. The position of the optical microscope (below the sample) allows the access of the AFM to the sample from the upper part. The AFM used in this thesis is a commercial instrument made by Digital Instruments. The instrument was equipped with a Nanoscope IIIa control electronics using the software version 5.12r2 (Veeco Metrology Group, Santa Barbara, CA).

2.2 AFM basics and optimization

The Atomic Force Microscope (AFM) is capable of resolving features of the order of nm or even smaller sizes, features that no optic technique is able to resolve due to the diffraction limit constraint (roughly λ/2). From its invention by Binnig et al., 1986, the AFM has evolved and new modes of operation such as dynamic mode, frequency shift and force spectroscopy have been developed and used for different purposes. In general, all these techniques rely on the detection of the cantilever bending by mean of one of the methods available for that purpose (interferometry, laser beam deflection, capacitative sensing and in early designs tunneling microscopy; Rugar et al., 1989).

The AFM employed in this thesis uses the laser beam deflection method for the cantilever bending detection. In this case, a laser beam is aligned in such a way that it is reflected off the backside of the cantilever. The beam is reflected towards a position sensitive photodiode detector, allowing cantilever deflections of less than a nanometer to be reliably detected. (see Figure 4). However, the cantilever noise is often more larger than this sensitivity.

In the Bioscope the AFM is positioned on top of the inverted microscope and the sample lies on a rigid stage. This has the advantage that large, heavy petri dishes with cell cultures can be imaged both by AFM and optical microscopy techniques. Note that most commercial as well as home-made AFMs scan the sample. Imaging of the samples by AFM thus requires the movement of the

cantilever in the x-y plane as the sample remains stationary. To achieve this cantilever movement, the tip is mounted to a piezoelectric tube scanner. Technically the challenge in implementing this design is to detect the cantilever deflection as it is scanned in x, y and z relative to the sample without artifacts.

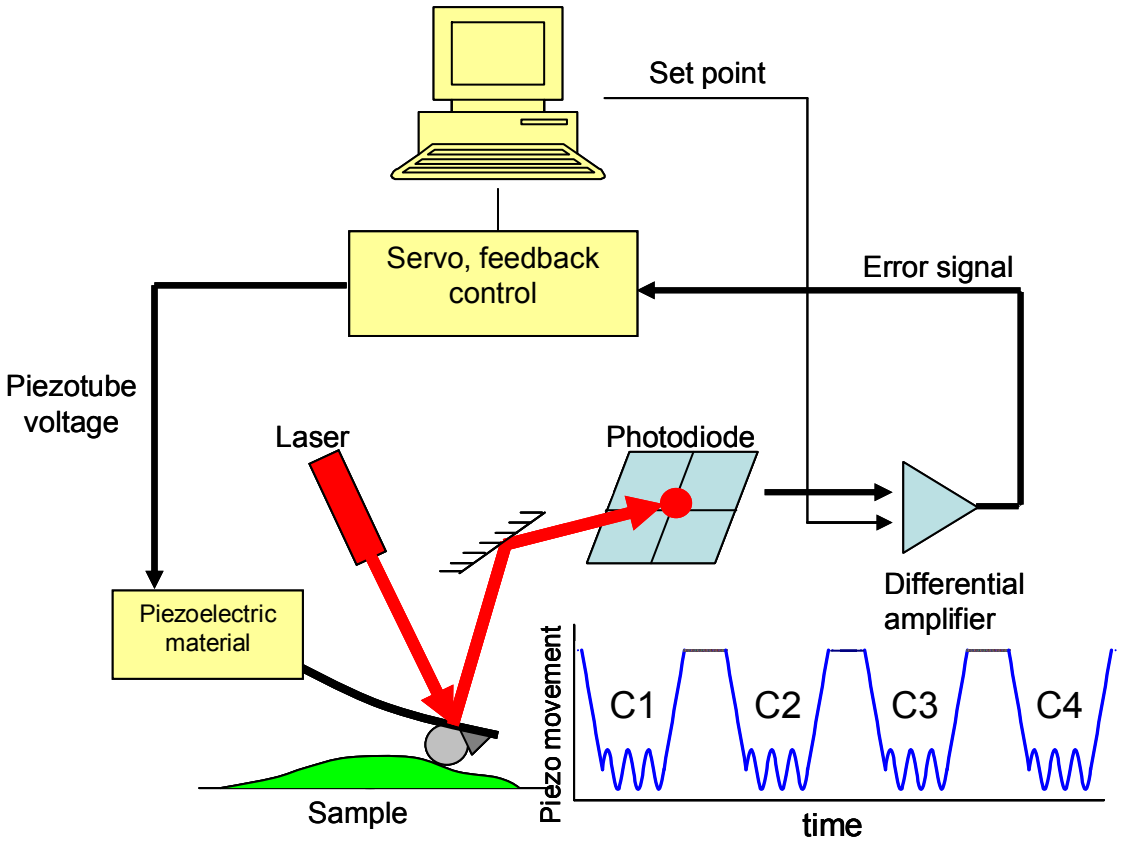

Figure 4: Main elements of the AFM. A laser beam hits the back of the cantilever and is reflected towards the photodiode in the AFM head. Probe-sample interactions bend the cantilever that results in changes in position of the laser spot at the photodetector. The output signal is constantly compared with a set point determined by the user and the error signal is sent to the servo. The information is used by the servo to determine the adjustments in the vertical position of the cantilever and to keep the sample-tip interaction constant. The drawing at the bottom-right of the figure depicts the typical movement of the cantilever in z when the force modulation technique is used. The amplitude and frequency of the oscillation was 7 nm and 10 Hz respectively and was applied for 15-20 s each cycle (represented as C1, C2,C3, C4).

The AFM is a very sensitive device with great potential to study small scale features (nm or even lower) with low interaction forces (pN). There are a

number of factors that need to be optimized carefully to achieve optimal imaging conditions, in particular for biological systems:

1. Optimization of feedback performance and image acquisition time. An artifact often observed during imaging with the AFM are feedback overshoots that appear most often in regions with abrupt changes in height, commonly found in biological systems which tend not to be very flat. Optimization of the feedback parameters (integral and the proportional gains) significantly reduce the overshooting although complete elimination is not always possible unless very low scan rates are employed. However, low scanning rates also can lead to drift artifacts (this occurs because of piezo creep and/or thermal drift) and a significant increase in image acquisition time, something that most of the time is not desirable when dealing with biological material. A good equilibrium between feedback and scan rate must be found in order to produce the more accurate images of the scanned samples.

2. Avoidance or minimization of optical interference patterns, which can originate from the reflection of the laser at the top and bottom side of the cantilever as well as the top of the sample (such as optically flat regions of the petri dish). This will result in noisy measurements (see Figure 5). This is particularly noticeable when force-distance curves are acquired. In these cases, a periodic wavy pattern is observed in the curve. Changing the position of the laser spot on the back of the cantilever or changing to a less reflective sample usually eliminates the interference.

3. Minimization of acoustic and floor vibrations which produce noise that affect the resolution of the AFM. The cantilever probe is prone to pick up such vibrations especially when the cantilever is in air. The minimization and damping of any vibrations thus is critical to obtaining high-quality data with any AFM. Our group has addressed this issue by locating the AFM in the basement of the M. H. Wong Building at McGill University on a floor vibrationally decoupled from the rest of the building. The basement was built on a separate foundation from the surrounding structure to remove vibrations from the building structure. An air-damped table on which the Bioscope AFM system rests gives additional

mechanical isolation. Care was taken not to mechanically short circuit the air table by clamping all cables tightly to it. The AFM is also covered with a home-made acoustic isolation hood (utilizing SOH-2 Sonex1 acoustical foam; Vibrasciences Inc., Branford, CT). All these measures lead to a minimization of vibration induced noise and instabilities.

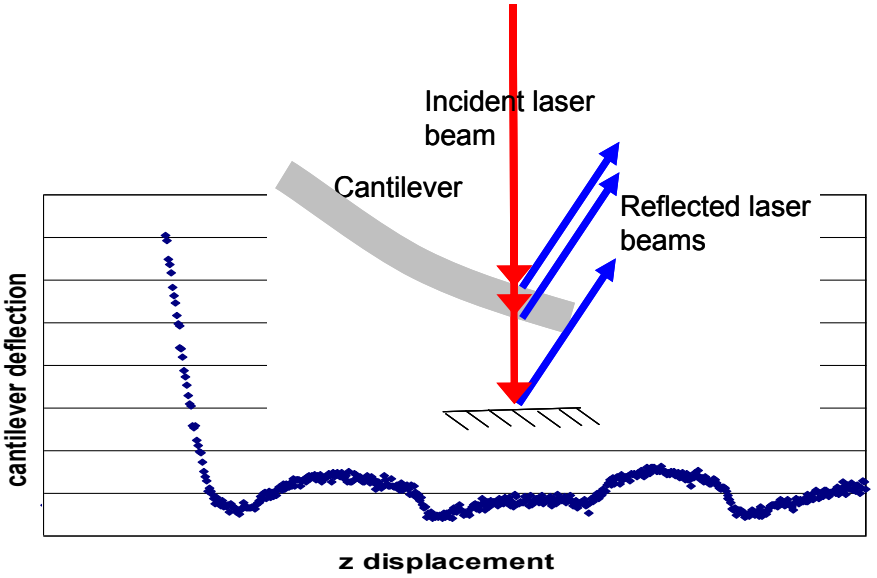

Figure 5: Interference of the laser reflected at three planes (upper and lower cantilever surfaces and the substrate) can negatively affect the data acquisition. It is particularly noticeable in force spectroscopy where the force-distance curves appear wavy. Changing the position of the laser beam in the back of the cantilever as well as using low refractive surfaces can eliminate the interference.

4. Minimization of interaction forces leads to high resolution AFM images on biological systems. In biological samples, the softness of the samples can reduce the resolution of the AFM images for features of interest such as i.e. pilus, flagellum, embedded proteins in the membrane, membrane protrusions. This occurs because excessive tip-sample interaction forces can easily and substantially deform and perturb the delicate, elastic cellular structures. Fixation of the samples, a method where the proteins that form the cell are covalently bound to each other, increases the overall resistance of the structures to deformation and is often used to image biological samples. However, that is not a choice if dynamic events are to be detected or if fixation alters the structures that

have to be observed. Reduction of the interaction forces is limited by external vibrations, electrical as well as optical interference noise.

5. The thermal bimetallic effect can result in variations of the tip-sample interaction force over time. This effect is especially relevant when scanning biological samples which are very delicate and are damaged easily when large forces are applied. The triangular cantilevers that have been widely used in this thesis are coated with gold on the backside to increase the reflection of the laser used to measure cantilever deflection. The bulk of the cantilever is made of Silicon Nitride (a temperature change of 1 mK leads to a deflection of typically 1 nm). Shining light on the cantilever is one source of heating and absorption induced thermal bimetallic bending that occurs slowly and only reaches an equilibrium after several minutes (~30 min). Thus, for all the measurements performed in this thesis, the cantilever was allowed to equilibrate before we proceeded to the collection of data.

6. To achieve good accuracy and precision, regular calibration of the AFM must be performed. This eliminates any artifact that could ultimately distort the images or produce false measurements of both, horizontal/vertical displacements or the strength of the probe-sample interaction forces. To assure quality data and optimal performance of the AFM, a calibration procedure was completed approximately every three months. A silicon calibration sample whose features are known and well characterized is used to calibrate the x-y axes as well as the z axes. Briefly, a topographic image of the calibration sample is taken and the motion of the scanner in the x-y axes is linearized (for details about the calibration procedures refer to the Bioscope manual). The size of the features is compared to the known characteristic sizes and recalibrated if necessary. A similar procedure applies to the calibration of the z displacement. In this case, the vertical movement of the z-piezo must be calibrated by using the known characteristic depth of the sample features. Finally, orthogonality in the x-y plane must be calibrated as well by measuring and adjusting the angles at which the features appear in the topographic image of the reference sample. The reason for potential changes in calibration constants is due to the fact that

piezoelements age (and change sensitivity) and that the elaborate cantilever piezoscanner with the integrated deflection measurement system can become misaligned due to uncorrected x-y and z piezo cross talk.

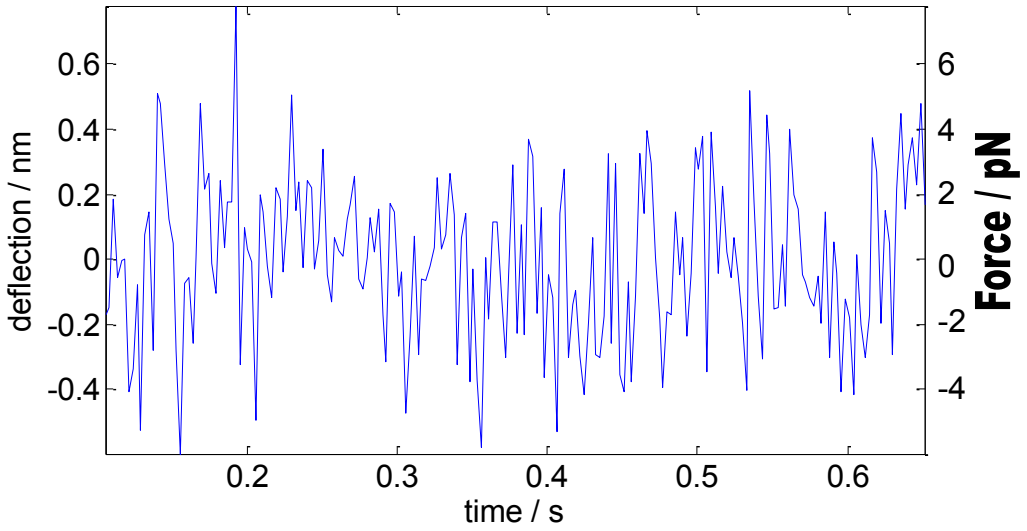

Figure 6: Estimation of the noise in the cantilever was performed by submerging it in liquid and taking the trace of spontaneous vibrations. It was found that the noise root mean square is equal to 0.25 nm for the cantilever used in this thesis (0.01 N/m spring constant). The data was acquired at 380 Hz. The use of stiffer cantilevers reduce the noise but they were not used in this thesis to avoid damage of the membrane due to large loads.

If all precautions described above are taken care of and the system is calibrated a benchmark measurement of the system and deflection is performed. Cantilever deflection data is collected with a 380 Hz bandwidth, while the z-position is maintained constant. For a cantilever with a spring constant of 0.01 N/m submerged in liquid stabilized at 37 C (*i.e.* same conditions as those employed when measuring cells) the measured standard deviation of the noise was found to be 0.25 nm. This is larger than what is achievable on many optimized high resolutions AFMs (where values as low as 10 pm are achievable), but one needs to consider that the Bioscope AFM is mounted on an inverted optical microscope. This (large) mechanical structure acts like a drumhead with substantial vibrational amplitudes. From Figure 6, we see that it is thus possible to observe cantilever deflections smaller than 1 nm under physiological conditions. Note that under realistic operational conditions detection of such

small values of the cantilever deflection is challenging. A possible explanations is that the noise of the electrical signal necessary to induce piezo motion to scan the cantilever in x and y or during acquisition of force distance curves (movement in z) induces piezo vibrations which couple to the cantilever An indication of this is that a lower deflection noise can be achieved by using higher frequency (*i.e.* stiffer) cantilevers. We however avoid the use of stiff cantilevers in this thesis as the larger spring constant leads to a higher force loading which can induce serious damages to the cell membrane.

2.3 Operation modes

2.3.1 Contact mode

In the contact mode of operation, the AFM cantilever is moved towards the sample until the cantilever-sample interaction leads to a bending of the cantilever due to Pauli repulsion. This event is detected optically by the laser beam deflection method. In our system the laser beam wavelength is 670 nm and it is focused on the back of the cantilever, close to the cantilever tip. The reflected laser beam is then detected in a split photodiode. When the cantilever bends as a consequence of tip-sample interaction, the laser spot on the split photodetector changes location. The difference between the photodiode output signal is proportional to the cantilever deflection. To maintain a constant, predetermined force, the AFM feedback system constantly compares the output signal with a reference (set point chosen by the user) and controls the cantilever movement to achieve a zero difference between the measured and the set point value (see Figure 4).

During imaging, the sample is scanned and the feedback controller keeps the cantilever bending (and hence the applied force) constant by dynamically moving the base of the cantilever and tip up or down (± z) with the help of a piezoelectric crystal. The voltage applied to the piezo necessary to adjust the z position of the cantilever is recorded and used to generate the topographic image of the sample. These images thus represent contours of constant force.

The lateral resolution of the AFM is a critical issue if small sample features are to be detected. Unlike optics, there is no resolution criteria related to some characteristic length scale in AFM. However, three parameters are relevant and determine the AFM resolution: sample-tip interaction force (in particular its decay length), tip radius and signal to noise ratio.

In biological systems, the sample stiffness is an important factor to consider if good resolution is needed. Care should be taken to choose the proper sample-tip interaction force. Due to the viscoelastic nature of the cells, relatively high interaction forces can mask soft surface features by smoothing them or simply breaking them. Internal structures can also be damaged by large forces and lead to cell death. However, the use of very low interaction forces is challenging and accomplished only under very well controlled situations and specific conditions. Le Grimellec et al., (1998) showed the viability to use the AFM to discern small granular features on the cell membrane without significant disruption (tip-sample interaction forces of the order of 20-50 pN were employed). Lateral resolution of 20 nm and sometimes 10 nm was achieved with indentations as low as 10 nm.

Lateral resolution is also affected by convolution effects due to the tip radius (see Figure 7) (Andrew Yacoot, 2008; Sun et al., 2002). The smaller the tip radius, the better images of small features reflect their true dimension. However, when imaging biological material, which is significantly softer than most types of substrates normally used in high resolution, AFM tips with a small radius of curvature are not recommended because the cell membrane can easily be punctured (the pressure applied by a sharp tip might be too high at the contact site). Thus a compromise between lateral resolution (*i.e.* tip radius) and sample yield strength is necessary. For the experiments presented in this thesis, where high resolution imaging was not the major aim, polystyrene beads radius of 4.5 μm (airway smooth muscle cells experiments) and 7 μm (experiments on neurons) were glued to the cantilevers and the tip-sample interaction forces were kept lower that 0.4 nN unless otherwise stated.

A study of the disruptive effects of scanning different types of cells at ~ 1nN force was conducted by You et al., (2000). In this study, the cells experienced morphological changes attributed to the constant movement of the cantilever during a one hour time lapse. Different cell types responded differently. This study also indicated that enhanced cell adhesion increased the tolerance of cells to the disruptive effect of scanning.

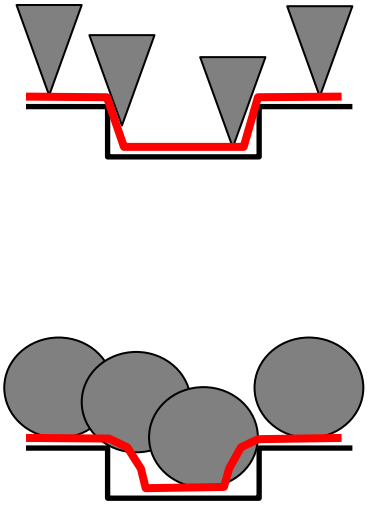

Figure 7: Sharp tips produce more accurate topography of the sample (upper diagram, black line, real topography; red line, topography generated by the AFM). However, they damage the cell membrane more easily due to high pressure at the tip end. It is common to observe overshoots at places where abrupt changes in height are present. They can be reduced by adjusting the feedback as well as the scanning speed. Larger surface contact (lower diagram) decreases the damage but the surface topography is not well followed.

Although the utilization of contact mode in live cells is to some extent limited by the forces the cells can support before being disrupted, there are a number of studies where this mode was employed. Some examples have been published by Schneider et al., 1997 and Espenel et al., (2008). In the first of the two manuscripts, the AFM was used in contact mode to detect changes in cell volume after treatment of endothelial cells of bovine aorta with aldosterone. This hormone is known to have acute, non-genomic effects on intracellular pH and intracellular electrolytes. The second manuscript studied plasma membrane microdomains and showed that membrane properties were markedly dependent

on temperature. These first temperature-dependent data show that large cell structures appeared essentially stable at a microscopic scale. On the other hand, as shown by contact mode AFM, the surface was highly dynamic at a mesoscopic scale, with marked changes in apparent topography, friction, and deflection signals. Sun et al., (2002) have used AFM to image cells but also to image biological molecules such as RNA and DNA although tip radius is still a limiting factor to obtaining good lateral resolution. Contact mode has been used to examine fixed cell cultures as well. Fixation cross-links the proteins that form the cell and make them stiffer relative to their live counterparts. The increased stiffness facilitates the scanning process since the cell structures are more resistant to deterioration and can even be used for more than one imaging session.

2.3.2 Tapping mode

Contrary to contact mode, where the cantilever is always in contact with the sample, in tapping mode, the cantilever interacts intermittently with the sample. In this mode, the cantilever is oscillated at its resonant frequency by a piezoelectric actuator. Upon approaching the sample and at the bottom of each oscillation cycle, the tip briefly interacts (‘taps’) the sample surface. This tip-sample interaction produce a decreases of the oscillation amplitude. The AFM feedback circuit is used to maintain a constant, reduced cantilever oscillation amplitude (*e.g.* to 80% of the interaction free amplitude) by adjusting the tip-sample separation. The feedback thus compensates for changes in the amplitude set value by changing the tip-sample separation z. Simultaneous topography and phase images can be obtained with this mode.

The use of tapping mode has some advantages relevant for biological samples. In particular, this mode significantly reduced probe-sample shear interactions, thus diminishing the damage that soft samples might suffer when scanned in contact mode. Oscillating the tip at high frequencies can take advantage of the viscoelastic nature of most biological materials, which tend to be stiffer (have a higher elastic modulus) at higher frequencies. Thus tapping

mode imaging on biological systems tends to give higher resolution images while minimizing damages from shear forces.

In addition to the topographic image, which provide information about the physical shape of the sample contour, phase images contain information of the mechanical properties of the sample. The phase lag of the tip movement relative to the excitation signal is monitored and recorded while the feedback keeps the oscillation amplitude at a fixed value. Phase image contains qualitative data of the mechanics of the sample but other techniques such as Force spectroscopy and Force modulation have to be used if quantitative data is required. Performing tapping mode in liquids brings additional advantages that include the elimination of capillary forces and the reduction of the van der Waals' forces. This, generally speaking, makes the imaging of biologically relevant samples, that are delicate and soft in nature, a bit less daunting (Hansma et al., 1994).

However, although tapping mode has advantages over contact mode, some issues can arise, especially when measurements are carried out under liquid which is a common procedure when investigating biological samples. The resonance frequency of cantilevers immersed in liquid is shifted towards lower frequencies compared to those observed when the cantilever is oscillated in air. Resonance peaks can disappear due to strong damping and new peaks (due to mechanical excitation of the liquid cell) might appear (Putman et al., 1994). This phenomena is known as the 'forest of peaks' problem and can make the identification of the cantilever resonance peak challenging (Schaffer et al., 1996). The quality factor of the cantilevers also decrease by 1 to 3 orders of magnitude in liquids as compared to air due to viscous damping, thus reducing AFM sensitivity (García and Pérez, 2002).

Despite that, tapping mode is widely used when low interaction forces are required and the mechanical damage of the sample is a concern. This mode has been used in experiments involving single and double stranded DNA, DNA-protein complexes (Muller et al., 1997; Kopp-Marsaudon et al., 2000; Sun et al., 2002), RNA (Kienberger et al., 2004), proteins (Möller et al., 1999; San Paulo

and García, 2000), polymers (Reiter et al., 2000) and living and fixed cells (Espenel et al., 2008).

2.3.3 Metrology and time resolution in contact and dynamic modes

Although AFM topographic measurements are very useful, it should be kept in mind that the height determined from images (both contact and tapping mode) is usually smaller than the nominal expected value for soft, easily deformable samples such as cells. Deformations occurs due to tip-sample interactions as well as dehydration (when scanning in air) .Convolution effects due to large tip radius of curvature also affect the measured lateral dimension of objects (García and Pérez, 2002). Under some conditions[2] an impressive lateral resolution of 1.1 nm (on proteins located in the purple membrane) has been achieved in tapping mode. The sample used were crystalline patches of the protein bacteriorhodopsin mounted on a solid, flat substrate with careful optimization of electrostatic screening (Möller et al., 1999).

Imaging of dynamic events such as cell division, filopodia extension, synapse formation and developing requires the acquisition of several frames in short periods of time. Current acquisition times are of the order of minutes which make the use of the traditional AFM a tool not suited for imaging highly dynamic events. Recently developed high speed AFM (HS-AFM) overcomes this problem (Casuso et al., 2009). HS-AFM has been mainly developed by three groups (Ando et al., 2001; Humphris et al., 2005; Hansma et al., 2006). For instance, Ando et al., (2001) were able to get 100x100 pixels images within 80 ms and therefore can generate a movie consisting of many successive images (80-ms intervals) of a sample in aqueous solution. The optimization of the AFM involved the use of small cantilevers with high resonance frequencies (450–650 kHz), small spring constants (150–280 pN/nm), a scan system free of resonant vibrations up to 60 kHz and several electronic components with a wide

[2] Minimization of the tip-sample interactions and the increased rigidity of the sample at higher frequencies due to viscoelasticity

bandwidth. This type of highly specialized equipment is not yet commercially available. Most recently, HS AFM has directly visualized the details of the motion of a single myosin motor protein on an actin filaments (Kodera et al., 2010).

2.4 The force sensor

2.4.1 Spring constant

In the AFM, the cantilever is the element that transduces the forces acting between tip and sample to optically detected mechanical deflections. For small forces (linear approximation) the deflection of the cantilever for a given force acting on it is given by the Hooks' law,

$$F = k * z \qquad \text{(Eq. 1)}$$

where *k* is the cantilever spring constant and *z* represent the vertical displacement (bending) measured at the cantilever tip. A good estimation of the cantilever spring constant is thus necessary to determine the force from the measured deflection z.

Several methods have been described in the literature to calibrate the spring constant of a cantilever.

Sader's method of calculating the spring constant for triangular cantilevers often used in biological experiments makes use of the parallel beam approximation (Sader, 1995) in which the two arms of the triangular cantilever are considered equivalent to a single rectangular cantilever plate of length *L* and width *2d*. For the triangular cantilevers, *L* is the length of one arm and *d* is its width. The parallel beam approximation method predicts that *k* can be calculated by the equation,

$$k = \frac{Et^3 d}{2L^3}\cos\theta\left\{1+\frac{4d^3}{b^3}(3\cos\theta-2)\right\}^{-1} \qquad \text{(Eq. 2)}$$

where *E* is the Young modulus of the material, *t* represents the thickness, theta is half the opening angle between the arms and *b* is the distance between the arms at the chip base. Calculation of the spring constant for the triangular cantilevers using the nominal cantilever dimensions provided by the

manufacturer (*L* = 310 µm, *b* = 225 µm, *d* = 20 µm, *t* = 0.55 µm and theta = 19.4; Veeco, model: MSCT-AUHW) and a silicon nitride's Young's modulus of 222 GPa (Nix, 1992) produces a *k* = 10.7 mN/m. The nominal value provided by the manufacturer is 10 mN/m, well within the 10% - 20% error generally accepted for the calculation of the spring constant using Sader's method (Sader, 2002).

A further method developed by Sader et al., (1995) to calculate the spring constant of triangular cantilevers was published in 1995 (such cantilevers were used in all the experiments described in this thesis unless otherwise stated). The method incorporates the viscosity and density of the medium in which the cantilever is immersed along with experimentally determined values of the resonant frequency and quality factor. The cantilever dimensions are also needed to calculate the stiffness of the cantilever. We found that results do not differ significantly from the values stated by the manufacturer.

Cleveland et al., 1993 developed a method that is based on measurements of the cantilever width and length as well as the cantilever's resonant frequency. The method relies on literature values for elastic modulus and density of the cantilever material.

The methods previously described make use of the cantilever dimensions to get the spring constant and are generally called "geometric methods".

"Thermal methods" measure the cantilever's thermal noise spectrum in order to calculate the cantilever spring constant (Hutter and Bechhoefer, 1993). In their approach, the cantilever is modeled as a harmonic oscillator in contact with a heat bath. In this case, the Hamiltonian describing the cantilever motion is given by,

$$H = \frac{p^2}{2m} + \frac{1}{2} m \omega_0^2 q^2 \qquad \text{(Eq. 3)}$$

Using the equipartition theorem, equation 4 can be obtained,

$$k = \frac{k_B T}{\langle q^2 \rangle} \qquad \text{(Eq. 4)}$$

Where $\langle q^2 \rangle$ is mean square amplitude of the cantilever oscillation due to thermal excitations. In order to measure the mean square amplitude of the

thermal fluctuations, the data is examined in the frequency domain. The power spectral density of the cantilever displacement fluctuations has a Lorentzian shape. Integrating this power spectrum over frequency gives the mean square of the fluctuations in the time-series data needed as input to equation 4.

There are other calibration techniques such as finite element analyses (Stark et al., 2001), methods that make use of nanoindentors (Holbery et al., 2000) and approaches involving manipulation of small particles (Cleveland et al., 1993). However, such techniques have some drawbacks such as complexity for quick use and the necessity of special equipment (Burnham et al., 2003).

A comparison of different calibration techniques found variations of 20% for the same cantilever (http://www.asylumresearch.com/Applications/CantileverCal/CantileverCal.shtml). In the present study, we found that the spring constant measured by the thermal method was within the value calculated by the Sader method and in good agreement with the nominal value given by the cantilever manufacturer. Thus, the nominal spring constant was used to calculate interaction forces in this thesis.

2.4.2 Attachment of polystyrene beads to cantilever tips

Many commercial probes, particularly the ones employed in this thesis (model: MSCT-AUHW, Veeco, Plainview, NY), have a sharp tip at the extreme end of the cantilever that interact locally with the sample. Although very localized interactions with sharp tips are desirable in many applications of AFM, it is not advantageous for the purpose of the experiments described in this thesis since they can lead to the damage of the membrane of living cells. To avoid harming the membrane, cantilevers with polystyrene beads attached to them were used throughout the experiments. An additional advantage of using beaded cantilevers is that the measured modulus is an average over an area. Calculation of the bead-membrane contact area was modeled with the Hertz theory. For a rigid spherical indenter in contact with an elastic material the equation

$$r^3 = \frac{3}{4}\frac{FR(1-\nu^2)}{E} \qquad \text{(Eq. 5)}$$

predicted the contact radius (Fischer-Cripps, 1999). Given a 0.3 nN force (typical for the measurements performed in this thesis) and a 4.5 μm diameter polystyrene sphere, the contact radius vary between 0.8 μm and 1 μm (the former for 'stiff' cells, the latter for softer cells). The attachment of the bead to the cantilever is described below.

Glass needles with sharp tips were prepared by pulling the two extremes of 1.5 mm diameter glass cylinders (World Precision Instruments, Inc., Sarasota, FL) with a micropipette puller (Sutter Instrument Co., Novato, CA). A small amount of UV curable glue (Electro-Lite corporation, Bethel, CT) was then deposited on the tip of the needle.

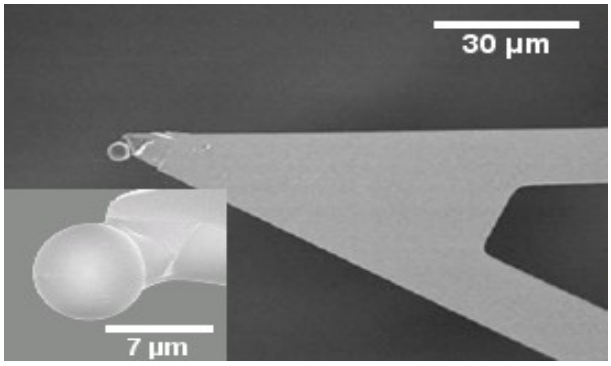

Figure 8: For most experiments presented in this thesis, a 4.5 or 7 μm diameter polystyrene bead was attached to the cantilever tip with UV curable glue. The bead prevented puncturing of the cell membrane due to the sharp tip.

A cantilever was placed sideways on a glass coverslip situated on the stage of the inverted optical microscope and the glass needle was brought into contact with the cantilever tip. A micromanipulator (Siskiyou, Inc., Grants Pass, OR) was used to precisely control the movement of the glass needle when transferring a small amount of glue to the cantilever tip. A coverslip, previously prepared by putting a drop of diluted polystyrene beads (Polysciences, Inc., Warrington, PA) and letting them dry, was mounted on the sample stage of the AFM. The cantilever was then mounted on the AFM head and moved downwards towards the coverslip until a polystyrene bead lying on the glass coverslip was touched by the cantilever tip. A bead was picked up from the substrate by

retracting the tip. The cantilever with bead was then placed for 30 s under a UV light to harden the glue (see Figure 8).

2.5 Force spectroscopy

Atomic Force Microscope Spectroscopy is a technique suitable to study the interaction forces between the probe and the sample. In this technique, the cantilever is moved vertically by ramping the z piezo, thus changing the tip-sample separation. Any lateral movement is disabled by keeping the x and y piezo extension constant. When the cantilever approaches to the sample, the tip-sample interactions (Pauli repulsion, van der Waals, ionic repulsion) increases and produces a bending of the cantilever. The approach is stopped when a deflection threshold (*i.e.* the maximum force) specified by the user is reached. Finally, the cantilever is retracted away from the sample to complete a force-distance curve cycle (see Figure 9). The force applied to the sample can be calculated by using Hooke's Law to convert the measured cantilever deflection to force (see Equation 1).

Unlike imaging in contact or dynamic mode, force spectroscopy is performed with the servo feedback loop deactivated. Since feedback loops always contribute some electrical noise, the smallest detectable force in force spectroscopy is usually smaller than the minimal applicable imaging forces. On graphs of force (deflection) vs. cantilever displacement two main portions of the curve can be distinguished: the contact and the non-contact regions. The non-contact region extends from the farthest cantilever-sample separation to the point where the first probe-sample contact occurs. (see Figure 9). The rest of the curve corresponds to the contact region where measurable physical tip-sample interaction occurs.

During the approaching and withdrawing parts of the cycle, different types of interactions act at distinct tip-sample separations. Long-range interactions include van der Waals and electrostatic forces and can be distinguished from contact and short-range interactions that include Pauli and ionic repulsion. Attractive capillary forces due to the formation of a thin layer of water connecting

both the tip and the sample surfaces might also appear when the probe is moving in air. However, when the sample is immersed in liquid, capillary and van der Waals forces, become too small to measure and not relevant (Heinz and Hoh, 1999). In addition, in physiological solutions (with ions present) electrostatic interactions are also negligible. This is advantageous for the experiments described in this thesis.

A distinctive feature of force spectroscopy is its ability to quantify interaction forces as low as nano and even piconewton. However, calibration of

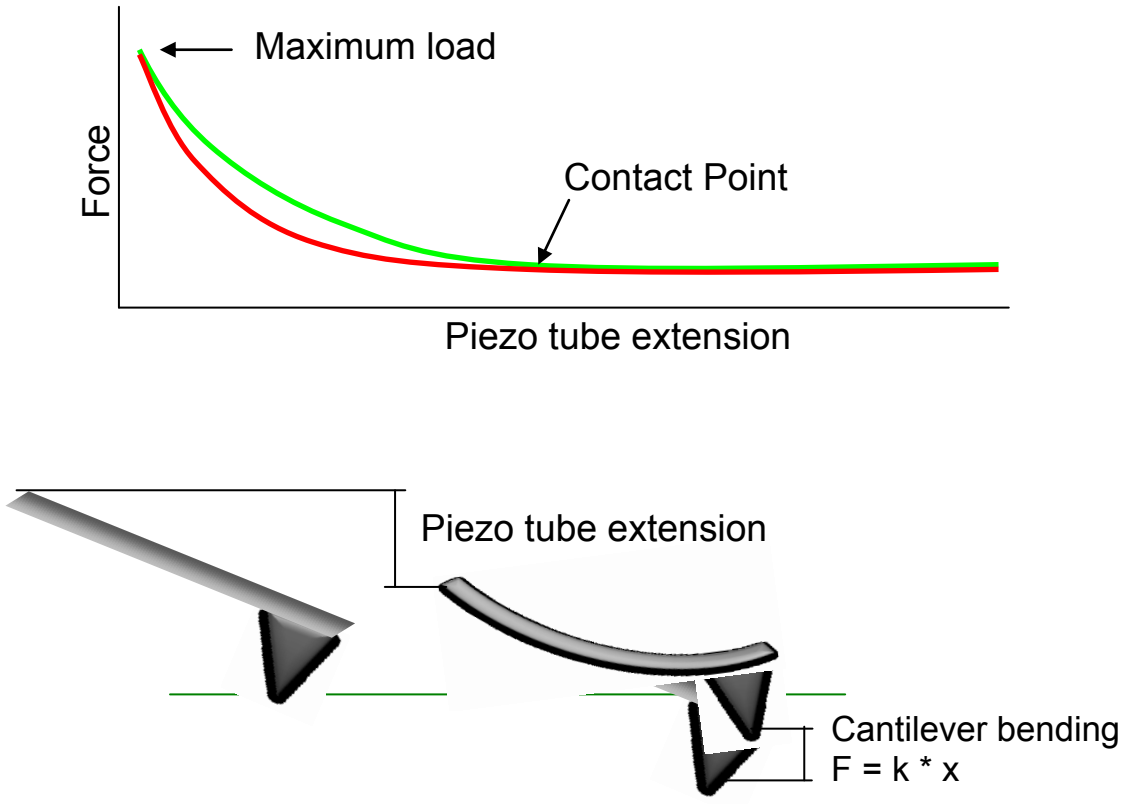

Figure 9: Force-distance curve on a soft substrate (upper panel). The region to the right of the contact point is called the non-contact region of the curve. Tip-sample interaction due to Pauli repulsion appears to the left of the curve. Approach (green line) and retraction (red line) lines in some cases do not overlap due to sample hysteresis. Cantilever bending begins after tip-sample interaction (left part of the lower panel). The piezo tube extends until the cantilever bending reaches a set point determined by the user (maximum load). The load is calculated as $F=k*x$. Subsequently, the cantilever is moved away from the sample and the cycle begins once more.

the deflection sensor is necessary (*i.e.* conversion factor of photodiode reading in V to nm deflection of the tip) and must be done before any quantitative measurement can be performed for each cantilever used. The photodiode output for a given tip deflection can vary depending on exactly where the laser beam is reflected off the cantilever. The regular calibration procedure requires the acquisition of a force-distance curve on a hard substrate (bare glass was used during the course of the experiments presented in this thesis). Because of the stiff nature of the glass, it does not deform and only the cantilever bends. Thus, the resulting cantilever deflection (which is proportional to the photodiode voltage) will be identical to the piezoactuator displacement which can be calibrated with a reference sample. (see section AFM basics and optimization). Finally, the inverse of the slope of the force-distance curve at the contact region (see Figure 10) is a measure of the cantilever deflection sensitivity (measured in nm/V).

$$def\_sensit = \frac{\Delta piezotube\_displacement}{\Delta photodiode\_voltage_{Rigid\_surface}} \qquad \text{(Eq. 6)}$$

Once the sensitivity is established, subsequent measurements of forces applied to non-rigid samples is possible by substituting ***z*** in equation 1 by

$$z = \frac{def\_sensit}{\Delta photodiode\_voltage_{non\_rigid\_surface}} \qquad \text{(Eq. 7)}$$

In this equation, the $\Delta photodiode\_voltage_{non\_rigid\_surface}$ is equal to the difference between the photodiode output voltage at the contact point and the voltage at any location on the contact region of the force-distance curve.

It should be pointed out that when indenting soft samples, a non-linear increase of the force is often observed at the contact region of the curve. This non-linearity arises mainly because the area of contact between the tip and sample increases with indentation (this will be discussed in more detail in the Hertz model section).

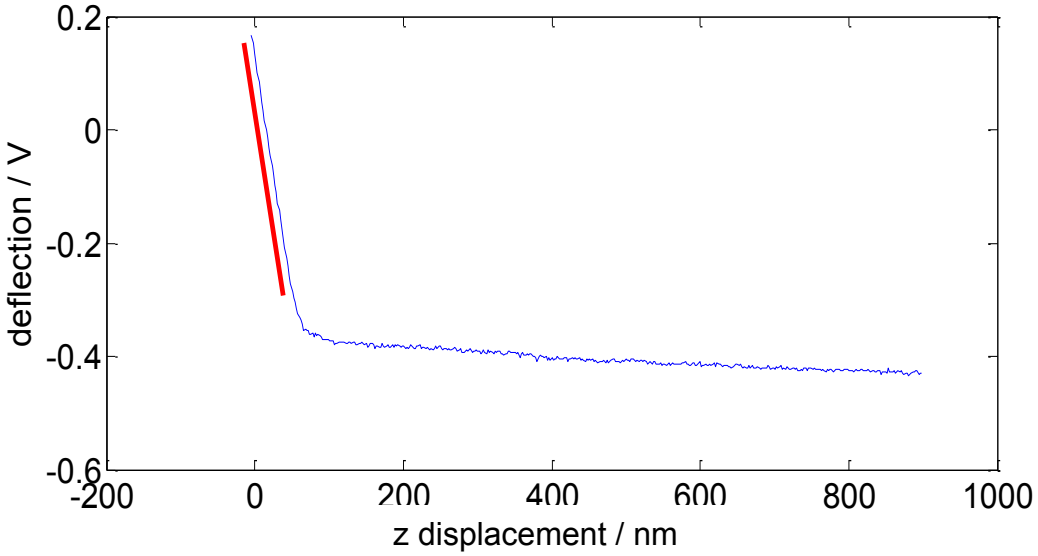

Figure 10: The stiffness of a rigid substrate allows the determination of the cantilever deflection sensitivity. Under these circumstances, the bending of the cantilever must be equal to the vertical displacement of the z-piezo tube at the contact region. The horizontal axes represents the calibrated z-piezo displacement and the y axes represents the cantilever deflection in Volt as measured by the position sensitive photodetector. The red line is a fit allowing the determination of the cantilever sensitivity. For the line shown here, we determined a deflection sensitivity of 128 V/nm

2.5.1 Force Volume Imaging

Force volume imaging is an extension of the force spectroscopy technique. In this case, the cantilever is moved in a defined pattern on the sample and a two-dimensional array of force-distance curves is obtained. After each curve is acquired and while the cantilever is not in contact with the sample, the piezotube displaces the cantilever laterally to a new position where another force-distance curve is obtained. This cycle is repeated until the whole area is covered. The resulting 4 dimensional data set $F(x,y,z)$ contains sufficient information to get a topographic image and an elasticity map of the samples (*e.g.* $dF(x,y)/dz$ for a certain value of z). A topographic image is generated by plotting the extension of the piezotube necessary to reach a defined force at each data point. The resultant image depicts the topography of the sample as contours of

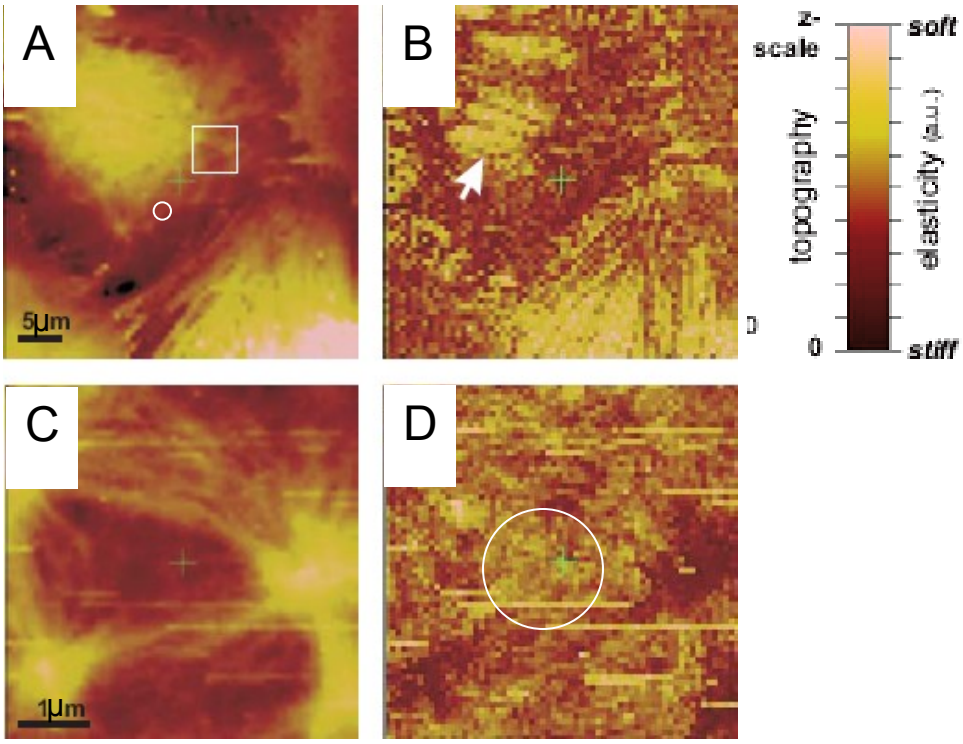

Figure 11: Force volume image of a confluent Airway Smooth Muscle Cell culture. The left images show the topography of the cells in the culture. The circles in the images A and D represent the approximate bead-cell contact area. Bright areas in A correspond to the cell nucleus. The z-scales in A and C are 1 µm and 0.3 µm respectively. It must be noticed that this scale does not represent the real height of the cells (from the underneath substrate to the top of the cell) since the confluence of the culture avoids the cantilever to reach the base of the cell at the edges). The upper right image (B) is the qualitative elasticity map generated by taking the indentation at a fixed z. The image shows homogeneity in the cell elasticity at regions around the cell nucleus. The area shown in C is a zoom of the region enclosed by a square in A. Similarly, D depicts the elasticity map of the area in C. It is noticeable that even though some fibers that connect the nodes are visible in C, they are not clearly visible in D. This is an indication that the mechanical properties of the cells measured with the AFM do not vary largely among regions of the same cell. Thus, the variations measured in this thesis have to be related to cell to cell variability in the mechanical properties. The Darker areas in the right imager correspond to stiffer regions. Posterior analysis of the force-distance curves in the array can produce quantitative data of the elastic properties of the sample. (Smith, 2004).

constant force[3] (z(x,y) for F = constant). It is thus in principle possible to generate images of surfaces at zero load (see Figure 11).

Relative elasticity of different regions of the sample can be qualitatively distinguished by several methods. For example, one can plot the slope of the F(z) curve (*i.e.* dF(x,y)/dz) at a fixed z value, look at the sample penetration (*i.e.*

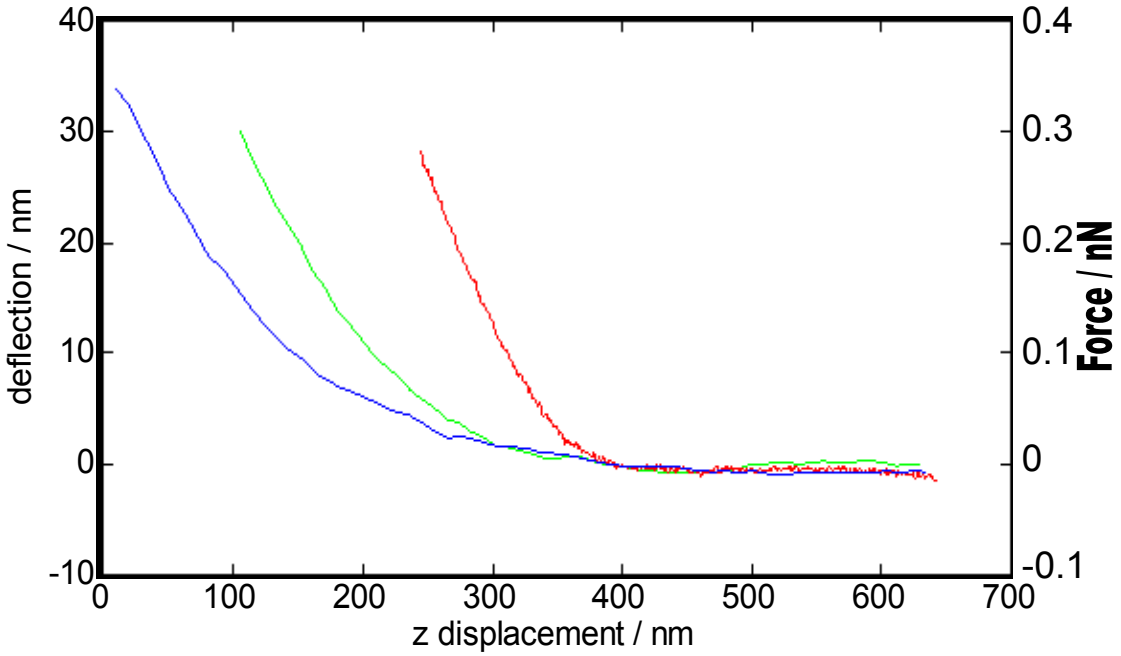

Figure 12: Three representative force-distance curves (approach) taken on different cells are shown. Each curve was obtained above a region between the cell nucleus and the cell edge. It can be noticed that for a fixed maximum force (0.3 nN in this case), the softer regions produce curves with larger indentation (blue line) that medium (green line) and stiffer regions (red line). This type of curves were used to fit to the Hertz model and calculate the Young's modulus and getting the indentation needed in equation 9 calculate the complex modulus of the cells. Note that the contact point particularly for indentation of soft samples is not obvious.

the indentation depth necessary to reach a maximum load) or measuring the cantilever deflection (*i.e.* force) at any indent depth between the contact point

[3]Force volume images are obtained in "relative trigger mode" which means that the maximum cantilever deflection is set constant and measured relative to the initial cantilever deflection.

and the maximum piezotube extension for each force-distance curve in the array (see Figure 11). Curves obtained on soft regions show a larger indentation depth than the indentations of relatively hard regions. Similarly, the cantilever deflection at a fixed z tend to be larger for curves taken on stiffer regions of the sample (see Figure 12).

Maps produced by force-volume imaging are useful to obtain a rapid and qualitative map of the spatial 3D extent of regions of relative elasticity differences of the sample. However, this method does not produce quantitative data regarding the elastic and/or viscous properties of the sample. To achieve this, other methods (Hassan et al., 1998) or further processing and analysis of the collected data has to be done as described in the sections “Hertz model” and “Force modulation”.

2.5.2 Hertz model

Elasticity and responsiveness of living cells to external forces are two interesting subjects from the perspective of tissue engineering, cell biology and cancer research. During tissue development, for instance, living cells respond to mechanical stimulus in their native environments with changes in morphology, membrane and nuclei structure (Lulevich et al., 2006), cell-spreading (Nathalie et al., 2002), actin and microtubule reorganization (Laurent et al., 2005), or cell motility (Petroll et al., 2004). So far, the investigation of single-cell mechanics had been difficult to perform since most of the techniques are intended to measure the mechanical properties of dissected tissue strips (strips are formed of hundreds or thousands of cells; Yuan et al., 2000; Holzapfel et al., 2004; Cavalcante et al., 2005) or averaging the mechanical properties of hundreds of individual cells (magnetic twisting cytometry; Fabry et al., 2001) where no control of the bead location on the cells surface is possible. The AFM, in contrast, can be used to test the mechanical properties of individual cells. One can then determine in principle how much of the distribution of various parameters observed in the aforementioned experiments is due to single cell or population heterogeneity. Furthermore, the AFM allows a fine control of the location of the

probe-cell contact and the duration of the interaction. Both, spatial and temporal control make this technique highly valuable. However, the characterization of cellular mechanics with the AFM is challenging mainly because the maximum cell height in the nuclear region is usually only a few micrometers and the thickness decreases considerably at regions close to the cell edge. This considerably limits the possibility of obtaining reliable measurements in those regions, a substrate effects or the mechanical properties of the nucleus can dominate. Although several theories describing contact mechanics in the context of cellular systems are available in the literature (Muller et al., 1983; Derjaguin et al., 1975; Johnson et al., 1971), the Hertz theory is the most often used model and has been used in several studies to characterize the cell mechanics of different types of cells (Rotsch et al., 1999; Sato et al., 2000; Yamane et al., 2000).

The Hertz model makes several assumptions: the material to be tested should be linear, elastic, isotropic and homogeneous with an infinite thickness while the indenter should be rigid, non-adhering and of known symmetric geometry (Hertz, 1882; Johnson, 1987). We will discuss these assumption in the following paragraph.

The requirements of rigidity and well known symmetric geometry are met by the spherical indenter used here. Small values of adhesion between the bead and the cell cannot be ruled out completely. However, the force distance curves used for the analysis did not show obvious signs of attachment (*i.e.* adhesion force was less that the detectable force noise). Although the other assumptions (linearity, elastic, isotropic and homogeneous) are generally not met by living cells, this model has been used to extract mechanical properties of cells in the past (Alcaraz et al., 2003; Smith et al., 2005; Rotsch et al., 1997). For instance, cells are likely not isotropic due to the presence of stress fibers in the cytoskeleton (actin filaments). However, at nm scales, the actin mesh might be reasonably homogeneous and isotropic (see Figure 13, Svitkina and Borisy, 1999). The infinite thickness assumption made by the Hertz model has been addressed by indenting the cells only a small fraction of the cell thickness (~ 10 – 20 %). Care was taken to indent only regions between the nucleus and the cell

edge where the cytoplasm is located. The determination of the place to indent was facilitated by the use of an inverted optical microscope that allowed the positioning of the bead tipped cantilever to the cytoplasmic region located between the cell nucleus and the cell edge.

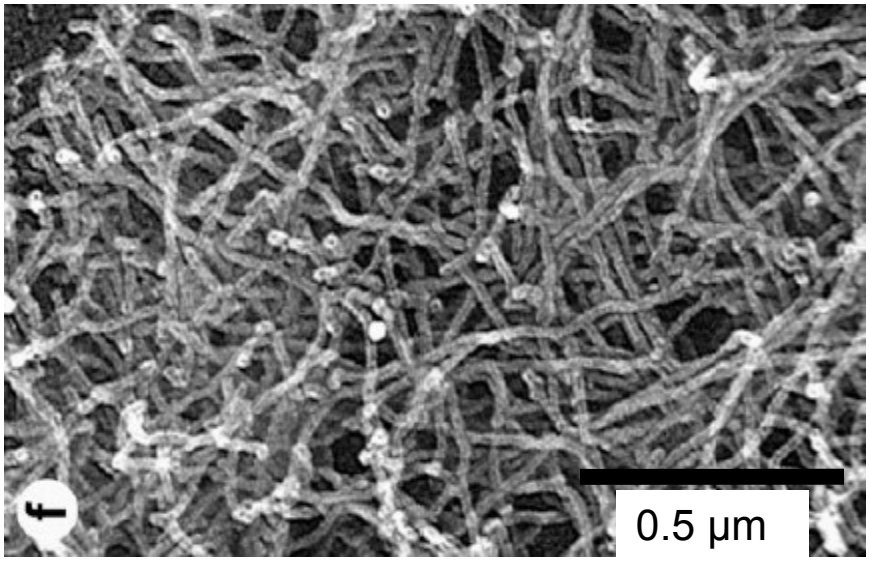

Figure 13: SEM image of the actin network in the lamellipodium of *Xenopus* fibroblasts. The height of this micrograph correspond to 1 µm which is approximately the calculated contact radius for a 4.5 µm sphere and a 0.3 nN load force typical for the experiments performed in this thesis. The AFM indentation contact area corresponds to roughly twice the area of this image, showing that the AFM is averaging over many actin fibers and is insensitive to their individual mechanical properties. Picture taken from Svitkina and Borisy, 1999.

One explanation for the success of the Hertz model in the context of AFM is due to the high spatial resolution/positioning capability and the high force sensitivity achievable in AFM force spectroscopy. At small indentation depths at selected locations only a small volume of the cell is probed, deviations from non-linearity, isotropicity and homogeneity are then only second order effects. Indeed, Smith et al., (2005) showed that force spectroscopy in the cytoplasmatic region of smooth muscle cells measuring the complex shear modulus showed a strong sensitivity to the degree of actin polymerization. Inhibitors of myosin light chain kinase activity had little effect on the stiffening response to contractile stimulation of the cells.

To calculate the elastic modulus, the Hertz model needs experimental input values of the load and penetration depth. During the experiments, typical loads of 0.3 nN and indentation depths between 200 and 400 nm were employed. The Hertz theory predicts that the force increases non-linearly with indentation depth according to the following mathematical relations,

$$F_s = \frac{4ER^{1/2}}{3(1-\nu^2)}\delta^{3/2}, \quad \text{spherical indenter of radius R>>δ} \qquad \text{(Eq. 8)}$$

$$F_c = \frac{2E\tan\theta}{\pi(1-\nu^2)}\delta^2, \quad \text{conical indenter of half-opening angle θ} \qquad \text{(Eq. 9)}$$

where *F* is the loading force, *E* is the Young Modulus, *u* is the Poisson ratio, *δ* is the indentation depth. For a spherical indenter, *R* is the sphere radius while theta represents half the opening angle for a conical indenter.

For the experiments performed here, cantilevers with glued beads were used for two reasons: first, conical indenters could damage the delicate cellular membrane and second because it was shown by Dimitriadis et al., 2002 that measurements of *E* performed with beaded cantilevers are more accurate than those performed with conical indenters. Thus, when analyzing data in this thesis the equation for a spherical indenter was employed.

After the collection of the force-distance curves, they were fit to the Hertz model using the Nonlinear Least Squares method. A numerical code implemented in the MATLAB software (version 7.10.0.499, (R2010a) The MathWorks Inc., Natick, MA, 2010) was employed to facilitate and speed up the calculation of the Young's modulus by fitting a large number of F(z) curves (see Appendix 1 for the code).

During the process to calculate the Young's modulus, the estimation of the indentation deep is required (see equation 8) and thus the contact point of the force-distance curves has to be determined. An analysis of the equation 10 reveals that the precision in the determination of the contact point (and thus the determination of the indentation deep) can importantly affect the calculated *E*

$$E = \frac{3(1-\nu^2)F}{4R^{1/2}}\delta^{-3/2} \qquad \text{(Eq. 10)}$$

If we take the derivative of this equation with respect to δ (which represent the indentation depth in the equation) and assuming that □δ represent the error on determining the contact point, we get the follow identity,

$$\frac{\Delta E}{E} = -\frac{3}{2}\frac{\Delta \delta}{\delta} \qquad \text{(Eq. 11)}$$

Thus, for small indentations δ such as the ones observed when indenting very hard substrates, the right term becomes large and then the relative error □E/E becomes large too. This means that only for large indents δ, the determination of the contact point will not substantially affect the determination of the Young's modulus and the limit for the validity of the Hertz model will depend solely on the material elastic limit.

Although the precision in the determination of the contact point is important, this is not an easy task when soft materials are tested since the curvature of the force distance curves at the contact point (see Figure 12) is small and force noise non-negligible. Determining this point by eye (although often done in the literature) is subjective and can lead to large systematic errors. Thus, an automatic procedure to systematically determine the contact point was implemented in MatLab. Briefly, an interval of the force distance curves that contained the contact region as well as part of the no-contact region was chosen. Several fits to equation 8 were performed in this interval in such a way that the probable contact point was displaced from the left to right (see Figure 14). The calculated Young's modulus, the goodness of the fit and the contact point for each fit were recorded. Clearly, many of the fits were not optimal (with poor goodness) but only the fit $f_H(\delta)$ with the larger goodness was kept (f_H is the fitted function that depends on the indentation δ, see equation 8).

To increase the robustness of the extracted Young's modulus a second analysis method was implemented as a cross check. A linear fit $f_L(\delta)$ to the non-contact region was performed and the standard deviation (σ) from points in the non-contact region relative to the best linear fit $f_L(\delta)$ was calculated. The value of $f_L(\delta)$ as well as $f_H(\delta)$ at the contact point ($f_L(Contact\ Point)$ and $f_H(Contact\ Point)$ respectively) were calculated. Only for curves where both fit methods yielded a

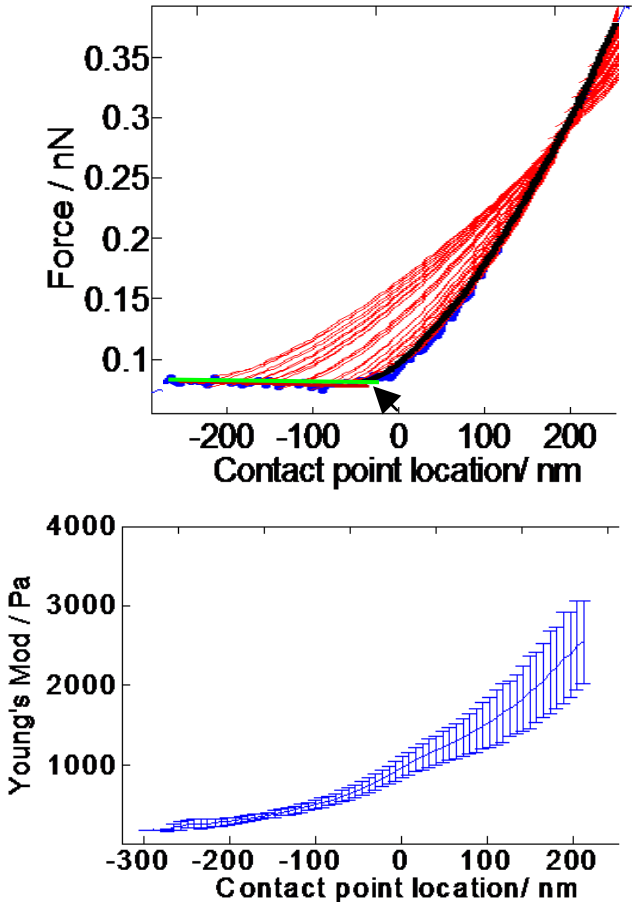

Figure 14: The upper panel shows a force-distance curve (blue line) obtained when a beaded cantilever (bead radius = 2.25 μm) was pushed into contact with a gel. The red lines represent several fits for different "contact points" along the force-distance curve. From all the contact points shown in the figure, only the one that produced a fit that satisfied the two following conditions was selected: a) the goodness of the Hertzian fit $f_H(x)$ (black line) had to be as close to 1 as possible and b) $f_H(\textit{contact point})$ is within the interval $f_L(\textit{contact point}) \pm 2\sigma$ (in this case, $f_H(x)$ represents the Hertzian fit while $f_L(x)$ represent the linear fit (green line) in the non-contact region, σ is the standard deviation from points in the non-contact region relative to the best linear fit $f_L(x)$). The arrow in the figure points to the curve that satisfied both conditions. The best fit is then used to determine E and the contact point. The plot in the lower panel was constructed by averaging the Young's modulus obtained from hundreds of fits separated equal distances from the best contact point for each of the many force distance curve employed. Thus, the error bars correspond to the variability of the Young's modulus for specific distances from the best contact point calculated in each force distance curve. In other words, the error bars in the graph represent the variability of E as a function of the contact point.

result for $f_H(Contact\ Point)$ within the interval $f_L(Contact\ Point) \pm 2\sigma$ the Young's modulus was flagged as having been determined reliably and thus deemed significant (see Figure 14 and Figure 15). This automized procedure thus systematically determined the contact point and Young's modulus.

Approximately 1000 force distance curves were used to compute *E* for each gel. From these, ~ 25 %, 50 % and 75% of the curves taken on stiff, medium and soft gels complied with the above conditions. It is plausible that this variable success rate is related to the fact that the calculation of the Young's

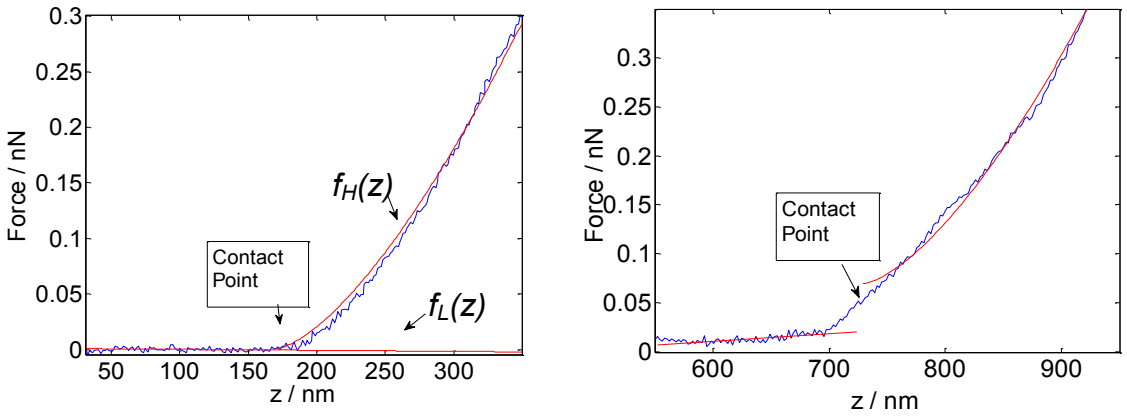

Figure 15: The left image shows a typical curve that fulfills the two conditions stated in the text in order to be considered significant. These conditions are that, $f_H(contact\ point)$ is within $f_L(contact\ point) \pm 2\sigma$ and that the goodness of the fit was better than 0.99. Clearly, the first condition is not satisfied for the curve shown in the right panel where a big discontinuity (gap) is observed at the contact point.

modulus of stiffer substrates is more sensitive to the precision in the determination of the contact point. The reported *E* and the error associated are the mean and the standard deviation of the calculated modulus for each gel stiffness.

2.5.3 Indentation Modulation

A more complete determination of the elastic properties of biological material can be achieved using the Indentation Modulation technique. Cells often are visco-elastic (*i.e.* have a frequency dependant elastic modulus). It is very

challenging due to instrumentation limitations to extract visco-elastic properties from force distance curves as described in the previous section. To implement the indentation modulation method a sinusoidal signal generated by a lock-in amplifier (Model SR810, Stanford Research Systems, Inc. Sunnyvale, CA) is fed into the AFM system. It oscillates the piezo tube of the AFM at a controllable amplitude and frequency. Consequently, a sinusoidal load is applied to the tested material through the beaded cantilever. The material response is then detected in the AFM photodiode output signal. This signal is analyzed with the lock-in amplifier, which allows a sensitive and quantitative determination of the resultant cantilever amplitude and phase. For a purely elastic material, the phase difference will be zero; the demodulated amplitude will be a reflection of the sample elastic modulus (more precisely the average of the bead-sample elastic modulus): soft samples will lead to a small cantilever deflection as the bead 'sinks' into the sample, whereas stiff samples will lead to a large cantilever oscillation amplitude. Calculation of the mechanical properties of the sample are performed by comparing the input and the output signals, including the phase shift (see inset in Figure 16). The resultant complex modulus (G^*) is an imaginary number, the elastic modulus correspond to the real part of G^* and the viscous modulus (also called loss modulus) correspond to the imaginary part of G^*.

When performing the indentation modulation technique, the cantilever movement before and after the application of the loading oscillation follows the same pattern as that of the cantilever when regular force-distance curves are taken (described in Hertz model section). However, in this technique, instead of a single transient pause of the cantilever movement at the farthest non-contact part of the cycle, a second pause is introduced at the maximum probe-sample interaction. This dwelling time is then used to induce the additional oscillatory load described above. The oscillation amplitude employed in the experimental procedure was 7 nm in all cases and the dwelling time was 15 - 20s. (see Figure 4)

Since the accurate measurements of the amplitude and phase shift are essential to calculate the complex modulus, a procedure to correct for phase

shifts and amplitude changes due to reasons other than the response of the sample needs to be performed. Briefly, a hard silicon cantilever with spring constant of the order of 40 N/m and resonance frequency ~ 300 kHz was driven towards a rigid glass surface and oscillated at frequencies lower than 1 kHz. The large difference between the cantilever resonance and the driving frequencies assures that phase shifts or resonant amplitude enhancement due to the cantilever resonance do not play any role in the induced cantilever oscillation. The measured output is only a consequence of the drive input signal. In addition, the rigidity of the cantilever and the high elastic constant (stiffness) of the glass substrate allows one to make the assumption that any movement of the piezo tube is instantaneously followed by the cantilever. Ideally, no difference in phase and amplitude between the input and output signals are expected. However, experimental results show a deviation from this expectation (Figure 16). Due to non-linearities in the z-piezo, the cantilever, the photodetector and the lock-in amplifier, the difference between the measured cantilever response and the driving signal is not zero. Data acquired during the experiments on cells must be corrected for this small deviation.

Strong attenuation of the amplitude and significant phase shifts are also observed at frequencies lower than 5 Hz. Such changes in amplitude and phase are attributed to ac coupling of the lock-in amplifier at low frequencies. The data presented in this thesis was acquired at 10 Hz where no large amplitude and phase changes were observed. Thus, attenuation at low frequencies was not a limiting factors but correction of the data was performed as well. The selection of 10 Hz for the experimental procedure was mainly done because low rather than the high frequencies are relevant for several physiological and cellular processes. For instance, the beats produced by the muscle of the heart can go from ~1 Hz at rest to ~3 Hz when exercising (Robert A. Robergs, 2002) and the breathing frequencies are lower than 0.5 Hz in any exercising condition (Tortora, 1990). At the intracellular level, molecular motors that generate muscle contraction such as myosin move along the actin filaments at a step rate of ~12 Hz (Pierobon et al., 2009).

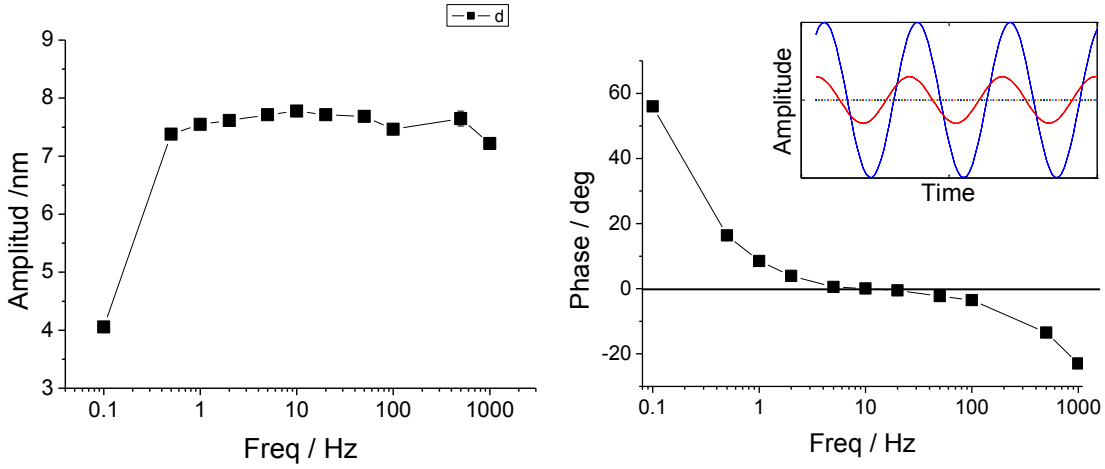

Figure 16: The indentation modulation technique requires the correction of the acquired data (amplitude and phase shift) from errors due to ac coupling in the lock-in amplifier and cantilever or piezo resonance. To get the correction values, a stiff cantilever (~40 N/m) with a 300 kHz resonance frequency was pressed against a piece of glass. An unperturbed, infinitely stiff system would produce curves with 7 nm amplitude and a zero phase shift. This does not occur and it can be seen in the figure that the corrections depend on the frequency due to the electrical and mechanical transfer function of our microscope. The error bars in the figure are very small and can not be seen. This is because the data was acquired with a large spring constant cantilever. This produced data with small noise. Inset shows typical data: the input signal (blue, piezo amplitude) generated by the lock-in amplifier differs from the output signal (red, response of the material measured by the cantilever). Phase shifts and amplitude differences are used to calculate the complex modulus of the samples.

The mathematical procedure used in this thesis to calculate the complex modulus of the samples is based on a first order approximation to the Hertz theory (Alcaraz et al., 2003; Alcaraz et al., 2002). Starting with equation 8 for a spherical indenter and taking the first order Taylor expansion we get,

$$F = \frac{4ER^{1/2}}{3(1-\nu^2)}\left[\delta_0^{3/2} + \frac{3}{2}\delta_0^{1/2}\delta_1\right] \qquad \text{(Eq. 12)}$$

In the above equation, δ_0 represents the value at the initial indentation (no oscillatory load included) and δ_1 the indention due to the oscillatory load. Taking $\delta_1 = \delta - \delta_0$ and since $E = 2G(1 + u)$ (Landau, 1986), equation 12 can be transformed to,

$$G = \left(\frac{1-\upsilon}{4\left(R\delta_0\right)^{1/2}} \right) \frac{F - F_0}{\delta - \delta_0} \qquad \text{(Eq. 13)}$$

In the frequency domain (Findley, 1976), the above equation takes the form

$$G^*(\omega) = \left(\frac{1-\upsilon}{4\left(R\delta_0\right)^{1/2}} \right) \frac{F(\omega)}{\delta(\omega)} \qquad \text{(Eq. 14)}$$

where G^* is the complex modulus and F and δ are the force and indentation due to the modulation.

An additional consideration must be made in order to get a good estimation of the complex modulus. The measurements are performed in liquid medium and the spring constant of the cantilever used is low (0.01 N/m). In these conditions, the hydrodynamic drag due to the movement of the cantilever in liquid can introduce errors. Alcaraz et al., (2002), proposed a methodology to correct for the hydrodynamic drag. In their theory, the cantilever is modeled as a sphere of radius a_{eff} submerged in a viscous medium and attached to a spring. The drag force oppose to the cantilever movement. Solving the equation of motion of the cantilever in liquid medium, the following equation for the hydrodynamic drag can be obtained,

$$H(\omega, h) = \frac{12\pi^2 \eta a_{eff}^2 \omega i}{h + h_{eff}} + r \qquad \text{(Eq. 15)}$$

where η is the liquid viscosity, a_{eff} is the effective radius of the cantilever, ω the frequency, i is the imaginary unity, h is the distance between the sphere and the plane, h_{eff} is the effective high of the tip of the “spherical” cantilever and r is a constant to correct for the fact that the drag away from the surface is not zero. Equation 15 was then used to fit the hydrodynamic drag data (for details about its calculations see below) obtained when the cantilever was oscillated at several height above the cell surface. The fit was extrapolated to zero height and such hydrodynamic drag was used to correct equation 13 (see Figure 17).

The complete equation to compute the complex modulus is given by,

$$G^*(\omega) = \frac{1-\upsilon}{4(R\delta_0)^{1/2}}\left(\frac{F(\omega)}{\delta(\omega)} - H(\omega,0)\right) \qquad \text{(Eq. 16)}$$

F(ω) and *δ(ω)* are measured experimentally. Since *F* is the Fourier transform of the force experienced by the cantilever due to the oscillation, it can be calculated using the equation $F = k^*z$ where *z* is calculated from the amplitude and phase shift acquired with the lock-in amplifier ($x = Ae^{i\theta}$). The denominator *δ* is calculated by subtracting *x* from the driving amplitude introduced by the piezoelectric tube (in our experiments this was always 7 nm). δ_o represent the initial indentation (before the oscillation is applied) and can be obtained from the force-distance curves (see Figure 12). *H* is determined from data fitted to equation 15 and extrapolated to zero height, *i.e.* contact (see Figure 17).

The noise in the amplitude and the phase measured by the lock-in amplifier outputs lead to an associated uncertainty in the calculated *G** value. As

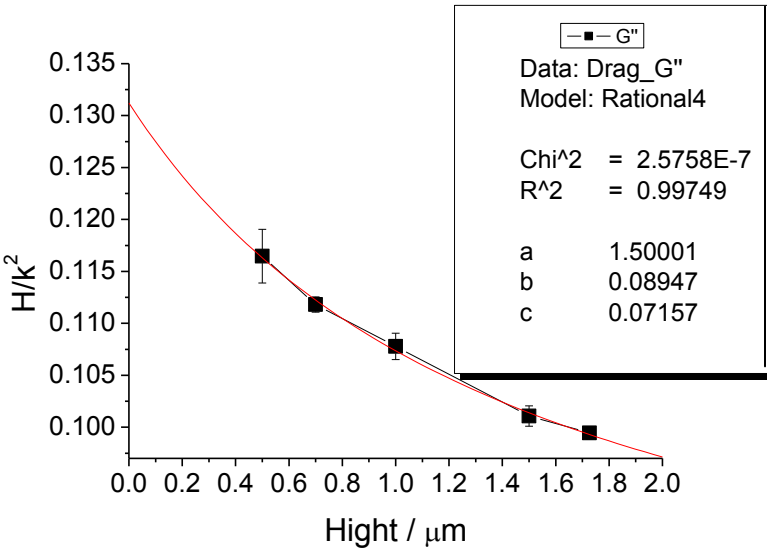

Figure 17: A typical curve used to estimate the hydrodynamic drag at zero height is shown in the figure. Equation 15 was used to fit the data and then extrapolated to zero. This value was subtracted from the *F(ω)/δ(ω)* in equation 14

a general rule, the amplitude and phase were calculated by averaging the last ~ 5 s of the data collected from the lock-in amplifier outputs and thus only the curves that showed a plateau at the end of the curve (see Figure 18) were

included in the analysis (each complete cycle lasted for 15 - 20 s, longer periods were avoided to prevent damage to the cells due to prolonged loads). Three to four cycles were averaged to calculate the viscoelasticity of a single cell at a single location (see Figure 18). Our analysis showed that variability between different cycles on the same location on the same cell was small (less that 100 Pa for the elastic modulus and less than 20 Pa for the loss modulus of cells plated on any substrate). In some cases, errors as small as 10 Pa in the elastic modulus and as low as a 4 Pa in the loss modulus were found. This is an indication of two things; that the method and the instruments used to get the data produce precise results and that these cells did not suffer large, detectable changes in viscoelasticity at the measurement location during the modulation cycle under the tested conditions. Variability in the measured values for G^* are thus NOT due to measurement noise, but are due to biological/sample variability.

A change in the amplitude (but not in the phase) was observed in the lock-in amplifier output of individual cycles only in a few cases but such data was not included to calculate G^* due to the fact that the lock in output signal requires some time (time constant of 3 s was used and the last 5 s were averaged) to

Figure 18: Traces of the lock-in output signals taken on the same cell and the same location at 90 s intervals during an indentation modulation experiment. The data was collected during four consecutive cycles (see inset in Figure 4). The traces were used to calculate the amplitude of the cantilever oscillation (left trace) and the phase shift (right trace). The data was scaled using the lock-in scaling factor (200 mV input per 10,000 mV output) as well as the cantilever deflection sensitivity (given in units of nm/V) in order to estimate the values in nm and radians of the amplitude and phase respectively (refer to text for details about the conversion). The data of the last 5 s was averaged since the signal only stabilizes after several seconds. The last 5 s (used to calculate the amplitude and phase) remained quite constant. Changes in G^* due to variations between cycles (the average of 3 to 4 cycles were used to calculate the viscoelasticity of a single cell) produce an error in the elastic modulus lower than 100 Pa and in the loss modulus lower than 20 Pa for any of the tested conditions. During the data acquisition, a region between the cell nucleus and cell edge was pressed with a force of 0.3 nN prior to the oscillatory load. The oscillation amplitude was 7 nm at a 10 Hz frequency.

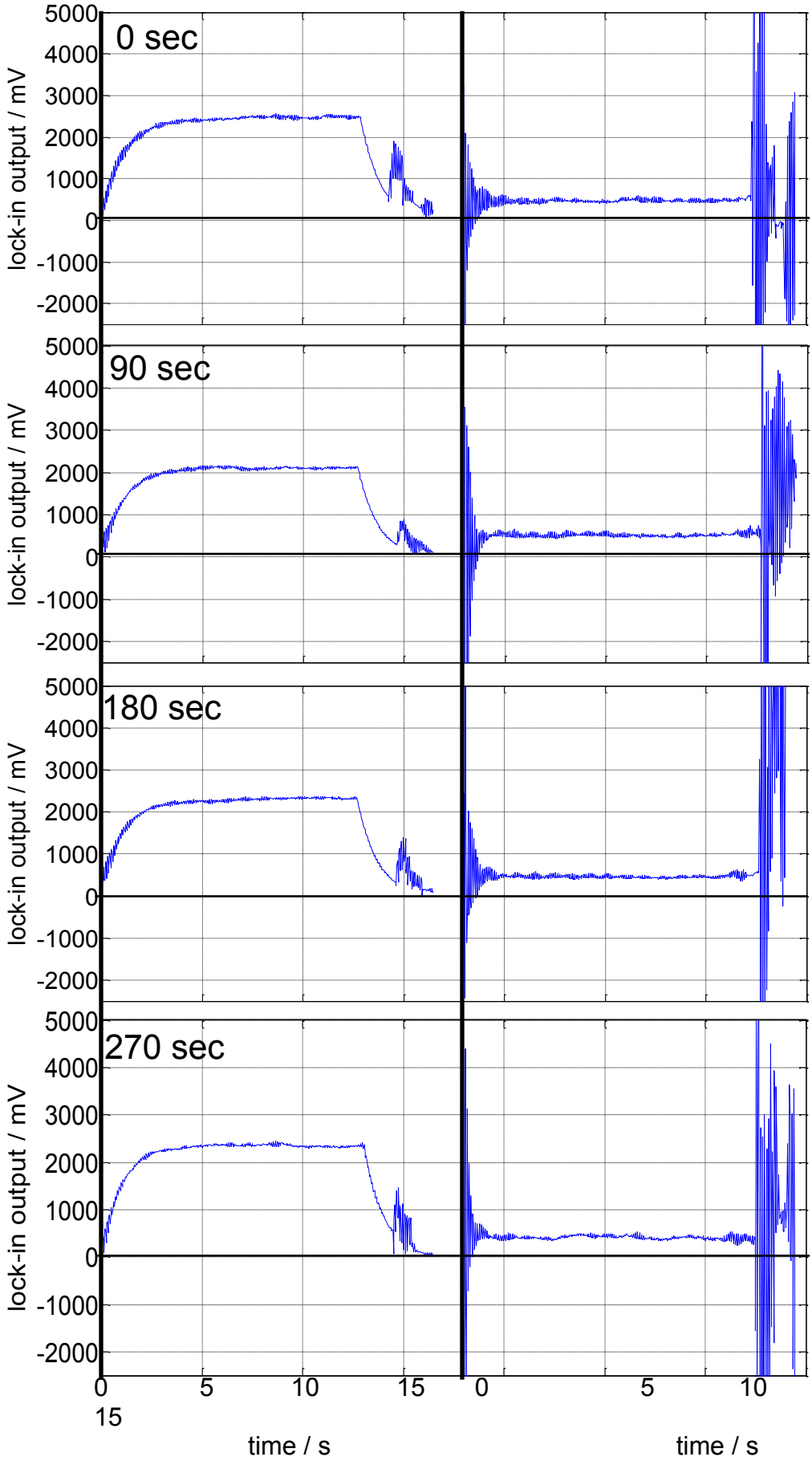
0 sec
90 sec
180 sec
270 sec
lock-in output / mV
5000
4000
3000
2000
1000
0
-1000
-2000
0
5
10
15
time / s

settle. Thus, if the input signal changes on time scales comparable to the lock-in amplifier time constant, the lock-in amplifier output signal is not a reliable measure of the input amplitude.

3 Cellular mechanics

It has been claimed in several manuscripts (*i. e.* Rosenblatt et al., 2004; Wang et al., 2009; Fletcher and Mullins, 2010) that the cytoskeleton importantly contribute to the cell mechanics. An elaborate array of protein fibers helps to maintain cell shape, produce locomotion, provides mechanical strength, aids in chromosome separation during mitosis, and facilitates the intracellular transport of organelles. This important structure surrounds the nucleus and is contained within the cytoplasm. In neuronal cells, the cytoskeleton extends to the neurites,

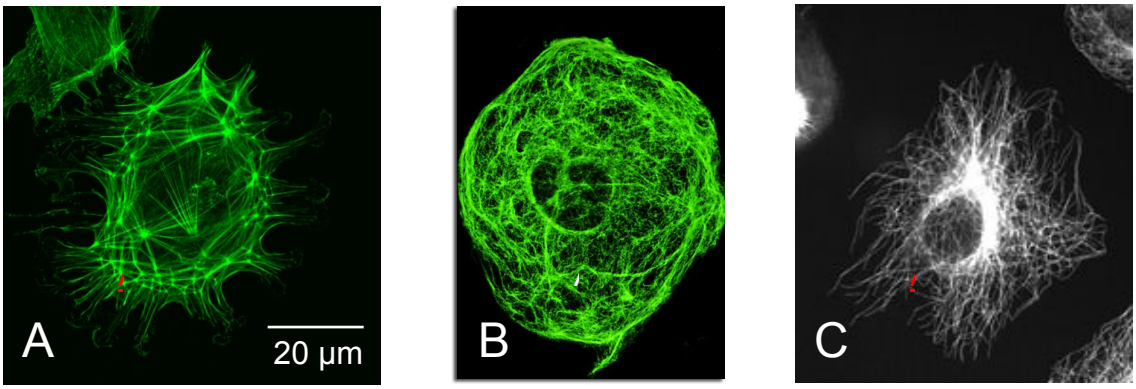

Figure 19: Cytoskeleton elements. A) Actin filaments are mainly found at the cortex of the cell and are involved in cell motility and force transduction. B) Intermediate Filaments from Rat Kangaroo Cell. It has been hypothesized that one of their functions is that of mechanical strength absorbers. C) Microtubules in a fixated cell extend mainly from the center of the cell towards the edges. Microtubules are important structures involved in protein transport. The scale is A is the same for the three figures. Sources: http://scienceblogs.com/, http://www.microscopyu.com/, http://en.wikipedia.org/ for actin, intermediate filaments and microtubules images respectively.

where besides conferring strength, it is involved in protein transport (Olson and Nordheim, 2010). There are three main protein filament components in the cytoskeleton; actin filaments, intermediate filaments, and microtubules (see Figure 19).

Actin filaments are the thinnest filaments of the cytoskeleton with a diameter of 8 nm. These filaments form a band beneath the plasma membrane that provides mechanical strength to the cell, links transmembrane proteins to

cytoplasmic proteins, generates locomotion of cells and interacts with myosin filaments to provide the force of muscular contraction. Actin filaments are flexible and relatively strong (Carlier, 1990).

In cells, actin is mainly found in two forms: monomeric (or globular) and filamentous actin (polymerized actin). The dynamic equilibrium between the two forms is controlled by a variety of factors that are typically only found associated with membranes and that ensure that the nucleation of new filaments occurs mainly from preexisting filaments growing towards the membrane (Bailly et al., 1999; Svitkina and Borisy, 1999; Pollard et al., 2000). Activation of cell surface receptors generate signals that lead to the nucleation of actin on one side, while at the opposite end, hydrolysis of ATP bound to polymerized actin followed by phosphate dissociation marks older filaments for depolymerization. Depolymerized actin is then recycled and returned to the pool of unpolymerized monomers (Pollard et al., 2000).

Actin filaments are a central structural feature of all muscle tissue. Controlled polymerization of branched networks of actin filaments produces force for cell motility. The structural and dynamic properties of actin depend, at least in part, on the form in which it is found in the cell (monomeric or filamentous) (Pfaendtner et al., 2010). Even more, newly formed F-ADP-Pi-actin filaments are more rigid than “old” F-ADP-actin filaments, a fact that could have implications in actin-driven motility processes (Carlier, 1990; Isambert et al., 1995).

Intermediate filaments (IFs), another important component of the cytoskeleton, constitute a major structural element of animal cells. Their major function is assumed to be an integrating device for the entire cytoskeleton (Kreplak et al., 2005).

There are several types of intermediate filament, each constructed from one or more specific proteins. Keratins, for instance, are found in epithelial cells and also form hair and nails; nuclear lamins form a meshwork that stabilizes the inner membrane of the nuclear envelope; neurofilaments strengthen the long axons of neurons and vimentins provide mechanical strength to muscle cells. Despite their chemical diversity, intermediate filaments, in conjunction with

associated proteins, play similar roles in the cell providing a supporting framework within the cell (Herrmann et al., 2007).

In vitro assembly of both recombinant and authentic IF proteins produced smooth-looking, flexible filaments by electron microscopy (EM) and Atomic Force Microscope (AFM). These fibers average 10 nm in diameter although estimation of their thickness varied among fixed and unfixed samples (Mücke et al., 2004; Mücke et al., 2005). Nanomechanical experiments with the AFM have demonstrated that IFs are characterized by a high propensity to withstand both tensile and bending stress (Kreplak et al., 2005; Kreplak and Fudge, 2007). In the cytoskeleton, IFs seem to work synergistically with the actin filaments and MT networks.

Finally, the microtubules are the third type of filaments that form the cytoskeleton. Well known functions of the microtubules include, cell transport and cell division in all eukaryotes (Nogales, 2003). During cell division, a large dynamic array of MTs, called the mitotic spindle, functions to physically segregate the chromosomes and to orient the plane of cleavage. In nondividing cells, MTs organize the cytoplasm, position the nucleus and organelles, and serve as the principal structural element of flagella and cilia (Desai and Mitchison, 2003). MTs are composed of repeating tubulin heterodimers and are present in all eukaryotes.

MTs are highly dynamic and can switch stochastically between growing and shrinking phases, both in vivo and in vitro. This nonequilibrium behavior is known as dynamic instability (Nogales, 2003). Possible functions of this instability include; allowing newly formed regions of cytoplasm to rapidly fill with MTs which, in turn, facilitate recruitment of membrane proteins through the MT transport system (Tanaka and Kirschner, 1991). The rapid remodeling of the MT mesh allows a more efficient three-dimensional exploration than equilibrium polymerization would permit, thereby enabling MTs to find specific target sites within the cell (Desai and Mitchison, 2003).

It has been shown that intracellular microtubules bear large-scale compressive loads from a variety of physiological forces (*i.e.* active viscoelastic

flow of the cytoplasm generates a slowly evolving stress field) that can cause both longitudinal compression and transverse shear stresses, depending on the details of the local stress field. Besides its intrinsic mechanical properties, MT resistance to compression is increased in vivo due to IFs reinforcement. In turn, the IFs ability to bend is reduced by the MT (Brangwynne et al., 2006).

Although polymers of the cytoskeleton are made of distinct subunits and differ in their properties, all those fibers are intricately linked together and interact specifically or nonspecifically with each other and other cellular components (Brangwynne et al., 2006). The resultant cytoskeletal organization ultimately plays an important role in transmitting compressive and tensile stresses and in sensing the mechanics of the microenvironment (Janmey and McCulloch, 2007). Interconnectivity creates continuous mechanical coupling through the cytoskeleton, which result in the distribution of internal and/or external forces throughout the cell.

One of the subjects studied in this thesis is the impact of a non rigid elastic substrate in cell mechanics. This is relevant because the live organisms, plants, animals and even bacteria are subject to a wide range of mechanical stress. Humans for example, due to their high mobility, have developed mechanisms to exert contractile forces that facilitate their displacement and limb motion. Other not controlled movements occur in the intestine and while breathing. At a microscopic level, it has been described that during inflammation, many immune system cells that normally move in the capillaries adhere to the walls and migrate towards the source of the inflammation. When adhered and before migration, shear stresses are applied on the cell surface due to the continuous movement of the blood in the clear of the capillary. While migrating, compressive loads that arise from their movement trough the small gaps that open between adjacent epithelial cells are exerted on the immune cells. Similarly, breathing and bone compression during movement are compressive and relaxation cycling processes that occurs all the time. The rhythmic beat of the heart is another example that shows the relevance of the mechanics of tissue. In muscle cells, very specialized structures called sarcomeres allow the movement of limbs and

application of large forces. In disease, it is now known that the cancer cell mechanics differ from normal in addition to other cell characteristics such as cell growth, morphology, cell–cell interaction, organization of cytoskeleton, and interactions with the extracellular matrix (Sokolov, 2007). Airway smooth muscle cells (AMSC) of asthmatic patients are more susceptible to contract when a stimulus appear (Jonas and Duschl, 2010; Shore, 2004).

In asthmatics, an increase in smooth-muscle mass is observed which in turn increases the contractile capacities of the airways. New findings show that the shortening velocities as well as the shortening capacities of ASMC of asthmatics are larger than that of cell from healthy people. mRNA expression and activity of myosin light-chain–kinase in the airway smooth muscle of patients with asthma was also determined and appears higher in asthmatic cells which could account for the increased velocity of shortening (Shore, 2004).

In dystrophin-deficient rat models, cultured myotubes were only one-fourth as stiff as normal cells (Pasternak et al., 1995). In osteoarthritis, cartilage chondrocytes display large viscoelastic moduli compared to cells from normal tissue (Farshid, 2000) and erythrocytes from patients with sickle cell disease (a type of anemia) are stiffer and more viscous than normal red blood cells (Nash et al., 1984). Thus, development of new approaches to reliable and fast measurement of the cell mechanics could potentially have an impact in diagnostics and the determination of the efficacy of therapeutics.

3.1 Methods to measure mechanical properties of cells

Several methods are used to study the mechanics of the cells. Optical tweezers have been used to test the mechanical properties of the filaments that form part of the cytoskeleton (see Figure 20; Footer et al., 2007, Liu and et al., 2005). However this method generally requires the isolation of individual filaments that are not part of a complete cell anymore. The technique relies in the optical trapping of a dielectric bead in a highly focused laser beam. The narrowest point of the focused beam contains a very strong electric field gradient. This tool can be used to measure small forces applied to the bead. For instance,

Simmons, (1993) have used an optical tweezers to measure or exert a force on single actin filaments. Beads were attached to rhodamine phalloidin labelled actin filaments and observed to move on a heavy meromyosin coated surface in the presence of ATP. The force needed to stop the movement of a trapped bead was assessed. Magnetic twisting cytometry (MTC) and glass needles can be used to test the mechanics of living cells but the first relies in the interaction between generally a type of integrin and its counterpart on the beads surface to promote adhesion (see Figure 20; Fabry et al., 2001). Thus, measured elastic properties are intrinsically related to the type of ligand or integrin at which the coated bead attached. In this case, a magnetic bead is dropped into the cell culture and twisting forces are applied by varying the direction of an external magnetic field. Viscoelastic properties of human ASMC have been measured with this technique by Fabry et al., 2001. In that study, they report that the stability of the cytoskeleton in closely linked to the so called effective noise temperature, a measured that arises from the fit of the measured viscoelastic properties at several frequencies to a power law.

Similar analysis performed by Smith et al., 2005confirmed this finding. However, a limitation of the MTC technique arises due to the fact that the location of the beads-cell contact is random and the collection of beads are distributed over the entire cell preventing measurements on specific sites on the cell or avoiding locations that are close to the edges where the cell thickness is small and contribution due to the substrate under the cell can lead to uncertainties. In addition, the beads are usually attached to focal adhesion points and thus directly interact with the cytoskeleton limiting measurements away from focal adhesion points. Generally speaking, these methods neither have control on the position of the bead-membrane contact resulting in beads that are distributed over the entire cell.

The glass needle technique, although it can be used to test the mechanics of the cells, does not allow to test the mechanics of the cells at very low force interactions and is thus only suitable for stiff cells.

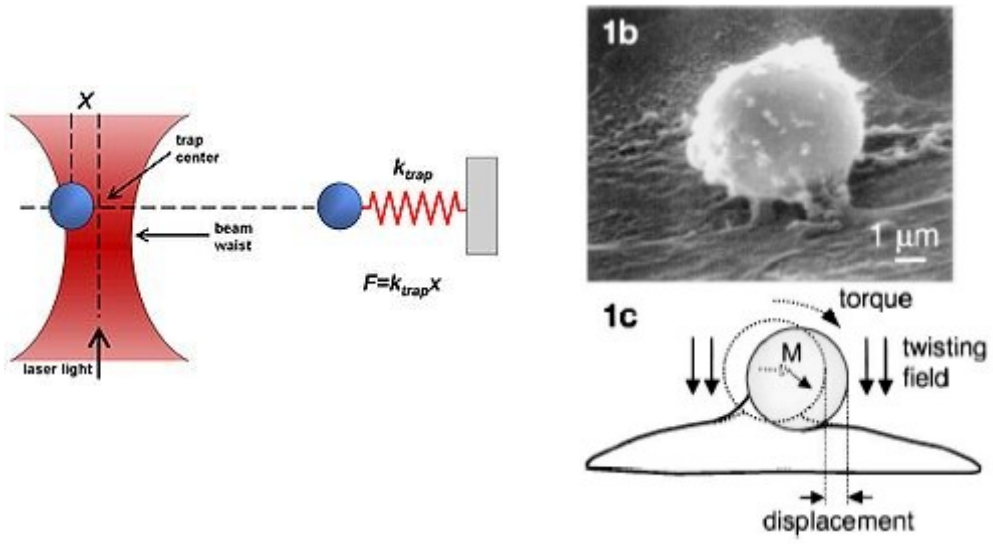

Figure 20: A bead trapped in the center of a laser beam. The force applied on the bead attached to molecule depends linearly on its displacement from the trap center (left image). Scanning electron microscopy of a ferrimagnetic bead that bind to the actin cytoskeleton of ASMC cells via integrins (upper right image). A magnetic field introduces a torque which causes the bead to rotate and to displace. M denotes the direction of the bead's magnetic moment (lower right image. Fabry et al., 2001).

Particle tracking is a technique where the movement of coated beads on the cell surface or beads engulfed by the cells is recorded. Information regarding the mechanical properties of the cytoskeleton by calculating the mean square displacement of the particle can be extracted. A review of this technique if found in Wirtz, 2009 paper.

3.2 Mechanical properties of cells.

After the introduction of the AFM (Binnig et al., 1986), the use of this tool has extended from the study of materials physics to a wide range of areas. Chemistry and biology have taken advantage of the capabilities of this technique and several studies on live or fixed cells have been performed over the past years. Mechanical properties of cell types such as fibroblasts (Rotsch et al., 1999) endothelial cells (Sato et al., 2000), astrocytes (Yamane et al., 2000) and other cell types have been investigated.

Force spectroscopy performed with the AFM is a technique that allows the testing of the mechanical properties of cells. Besides, this tool provides excellent control on the position of the cantilever-sample as well as allows the application of forces in the range of pN to several nN in a controlled fashion.

Investigations of some biological processes that include changes in deformability and adhesion of endothelial cells in contact with monocytes have been reported by Kataoka et al., 2002. A study of the mechanical response of endothelial cells to a shear flow was performed by Sato et al., (2000). In these experiments the cells were exposed for several hours to a shear flow at the end of which the AFM was used to asses changes in cell rigidity. A larger Young's modulus was found at the upstream side of the cells after 6 h exposure but this stiffness polarity disappeared after long exposure times.

Changes in stiffness during the cell cycle have been found (Dvorak and Nagao, 1998). In particular, a marked but transient decrease in stiffness occurs in the mitotic spindle region during anaphase.

Cell cytoskeleton observation by contact imaging AFM has been achieved in fixed cells (Hofmann et al., 1997) and samples consisting of inside-out orientated plasma membrane with overhanging cytoplasmic material (Santacroce et al., 2006). Those studies showed that the length and thickness of filaments vary in the same cells and that the thinnest fibres have a height of 7 nm, which is in good agreement with the diameter of a single actin microfilament measured for isolated actin fibers.

Measurements of the stiffness of smooth muscle cells in response to contractile agonist were published in 2005 by Smith et al., (2005). In those experiments, and highly relevant to our experiments, it was shown that inhibition of myosin with 1-(5-iodonaphthalene-1-sulfonyl)-1H-hexahydro-1,4-diazepine hydrochloride (ML-7) as well as treatment of cell cultures with cytochalasin-D (it induces actin depolymerization) cause a decrease in cell stiffness. These results indicate that the cortical actin has an important role in the cellular mechanics

The aim of this thesis is to demonstrate that force spectroscopy as well as manipulation modes of AFM, in combination with other techniques, can be a

powerful new tool that can help to understand biological systems. We demonstrate that AFM can be used to measure mechanical properties of cells and substrates and can be used in novel ways using manipulation modes to study biological interactions. Comprehensively answering biological questions is beyond the scope of this thesis, but it will (and already has) stimulated the use of these techniques to answer interesting, fundamental questions in biology (Meakins Christie Chest Hospital, lab of James Martin; Montreal Neurological Institute, labs of David Colman and Timothy Kennedy).

4 Material and Methods (Airway Smooth Muscle Cells)

4.1 Experimental Setup (Temperature and pH control).

Heated stage. When performing experiments on cell cultures, two important conditions have to be observed in order to keep cells alive and in good condition; the temperature must match the temperature of the organism from which the cells were obtained (37 C for mammals) and the pH of the culture medium must be buffered to physiological pH (*i.e.* close to neutral). Cell culture incubators are typically used to meet these two requirements.

However, during AFM measurements, the cell cultures are taken out of the incubator. Without proper control of temperature and pH, the cells can easily be harmed. In many cases, due to the nature of the measurements, the culture dishes should be kept outside for prolonged periods of time (the dishes were kept three or even four hours outside the incubator when measuring recruitment times of the presynaptic proteins, see section 6). To avoid the damaging effects of changes in temperature and pH to the cell cultures, both conditions were controlled in the Bioscope AFM as described below.

A heated stage (Micro-Incubator chamber, model DH-35i, Warner Instruments, Inc., Hamden, CT) connected to a temperature controller (model, TC-344B, Warner Instruments, Inc., Hamden, CT) was employed to keep the temperature of the cellular cultures at 37 C throughout the experimental procedure. Bottom glass petri dishes (MatTek Corp., Ashland, Massachusetts; 35 mm diameter) were positioned and secured to the heated stage. The range for temperature control that can be achieved with the setup goes from room temperature to 50 C.

Heat transfer in this stage is achieved by thermal conduction. A metallic ring is put around the 35 mm diameter bottom glass Petri dishes. This metallic ring is heated to the set temperature. Thermal equilibrium between the ring and the medium in the dish is reached after a few minutes. Two thermistors keep track of the temperature; the first reads the temperature at the metallic ring while

the second can be positioned inside the liquid medium. Since the AFM cantilever holder is always occupying a significant part of the space inside the Petri dish, reading of the temperature of the culture medium at all times is limited. However, to ensure that the temperature of the culture medium was optimal for live cells (37 C), one temperature sensor was placed at the bottom-center of a Petri dish filled with culture medium and the readings of the in-liquid sensor and the metallic ring temperature sensor were recorded. In order to get 37 C at the center of the Petri dish, the metallic ring must be heated up to 38 C by fine tuning of the electrical power (*i.e.* adjusting the voltage) applied to the heating elements. Thus, the temperature of the metallic ring was used as an indication of the temperature reached at the center of the dish during the experimental procedure.

pH control. There are generally two ways to keep pH constant in a cell culture; by using bicarbonate buffers or by using 4-(2-hydroxyethyl)-1-piperazineethanesulfonic acid (HEPES). The first method requires a constant supply of CO_2 and is commonly used in biological incubation systems. This method relies on the diffusion of carbon dioxide (CO_2) into the culture medium through the liquid-gas interface. The diffused CO_2 combines with the water molecules in the medium to form carbonic acid (H_2CO_3), which in turn dissociates to form bicarbonate (HCO_3^-) and hydrogen ion (H^+) lowering the pH of the medium to values where cells can survive.

$$CO_2 + H_2O \leftrightarrow H_2CO_3 \leftrightarrow HCO_3^- + H^+$$

Additional slow acidification of the medium due to excretion of byproducts produced by the cell in the culture is thus counterbalanced by the buffering capacity (moles of acid or base added in buffers solution / change in solution's pH) of the CO_2/H_2CO_3 system.

Although the HEPES system has an good buffering capacity at neutral pH (where cells grow better), its use was avoided in this thesis due to reports that link the utilization of HEPES to the formation of cytotoxic products within 30 min after exposure to light (Zigler et al., 1985). Experiments where illumination was used to observe fluorescently tagged cellular structures would increase this cytotoxic effect.

In order to keep cells alive outside the incubator during significant periods of time (hours), a plastic box that covers the cell culture and isolates it from the surroundings was designed and made-up in the machine shop facilities of the Physics Department (see Figure 3). Basically, the box can be regarded as a customized incubator. 5% CO_2 gas is injected continuously by means of a needle introduced through a rubber sheet that seals the upper part of the box. A hole made in the rubber sheet that tightly fits to the skirt that protects the electronics in the base of the AFM piezo tube allows the access of the cantilever to the cells plated on the Petri dish. A piece of moist tissue is placed inside the box to reduce the rate of evaporation of the culture medium.

4.2 Cell isolation and cultures for the AFM experiments.

Tracheal smooth muscle cells of Brown Norway rats (Harlan Sprague Dawley, Wallkerville, MD, USA) were isolated and cultured as previously described by Tolloczko et al., 1995. Briefly, the cells were enzymatically dissociated with 0.05% elastase type IV and 0.2% collagenase type IV and cultured in 1:1 Dulbecco's modified Eagle's medium -Ham's F12 medium (DMEM-F12) supplemented with 10% fetal bovine serum (FBS), 0.224% NaHCO3 and 100 U/ml penicillin, 100 µg/ml streptomycin and 25 µg/ml amphotericin in a 5% CO2 incubator. Cell culture reagents were purchased from Invitrogen (Canada Inc., Burlington, Ontario).

For AFM experiments, cell in the first or second passage were plated in bottom glass culture dishes (MatTek Corp., Ashland, Massachusetts), let grow until 60 – 70 % confluence was achieved and starved for 24 hours prior to experiments in DMEM medium with 0.5% FBS. This assured that the cells were always in the same phase of the cell cycle when the measurements were performed. This level of confluence allowed a reliable discrimination of the nucleus and cell borders. On the day of experiments, the culture dishes were mounted on the microscope heated stage with ~1.5 ml of medium. The home made CO_2 box was placed around the culture dish and 5% CO_2 was injected continuously to keep the pH of the medium neutral. The temperature of the

culture was kept at 37 C by mean of the heated stage (DH-35iL, Warner Instruments, 1125 Dixwell Avenue, Hamden, CT). A moist tissue placed inside the box helped to maintain humidity and prevented evaporation of the medium.

Usually, the plates were prepared such that we had at least three cell cultures, each one with a different substrate ready on the day of the AFM measurement. Experiments were performed only ~30 min after the cell culture was placed on the stage to give time for the cantilever stabilization (this was necessary to avoid the bending of the cantilever due to the bimetallic effect; see introduction). This allowed for a maximum of three cells (although usually two cells) to be measured per dish due to the time it takes to perform these experiments.

4.3 Cell localization and methodology to identify the area to indent.

The combination of the AFM with the inverted optical microscope allows a precise positioning (few micrometers using low magnification objectives and ~1 μm or less for high magnification objectives) of the cantilever relative to the cell. We took advantage of this attribute of the set up to perform the measurements that let us determine the mechanical properties of the cells. The steps described below were followed:

1. Turn on the heated stage, mount the dish in the microscope stage and position the AFM head above the culture dish, ready for the experiments. Inject 5 % CO_2 into the box that enclosed the cell culture.
2. Let the system stabilize for at least 30 min.
3. Localize a cell in the culture with the nucleus and the cell edge clearly visible. This step was the most challenging of all since the nucleus is not all the time clearly visible and the angle at which the dish is illuminated from above has to be adjusted a few times before a clear image is obtained. For future experiments, it is recommended to use a phase contrast microscope which produce images more suited for nuclear localization.

4. Localize a region between the cell nucleus and the cell edge.
5. Align the site to indent to the center of the bead. This was achieved by first focusing on the cells and situate the mouse pointer on the computer screen at the position to indent. Then, the bead was focused and moved laterally until its center was positioned on the pointer tip.
6. Approach of the cantilever to the cell followed and the measurements performed.

The completion of these steps allows us to systematically measure the mechanical properties of the cells only on regions that lie between the nucleus and the cell edge. The use of spherical beads for the experiments was chose over conical tips even though the mechanical properties of the cells could in principle be measured directly with such sharper tips. We thus, however, avoid the potential of a sharp end of a conical tips to potentially disrupting the cell membrane or cell interior structures.

4.4 Polyacrylamide gel preparation.

Polyacrylamide sheets can be directly prepared on glass surfaces. However, those sheets detach easily from the glass. A procedure to adhere the gels to the glass needed to be found. To achieve that, we implemented a method previously described by Wang and Pelham, (1998) where polyacrylamide sheets are covalently attached to an activated glass substrate.

Glass activation. Gels with three different mechanical properties were prepared. Briefly, a small amount of 0.1 N NaOH was pipetted on the glass surface of 35 mm diameter bottom glass Petri dishes (MatTek Corp., Ashland, Massachusetts) and let dry. Covalent binding of the linker to the glass was achieved by depositing 200 µl of 3-aminopropyltrimethoxysilane in the bottom of glass dishes followed by a 5 min incubation time. Distilled water was added after incubation and the dishes were agitated for 10 min. Finally, the dishes were rinsed several times with distilled water and activation of the covalently bound silane molecules was accomplished after 30 min incubation with 0.5% glutaraldehyde in PBS solution.

Gel Preparation. Solutions of 10% Acrylamide-0.03% Bisacrylamide, 10% Acrylamide-0.26% Bisacrylamide and 20% Acrylamide-0.5% Bisacrylamide were prepared in distilled water. In all three cases, polymerization was initiated by adding 1/200 volume of 10% ammonium persulfate (10% APS) and 1/2000 volume of N,N,N',N'-Tetramethylethylenediamine (TEMED). 15µl of the mixture was pipetted into the activated glass and covered with a coverslip pretreated with dichlorodimethylsilane (Acros Organics; Geel, Belgium) to facilitate its later removal. Prior to gel functionalization, the substrates were rinsed several times with 50 mM HEPES. The reagents used for the glass activation as well as gel preparation (excluding dichlorodimethylsilane) were purchased from Sigma-Aldrich Canada Ltd., Oakville, Ontario.

4.5 Gel functionalization.

It has been shown in this and other studies (Paszek et al., 2005; Discher et al., 2009) that bare polyacrylamide gels have a reduced capacity to promote cell adhesion. Functionalization of gels with molecules that promote adhesion is thus necessary. Besides promoting adherence to the substrate, functionalization also provides an environment that resembles to some extent the presence of intercellular proteins (extracellular matrix proteins) in tissues. Particularly, smooth muscle cells secrete extracellular matrix proteins into the intercellular spaces that serve as support, provide an adhesive surface and could be involved in cell signalization and transduction of mechanical forces among cells (Ingber, 2002; Chiquet, 1999; Chiquet et al., 2003).

Polyacrylamide functionalization was performed according to the procedure described in Wang and Pelham, 1998. 1 mM Sulfo-SANPAH (Thermo Scientific, Nepean, Ontario) prepared in 50 mM HEPES (preparation performed in darkness due to the photosensitivity of Sulfo-SANPAH) was pipetted onto the polyacrylamide gel. The surface was exposed for 6 min to the 30W germicidal lamp (UV light) of a culture hood. Care was taken to place a thin layer of the solution on the gel surface and distribute it evenly. Large amounts of solution resulted in poor functionalization. Elimination of the darkened solution, addition of

new 1mM sulfo-SANPAH solution and a new exposure to UV light followed. Unbound sulfo-SANPAH was removed by adding 50 mM HEPES to the dish and placing it in a shaker for 15 min. The step was repeated until the red residues of unbound sulfo-SANPAH disappeared.

Fibronectin from human plasma (Sigma-Aldrich Canada Ltd., Oakville, Ontario) was employed for gel as well as glass functionalization but concentrations of the fibronectin solution used for functionalization varied among the different substrates. For the 10% Acrylamide-0.03% Bisacrylamide gel, 70 µg/ml of fibronectin diluted in PBS was used; for the 10% Acrylamide-0.26% Bisacrylamide gels, the concentration was 8 µg/ml, for 20% Acrylamide-0.5% Bisacrylamide gels, the fibronectin concentration was 6 µg/ml and for glass functionalization, the concentration used was 4µg/ml. The dishes were incubated in a shaker overnight at room temperature.

Unbound fibronectin was removed by aspiration and washed with PBS. UV irradiation for 20 min under the germicidal lamp of a sterile hood assured the elimination of any bacteria or fungi in the substrate. Before sterilization, a thin layer of sterile water was placed onto the substrate to prevent gel drying. Dehydration of the polyacrylamide sheet can result in gel shrinking and detachment.

1.5 ml of DMEM supplemented with 10% FBS was deposited in the Petri dishes and incubated for at least 30 min before cell plating. This step permitted the absorption of the medium into the gel.

4.6 Gel characterization.

Protein content. Content of fibronectin bound to the functionalized gels as well as glass coverslips was quantified with a modified Enzyme-linked immunosorbent assay (ELISA, Ma et al., 2010). First, the functionalized surfaces as well as controls (no functionalized gels and glass plates) were covered with 1 ml of blocking buffer (3% bovine serum albumin in PBS) for 2 h at room temperature. Albumin blocks the remaining sites where fibronectin is not bound. The dishes were subsequently washed three times with PBS. Anti-Fibronectin

antibody produced in rabbit (Sigma-Aldrich Canada Ltd., Oakville, Ontario) was diluted 1:5000 in blocking buffer, added to the dishes and incubated for 2 h at room temperature. Unbound antibodies were removed rinsing three times the dishes with PBS. The secondary antibody used was the goat anti-rabbit IgG–FITC antibody (Sigma-Aldrich Canada Ltd., Oakville, Ontario) and was diluted 1:320 in blocking buffer. The antibody was added to each dish and then incubated for 2 h at room temperature. The dishes were subsequently positioned on the microscope stage and the FITC dye was excited (excitation wavelength, 495 nm) with an HBO 50 W mercury lamp and proper filters. The emission signal (wavelength pick at 521 nm) was collected with a 60x oil immersion objective and images of the sample acquired with a CCD camera (Cascade:1k camera, Photometrics; Tucson, AZ) mounted in an inverse optical microscope (Axiovert S100 TV, Carl Zeiss Canada Ltd., Toronto, Ontario). The images collected were later subject to fluorescence intensity analysis using the public domain NIH Image program (developed at the U.S. National Institutes of Health and available on the Internet at http://rsb.info.nih.gov/nih-image/). Bare substrates (no fibronectin) were used as controls for all experiments performed to determine protein content.

Gel stiffness. Measurement of the gel elasticity was performed with the AFM (for details refer to section Force volume) on at least four places on the gels. Triangular cantilevers (C-triangular Microlever; Veeco) with spring constant of 0.01 N/m and 4.5 μm diameter polystyrene beads (Polysciences Inc., Warrington, PA) glued to the cantilever tip were used. Maximum loads of 0.4 nN were applied in order to get the force-distance curves employed to calculate the Young's modulus of the gels.

4.7 Proliferation assay.

To examine the effect of the matrix stiffness on the proliferation rate, airway smooth muscle cells from Brown Norway rat were seeded in both polyacrylamide gels and glass functionalized with fibronectin. Cells plated did not exceed the fifth passage on DB Falcon^{TM} cell culture flasks (BD Biosciences;

Mississauga, Ontario) in all the cases. Cells cultures were incubated at 37 C and 5% CO_2 with complete DMEM medium until 60 – 70 % confluence was reached. Subsequently, cell cultures were starved in 0.5% FBS medium for 24 hours to assure that the cells were in the same phase of the cell cycle at the beginning of the proliferation assay.

One day prior to the assay, the starvation medium was removed and substituted with 10% or 0.5% FBS culture medium. Six hours after the medium exchange, bromodeoxyuridine (BrdU; BD Pharmingen, 550891) diluted in DPBS (Gibco) was added to the cultures at a final concentration of 10 μM. The cultures were incubated another 18 h to permit the BrdU to incorporate into newly synthesized DNA strands.

Prior to cell harvesting, the cells were washed three times with HBSS to eliminate cellular debris or floating dead cells from the dish. The remaining cells adhered to the polyacrylamide gel were then detached with 0.5 ml of 0.25% trypsin. After inactivation of trypsin with 2 ml of 10% FBS medium, the cell suspension was transferred to Falcon tubes (BD Biosciences) and spun at 1400 rpm in a refrigerated centrifuge (4 C). The supernatant was removed and 1 ml of staining buffer (1X PBS, 3% FBS, 0.09% sodium azide) was added to the remaining pellet followed by brief vortexing and spinning. Cells were permeabilized with 100 μl of cytofix/cytoperm for 20 min on ice and washed with Perm/wash buffer. Remaining traces of cytofix/cytoperm were eliminated with 1 ml of staining buffer. The cell pellet was then stored in freezing medium (10% DMSO, 90% heat inactivated FBS) at -80 C.

To prepare the cells for the cytometer reading, the cells were once more permeabilized with 100 ul of Cytofix/Cytoperm for 5 min at room temperature, washed with Perm/Wash buffer and re-suspended in 100 μl of DNase. Cell suspension was incubated for 1 h at 37 C followed by addition of 1 ml of Perm/Wash buffer and spinning.

Anti-BrdU antibody diluted in Perm/Washer buffer was mixed with the cell pellet and incubated for 30 min at room temperature. The Anti-BrdU antibody solution was then eliminated by adding 1 ml of Perm/Wash buffer. For

fluorescence-activated cell sorting (FACS), the cell pellet was diluted in 0.5 ml of staining buffer.

Cells were analyzed by FACScan (Beckman counter) with MultiCycle for Windows software (Beckman counter) for detailed cell cycle status. The percentage of proliferative cells in each condition was determined.

4.8 RNA extraction protocol.

Airway smooth muscle cells were cultured on polyacrylamide gels coated with fibronectin. At 60 -70 % confluence, the cell cultures were starved in 0.5% FBS medium for 24 hours to assure that the cells were in the same phase of the cell cycle at the time of RNA extraction. On the day of the experiment, the culture medium was removed from each dish. Cells were washed with PBS twice and the RNeasy Mini kit® (QIAGEN) was used to extract RNA following the manufactures protocols.

Briefly, cells were disrupted with 350 µl of RLT buffer plus 5% beta-mercaptoethanol. Cell lysate was mixed by pipetting and transferred to QIAshredder spin column placed in 2 ml collection tube and centrifuged in order to homogenize. One volume of 70% ethanol was added to the homogenized lysate and the mixture was transferred to RNeasy spin column placed in 2 ml collection tube. The tubes were centrifuged for 15 s at 8000 x g. 700 µl of RW1 buffer was added to the RNeasy spin column and then centrifuged 15 s at 8000 x g. The RNeasy spin column was then washed with 500 µl of RPE buffer twice, centrifuged for 2 min at 8000 x g and transferred to another collection tube. The RNA was eluted by adding 30 µl of RNase-free water directly to the spin column membrane and centrifuged for 1 min at 8000 x g.

The total RNA was quantified with a NanoDrop (Thermo Fisher Scientific Inc. 81 Wyman Street Waltham, MA) and integrity was verified in an Experion machine (Bio-Rad, 1000 Alfred Nobel Drive Hercules, CA). The extracted total RNA was sent to the Génome Québec Innovation Centre at McGill University for gene expression assay exploiting Illumina array based technologies.

4.9 Immunofluorescence.

Cell cultures were cultured in DMEM supplemented with 10% FBS until ~ 60 -70 % confluence was reached. Then, the cell cultures were starved in 0.5% FBS medium for 24 hours to assure that the cells were in the same phase of the cell cycle. Cell fixation was performed with 3.7% paraformaldehyde diluted in PBS. Adherent cells were permeabilized with 0.1% saponin in PBS for 15 min followed by the addition of blocking buffer (5% milk, 0.1% saponin in PBS). The cultures were incubated 30 min and then the cells were labeled with FITC-phallodin (33.3 µg/ml) diluted in PBS plus 0.1% saponin for 1 h. Prior to the imaging procedure, the cultures were washed four times with PBS to remove the excess of dye. An HBO 50 W mercury lamp and proper filters were used to excite the FITC dye (excitation wavelength, 495 nm) and the emission signal (wavelength pick at 521 nm) was collected with a CCD camera (Cascade:1k camera, Photometrics; Tucson, AZ) mounted on an inverted optical microscope (Axiovert S100 TV, Carl Zeiss Canada Ltd., Toronto, Ontario).

4.10 Analysis of the data

Young's modulus and complex modulus

Due to the large number of data sets, in particular when analyzing force-distance curves collected in the Force-Volume mode of operation (~ 750 force-distance curves are taken at several positions above the polyacrylamide gels), MatLab programming routines were implemented and employed to fit the curves to the Hertz model and calculate the corresponding Young's Modulus (see code in the Appendix). Details of the procedure to calculate the mechanical properties can be found in the section Hertz model and Indentation modulation.

For the calculation of the complex modulus, the lock-in output data was visualized using the WinWCP version 4.1.5 software (http://spider.science.strath.ac.uk/sipbs/showPage.php?page=software_winWCP). Averaging of the last 5 s of the curves (see Figure 18) was performed and the data exported to Microcal OriginPro, version 6, where the calculation of the Complex modulus was completed.

Images and Gene Array data

All images taken with the optical microscope, either bright field or fluorescent images, were processed with the Image J software (NIH, http:// rsbweb.nih.gov/ij/index.html) when needed. FlexArray software (Genome Quebec) was used to normalize the gene array row data and to perform further the analysis such as one-way analysis of variance (ANOVA).

5 Application of force spectroscopy to Airway Smooth Muscle Cells (Results)

5.1 Gel functionalization and its mechanical properties

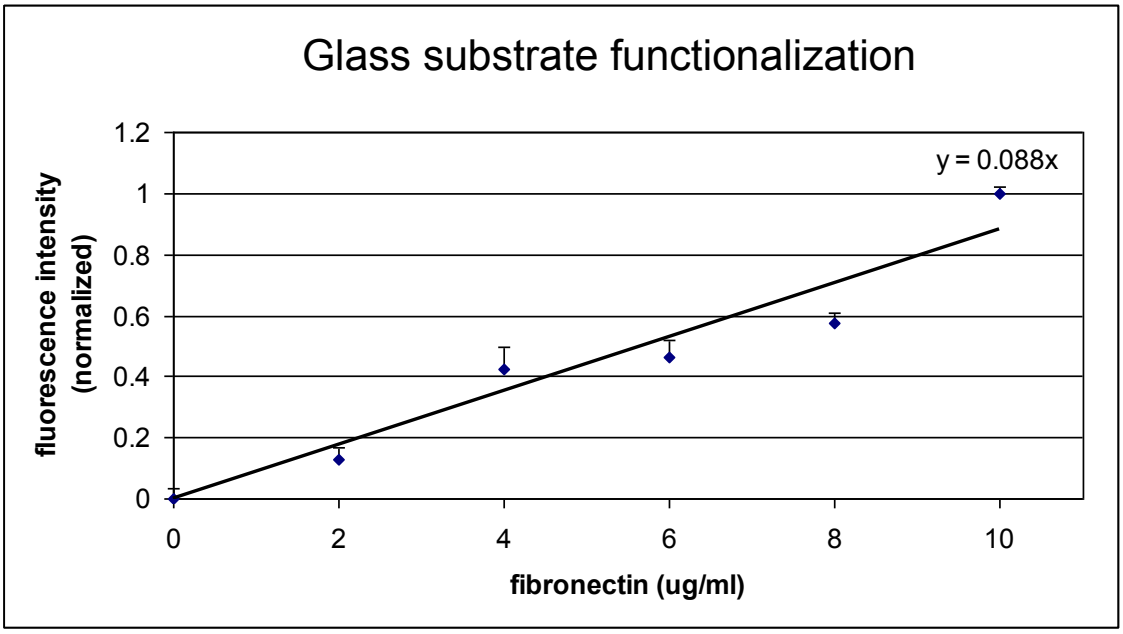

Figure 21: Glass substrate functionalization. Glass bottom Petri dishes were coated with a layer of fibronectin by passive absorption. Fibronectin diluted in PBS at final concentrations 10 µg/ml, 8 µg/ml, 6 µg/ml, 4 µg/ml, 2 µg/ml and 0 µg/ml was added to glass bottom Petri dishes and incubated overnight at room temperature. The amount of fibronectin deposited on the glass was quantified by fluorescence intensity (refer to material and methods for details) and normalized with the fluorescence intensity measured at 10 µg/ml.

Polyacrylamide substrates are highly inert and lack the capacity to promote cell adhesion. Surface functionalization was necessary in order to achieve cell adhesion and cell growth. Functionalization of the polyacrylamide gels was attempted at first by passive absorption using fibronectin diluted in PBS. Overnight incubation at room temperature did not result in fibronectin deposition on any of the polyacrylamide gels. However, functionalization of glass substrates by passive absorption did produce surfaces coated with a thin layer of fibronectin. Fibronectin functionalization of gels was only possible after pre-

treatment of polyacrylamide sheets with the crosslinker sulfo-SANPAH which binds covalently to the gel by one extreme while the other extreme reacts with the amino groups (*i.e.* lysine) present in the proteins.

Assessment of the relative content of fibronectin in all the substrates was achieved by sandwich Enzyme-linked immunosorbent assay (ELISA). Fluorescence intensity of Anti-Rabbit IgG-FITC antibody bound to anti-fibronectin antibodies was measured and the fluorescent intensity of the glass functionalized with a solution of fibronectin (see Figure 21) at an initial concentration of 10 μg/ml was employed to normalize the data.

Comparison of the fluorescence intensity measurements of the functionalized gels vs. functionalized glass showed that functionalization of glass was more efficient than any of the polyacrylamide gels functionalized. Adjustments in the concentration of fibronectin solution used for gels functionalization were necessary. Measurements showed that for the 10% acrylamide-0.03% bisacrylamide gel, the concentration of the fibronectin solution was 70 μg/ml; for the 10% acrylamide-0.26% bisacrylamide gel, the concentration was 8 μg/ml and for the 20% acrylamide-0.50% bisacrylamide gel the concentration was 6 μg/ml. In all the cases, the fluorescence intensity measured in the three gels was equivalent to that measured on glass functionalized with a 5 μg/ml fibronectin solution.

Confocal microscopy performed on polyacrylamide gels showed that fluorescent antibodies do not penetrate the matrix bulk and remain bound to fibronectin molecules covalently linked to the gel surface (see Figure 22). This assured that the determination of the fibronectin content on the gels by ELISA only accounts for the protein located on the gel surface. Only the superficial fibronectin layer promotes cellular adhesion. Seeding of smooth muscle cells on the functionalized substrates confirmed that the amount of fibronectin covering the surfaces was appropriate to support cell adhesion.

Following functionalization, the mechanical properties of the gels were tested by performing AFM spectroscopy on three different 100 μm x 100 μm square areas on the polyacrylamide gels. The Force-Volume imaging technique

was employed to collect 256 force distance curves over a single area for a particular substrate. A total of ~ 3,800 curves were taken in a 5 day period for each substrate but only the curves that complied the conditions stated in section 2.5.2, Figure 14 and Figure 15 were included to calculate the Young's modulus. The conditions in which the gels were stored during the 5 day period were the same at which the cell cultures were kept, to say, in an incubator at 37 C and submerged in complete DMEM medium. The array of force-distance curves obtained was then used to calculate the Young's Modulus (refer to section 2.5.2 for details about the calculations) which was averaged per day and per substrate (see Figure 23). No difference in elasticity was noticeable between functionalized and no-functionalized gels prepared with the same concentrations of acrylamide/BIS-acrylamide.

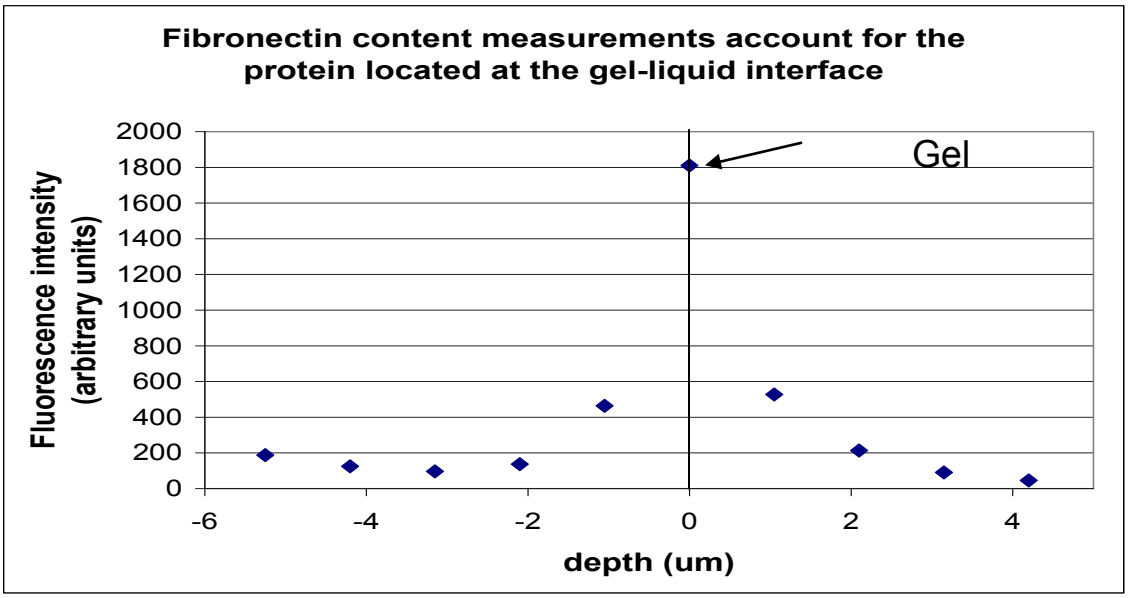

Figure 22: Fibronectin content measurements account only for the protein located at the gel-liquid interface as demonstrated with Confocal microscopy imaging. Fluorescence measurements at several planes within the gel (negative values at the "x" axis), at the gel-liquid interface (0 um at the "x" axes) and above the gel (positive values at the "x" axis) showed a sharp peak at the gel surface.

On average, the elastic properties of the gels were from soft to hard matrix: 900 ± 200 Pa, 3,700 ± 300Pa, 6,300 ± 500 Pa. The Young's modulus of glass computed using the same methodology was 240,000 ± 30,000Pa (see

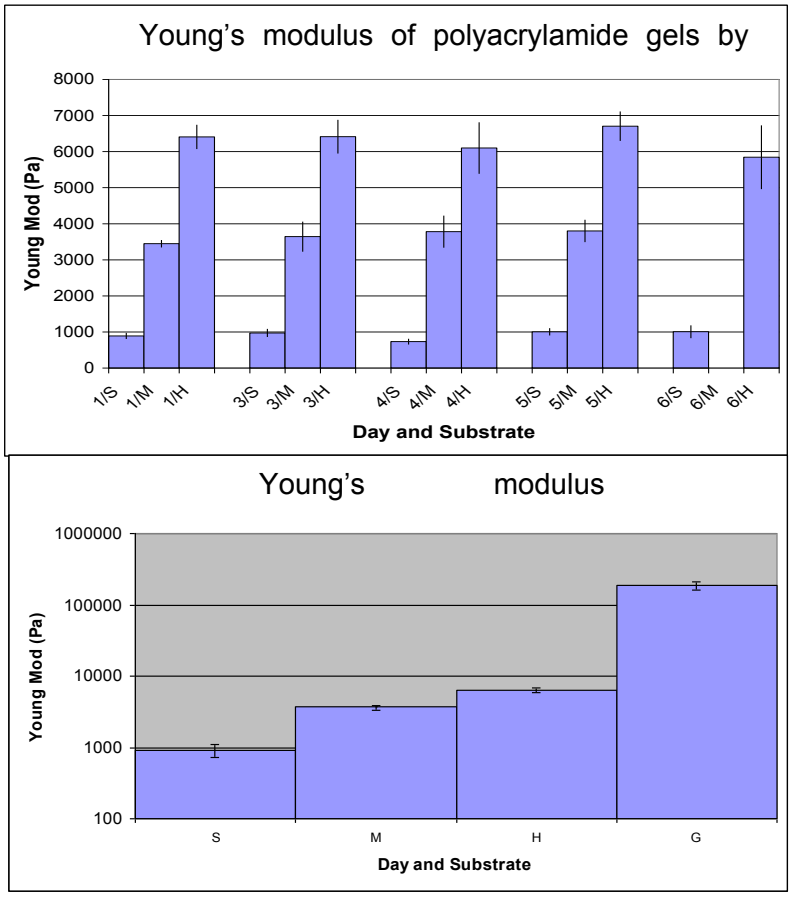

Figure 23: Young's modulus of polyacrylamide gels determined by fitting equation 8 to the force distance curves taken on the polyacrylamide gels. Upper panel: The Atomic Force Microscope force-volume method was employed to measure the Young's Modulus of the gels. No significant differences were observed after six days. The number before the slash character in "x" represents the day at which the measurements was done while the letter after the slash denote the polyacrylamide gel measured. Each data point is the average of more than 800 measurements, the error bar is the standard deviation. Lower panel: The Young's modulus of very stiff materials (such as glass and polystyrene) becomes inaccurate do to the high sensitivity of the Hertz model to small variations in the indentation depth (for details refer to section 0 in the text). However, the model can be used to calculate the Young's modulus of softer materials (*i. e.* polyacrylamide gels; larger indentations) since the determination of the Young's modulus is less affected by the changes in the indentation depth and do not have the limitation that arises due to the use of an indenter softer than the material to measure. S ('soft') stands for 10% acrylamide 0.03% bisacrylamide, M ('medium') stands for 10% acrylamide 0.26% bisacrylamide, H ('hard') stands for 20% acrylamide 0.50% bisacrylamide and G stands for glass.

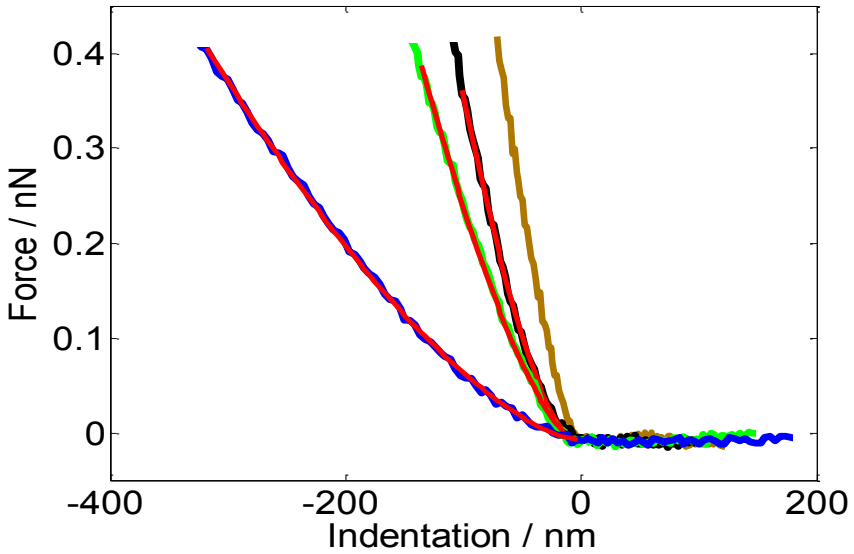

Figure 24: Representative force-distance curves taken on glass (brown), stiff (black), medium stiffness (green) and soft (blue) polyacrylamide gels. The red lines represent Hertzian fits to the data. The softer the substrate, the larger indentation for a given force.

Substrate	**10% acylamide, 0.03% BIS-acrylamide**	**10% acylamide, 0.26% BIS-acrylamide**	**20% acylamide, 0.50% BIS-acrylamide**
Short name	10T-0.03C	10T-0.26C	20T-0.50C
Elasticity (Pa)	900 ± 200	3700 ± 300	6300 ± 500

Table 1: The table shows the elasticity of polyacrylamide gels prepared with three concentrations of polymer and cross-linker as well as glass

Figure 24 for representative force-distance curves taken on all the substrates and used to compute the Young's modulus. For the procedure to find the best fit using equation 8 see Figure 14, Figure 15 and text below). It is obvious that the measured value of the Young's modulus of glass is significantly lower than that reported in the literature (~ 70 GPa, Poisson ratio 0.24; Makishima and Mackenzie, 1973; Makishima and Mackenzie, 1975). We explore the origin of this inconsistency in section 2.5.2 .

5.2 Sources of uncertainty and applicability of the Hertz model to determine the Young's modulus of substrates.

The smaller measured value for *E* of 0.24 ± 0.03 GPa as compared to the accepted literature value of several 70 GPa for glass is due to two main reasons. First, the Hertz model assumes that when two bodies are in contact, one of them has to be rigid and non-deformable. The measured Young's modulus then correspond to that of the deformable material. Since our measurements are performed by pressing a polystyrene bead attached to the AFM cantilever to the glass substrate (polystyrene being softer than glass), it is a reasonable assumption that the measured value might correspond to the Young's modulus of the bead instead of the glass plate (rigid material). The value reported in the literature for polystyrene is between 2 - 4 GPa (Lubarsky et al., 2004; Miyake et al., 2006; Brighton, 1979). Our measurements of 0.24 GPa is still an order of magnitude smaller. To understand the origin of this difference, we should refer to section 2.5.2 and to equation 10 used to compute the Young's modulus and fit the force-distance curves. In the section, one can find an overview of the impact of the precision to determine the contact point in *E* and study the influence of the indentation deep in substrates with different stiffnesses.

For instance, indentation depths for gels are from ~ 70 nm to ~ 300 nm depending of the acrylamide and bisacrylamide concentrations. Thus, if we take the equation 11 in section 2.5.2, we can estimate that for a $\Delta\delta$ = 15 nm and indentation of the order of 70 nm (typical for the hard gels), $\Delta\delta/\delta$ gives a 30 % relative error on $\Delta E/E$. Smaller indentations of the order of 40 nm or lower (*i. e.*

for glass substrates) and uncertainties in the determination of the contact point of 10 nm produce relative errors in ΔE/E of the order of 40 %. However, for the large indentations observed on the softer gels (δ = 300 nm) and with Δδ = 20 nm, Δδ/δ gives a 10 % relative error on ΔE/E. This analysis demonstrates that the consequence of how precise the contact point can be determined is less dramatic for soft materials where indentations are large. The above result also imply that the Young's modulus of the soft and medium stiffness gels reported above are the most reliable while the modulus calculated for the hard gel and glass are less reliable due to systematic errors in contact point determination. This is confirmed when the modulus *E* measured and calculated here is compared to the values reported in the literature for glass or polystyrene.

Note that a further possible explanation for the discrepancy for the polystyrene value is the fact that as we used very small indentation depths the swelled surface layer of polystyrene might be softer than the bulk value reported in the literature. Due to the systematic error in *E* as a result of the contact point determination uncertainty in the present experiments this hypothesis cannot be experimentally tested in the current set-up. Polysterene surfaces are however known to change and age; polysterene spheres stored for extended periods of time look very 'fuzzy' in SEM images, in contrast to freshly acquired and imaged samples.

Other sources of systematic error than would mainly affect the determination of Young's modulus of hard substrates such as glass include the cantilever bending due to its movement in liquid. The $\delta^{-3/2}$ part of equation 10 predicts that small measurement errors due to fluid-induced cantilever bending (*i.e.* drag) in the determination of the indentations δ are not significant for large indentations. For small indents in stiff substrates this can however become a major source of systematic error. One would need to perform a careful systematic study of cantilever drag not only in liquids, but also close to surfaces.

5.3 Cell morphology on gels and actin network.

During the course of the experiments, it was apparent that the shape and size of the cells varied depending on the stiffness of the underlying substrate. In general terms, rounded and small cells thrive on the softer gel (10T-0.03C) while extended and larger cells thrive on the medium (10T-0.26C) and high (20T-0.50C) stiffness polyacrylamide sheets as well as on glass substrates (see Figure 25). In all cases, the substrates were functionalized with fibronectin as described above.

The area of cells was determined by applying an appropriate intensity threshold. This was performed for ~ 30 cells for each substrate. The measurement of the cell area and the cell perimeter were performed with the Image J software (NIH, http:// rsbweb.nih.gov/ij/index.html). Note that as described in the methods section these cells were all in an arrested state of development, having been starved for 24 hours.

Fitting the area of cells to a Poisson distribution produced a maximum likelihood estimate for cell area on the soft, medium, hard and glass substrates of 1130 μm^2, 2060 μm^2, 2450 μm^2, 2105 μm^2 with 1120 – 1140 μm^2, 2045 – 2075 μm^2, 2430 – 2465 μm^2, 2090 - 2120 μm^2 95 % confidence intervals respectively (see Table 2). Histograms in Figure 26 show a broad distribution of the area covered by cells within the same type of substrate.

	Maximum likelihood estimate of area [$\mu m^{2]}$	95 % confidence interval [$\mu m^{2]}$
Soft gels	1130	1120 – 1140
Medium	2060	2045 – 2075
Hard	2450	2430 – 2465
Glass	2105	2090 - 2120

Table 2: Maximum likelihood of the area for cells cultured on the four substrates computed from a Poisson distribution of the areas (~ 30 cells per substrate) .

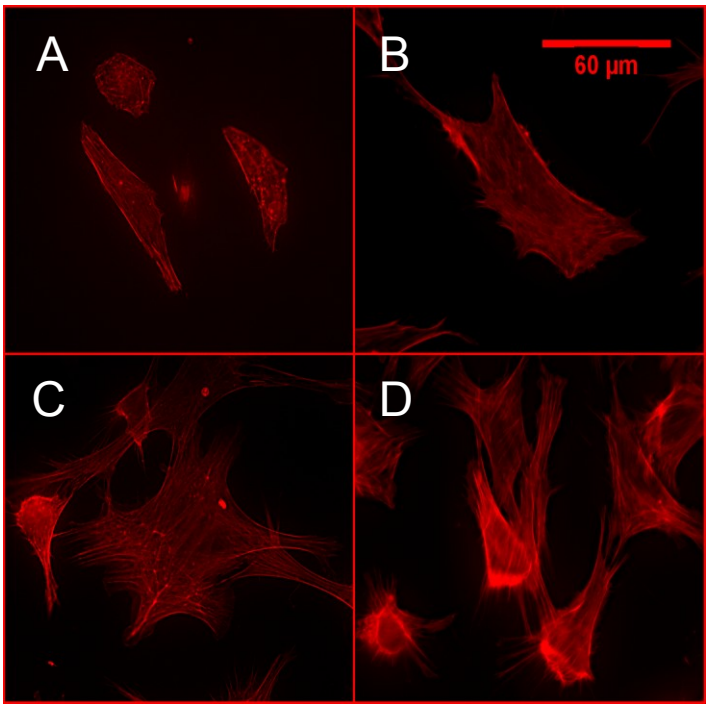

Figure 25: Cellular morphology of Airway Smooth Muscle Cells growing on three polyacrylamide matrixes and glass. Cells in the soft matrix (A) look round and small in sizes compared to that growing on medium (B) and stiff (C) gels as well as glass substrates (D). Filopodia appears absent in cells growing on the soft gel. Cells were labeled with Red Phalloidin which binds to the polymerized actin in the cell. Scale bar is the same for all four figures.

We find that the cells grown on the soft gels cover roughly half the area of cells grown on the other substrates. When inspecting the histogram of the cells one also notices that the width of the area distribution is not changed.

Cell morphology varied among the substrates. Thus, cell roundness was quantified employing the following equation for cell circularity,

$$C = \frac{4\pi A}{p^2} \qquad (2)$$

where *A* represents the area of the cell and *p* the perimeter. In this context, a value of 1 indicates a perfect circle while lower values indicate that elongated structures are present (in this case, lamellipodia and filopodia, see Figure 25 and Figure 27).

No important differences appeared among cells plated on the medium stiffness gel, hard gels and glass substrates (all exhibited low circularities). The

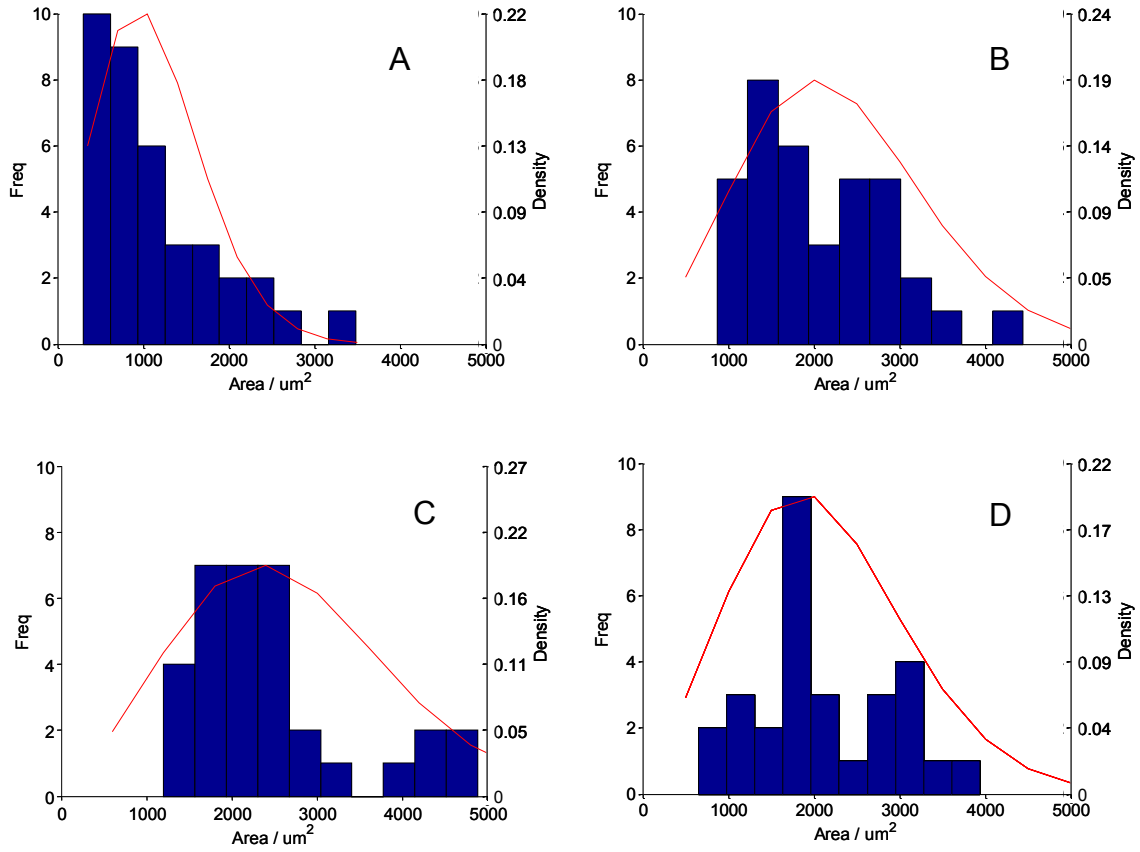

Figure 26: Histograms of the cell area distribution. The cells were cultured on soft (A), medium (B), hard (C) and glass (D) substrates. To assure the cells were in the same mitotic stage, the cultures were allowed to develop until ~60% confluence was reached and then subjected to a 24 hour starvation period. A shift to larger areas is observed between cultures on soft gels and stiffer substrates. The red lines represent the Poisson distribution fit. The maximum likelihood estimate for cell area on the soft, medium, hard and glass substrates are 1130 μm^2, 2060 μm^2, 2450 μm^2, 2105 μm^2 with 1120 – 1140 μm^2, 2045 – 2075 μm^2, 2430 – 2465 μm^2, 2090 - 2120 μm^2 95 % confidence intervals respectively.

cells exhibited elongated shapes with several filopodia and lamellipodia protrusions in all cases (see Figure 28). However, circularity of cells on the soft gels clearly shows a wider distribution with slightly higher C values in some cases. This is consistent with the observation of more rounded cells with no filopodia and lamellipodia in cells plated on soft substrates (see Figure 25 and Figure 28).

Poisson distribution fitting of the circularity data showed that the maximum likelihood for circularity for cells cultured on the soft, medium, hard gels and glass

are 0.23, 0.07, 0.06 and 0.06 with 0.11 - 0.45, 0.01 - 0.22, 0.01 - 0.22, 0.01 - 0.24, 95% confidence interval respectively.

It is widely assumed that the underlying cytoskeleton network, in particular, the actin filaments are a predominant factor determining cell shape (Disanza et al., 2006, Pollard and Cooper, 2009, Mogilner and Rubinstein, 2010). Thus, the differences in cell morphology observed optically and confirmed with cell area and cell circularity measurements could be potentially linked to variations of the actin distribution in the cells cortex. Furthermore, cortical actin

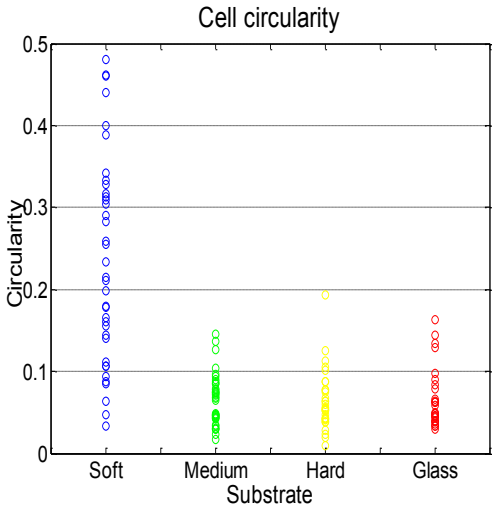

Figure 27 Cell circularity. Cells on soft gels exhibit more circular shapes than cells in the other three conditions. Circularity of 1 represent a perfect circle. S, soft gel; M, medium stiffness gel; H, hard gel and G, glass.

might have an impact on cell mechanics, the main subject of this study. We thus observed the location of actin filaments by labeling the cells with Texas Red Phalloidin. This probe is produced from a mushroom toxin conjugated with a Red dye that is excited at 595 nm and emits at a wavelength of 615 nm. The toxin has a high affinity for filamentous actin (F-actin) and binds specifically at the interface between adjacent F-actin subunits. Texas Red Phalloidin does not bind to actin monomers (globular actin or G-actin which are widely distributed in the cell cytoplasm). The high affinity of this probe for filamentous actin allows the study of the actin mesh distribution.

Texas Red Phalloidin revealed a large number of lamellipodia and filopodia on cells plated on the harder substrate (20T-0.50C and glass) although those structures were also present in medium stiffness gels (10T-0.26C) but almost absent on the soft gels (10T-0.03C, see Figure 28). Furthermore, the organization and the length of the actin filaments tend to increase with substrate stiffness. Cells growing on the stiffer gel and glass show regions were the actin is organized in a network that is highly nodal (see Figure 28B and E).

AFM imaging and force volume experiments of this type of cells had previously showed the same type of actin organization, including the observation of adhesion centers and nodes. (Smith et al., 2005).

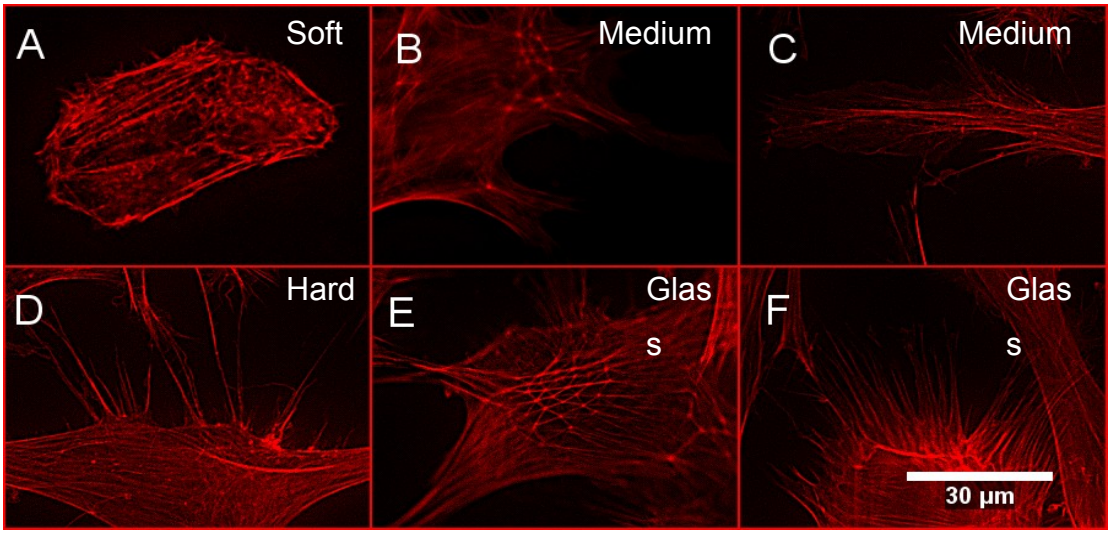

Figure 28: Actin arrangement detected optically by staining with Texas Red Phalloidin. Actin filaments show a poor organization in Airway Smooth Muscle cells plated on soft substrates (A). This cells appear rounded with very few or no lamelipodia and filopodia. Actin becomes increasingly organized with matrix stiffness (B and C, medium stiffness; D, hard matrix; E and F, cells growing on glass) as it appears in the central part of image B and E where nodes become visible close to the edge of the cell. Filopodia-like structures are visible in cell plated in medium stiffness gels (B) but length and number of such structures increases in cells plates on stiff gels (D) and glass substrates (F). Panel E (cell on glass substrate) shows a cell with a very well organized actin mesh with nodes that interconnected by actin filaments. Scale bar is the same for all the images in the panel.

5.4 Dependence of the elastic properties of ASMC on the substrate stiffness.

It has recently been reported that several cellular characteristics of *in vitro* cultures are significantly linked to the mechanical properties of the matrix in which they grow (Engler et al., 2006b; Saha et al., 2008b; Discher et al., 2009). Thus, when investigating cellular behavior, matrix stiffness is an important parameter to take into consideration if conclusions relevant to the *in vivo* environment are to be drawn. In the present study, we were motivated to determine whether the intrinsic viscoelastic properties of the cells are affected by the mechanical properties of the matrix and give and initial exploratory view of the effect of the matrix mechanics on other biologically relevant parameters such as gene expression (genotype), cytoskeleton organization and proliferation (*i.e.* cell viability). The present study should be seen as a starting point for future more directed, biologically focused studies.

As described, polyacrylamide gels with three stiffnesses were prepared by mixing 10 % w/v polyacrylamide with 0.03 % and 0.26 % w/v of the cross linker BIS-acrylamide or 20 % w/v polyacrylamide with 0.50 % BIS-acrylamide and used for cell growth. Cell cultures on glass were also included.

Prior to the measurement of the mechanical properties of the cells, they were starved for 24 h in DMEM supplemented with 0.5 % FBS. This assured that all the cells were in a non-proliferate stage of development and thus the cell cycle phase does not play any role in the measured cell mechanics.

Force modulation measurement (refer to section 2.5.3 for details of the procedure) were performed on the cytoplasm of cells (for a description of the method used to determine the location to measure refer to material and methods section). The experimental conditions employed were: a maximum prior-to-modulation loading force of 0.3 nN and an additional oscillatory load of 7 nm amplitude and 10 Hz frequency during ~ 15 sec followed by 20 sec unloaded period to allow the cell relaxation and avoid damage. Due to the fact that the preparation procedure as well as the cantilever drift stabilization, cantilever sensitivity calibration, cell location, positioning and drag calibration were time

consuming, a maximum of three cells per dish were measured per day although two cells was typical. For the duration of the measurements, the cells were supplied with CO_2 and kept at 37 C to prevent cellular deterioration. Each cell was measured in a unique location between the nucleus and the cell edge. Multiple measurements at different regions in a single cell were avoided to prevent changes in cell mechanics due to prolonged loads. Even though the measurements were performed on a sole location on the cell, previous results from Smith et al., (2005) (see Figure 11) indicate that the data collected from several cells in this thesis gives a representative view of the cells under the specific tested conditions. In Figure 11B, it is possible to observe that the relative elasticity of the region around the cell nucleus is homogeneous and differences in elasticity are only evidenced at submicron areas (see Figure 11D). Since the cell-bead contact area for the experimental conditions used in this thesis is ~ 3 μm^2 (the contact radius is ~ 1 μm), it is reasonable to think that this methodology is a very good approach to compute the overall mechanical properties of individual cells. It is an indication that the AFM measurements are not sensitive to the properties of individual fibers but it is an average of the elastic properties over an area that contains several filaments.

On a typical day, cells on a maximum of three dishes were measured. The total number of culture dishes employed and analyzed for the results presented in this thesis were: 13, 10, 12 and 13 dishes for the cell cultured on glass, hard, medium and soft substrates respectively. We thus report the results of 16-28 cells measured per substrate.

We found that the complex modulus of airway smooth muscle cells plated on the substrates demonstrated that the elastic modulus of the cells tends to increase until a maximum that is reached for hard matrices (see Figure 29). For the conditions tested, the storage modulus was, 820 ± 360 Pa, 820 ± 280 Pa, 650 ± 300 Pa and 340 ± 160 Pa for the cells plated on glass, stiff gel, medium stiffness gel and soft gel respectively. The fairly large standard deviations is due to cell variability, as measurement errors are substantially smaller.

The experimental errors due to uncertainties in the estimation of the contact point were estimated by substituting the typical values of the real part of equation 14 (0.215 Pa $m^{1/2}$ for the softest and 0.367 Pa $m^{1/2}$ for the glass substrates) and maximum estimated deviations of 20 nm from the typical indentations δ_0 (400 nm for cells on the softest and 200 nm for cells on glass) into the equation 14. One thus obtains an estimate for the experimental error in determining the elastic modulus from force modulation. We obtain of 2.5 % for cells plated on softer matrix and 5 % for cells cultured on the glass substrate, nearly an order of magnitude smaller than the observed standard deviation. Additionally, it was shown in the material and methods section that the error due to the lock-in amp output signals is in all the cases less than 100 Pa for cells plated on stiff gels and ~ 20 Pa for cells cultured on the soft gels. Together, this strongly indicates that the differences in the elastic modulus means as well as the standard deviation are due to biological variability. A histogram of the elastic modulus is shown in Figure 30.

Note that the absolute variability of the elastic modulus was narrower in cells plated on the softer gel (160 Pa versus 280-360 Pa). As can be seen in Figure 29, a trend that shows an increase of the mean elastic modulus of cells plated on medium and hard gels is not statistically significant using the one-way analysis of variance statistical analysis (one-way ANOVA) method. .The analysis was performed in MatLab software, for an example of the methodology refer to Appendix 2). ANOVA is used to discern whether or not the means of several populations are statistically different or equal. It assumes that there is only one factor that varies among the groups (in our case the substrate stiffness), that there is independence of cases, equality of variances and the random variable must be normally distributed. This assumption of only one variable is reasonable since the culture dishes were all kept under the same incubation conditions and the cells were in an arrested growth phase when the measurements were performed. In other words, the results of these measurements, although an average of cell plated on several dishes, are expected to be significant for each group since all condition except the substrate were kept constant.

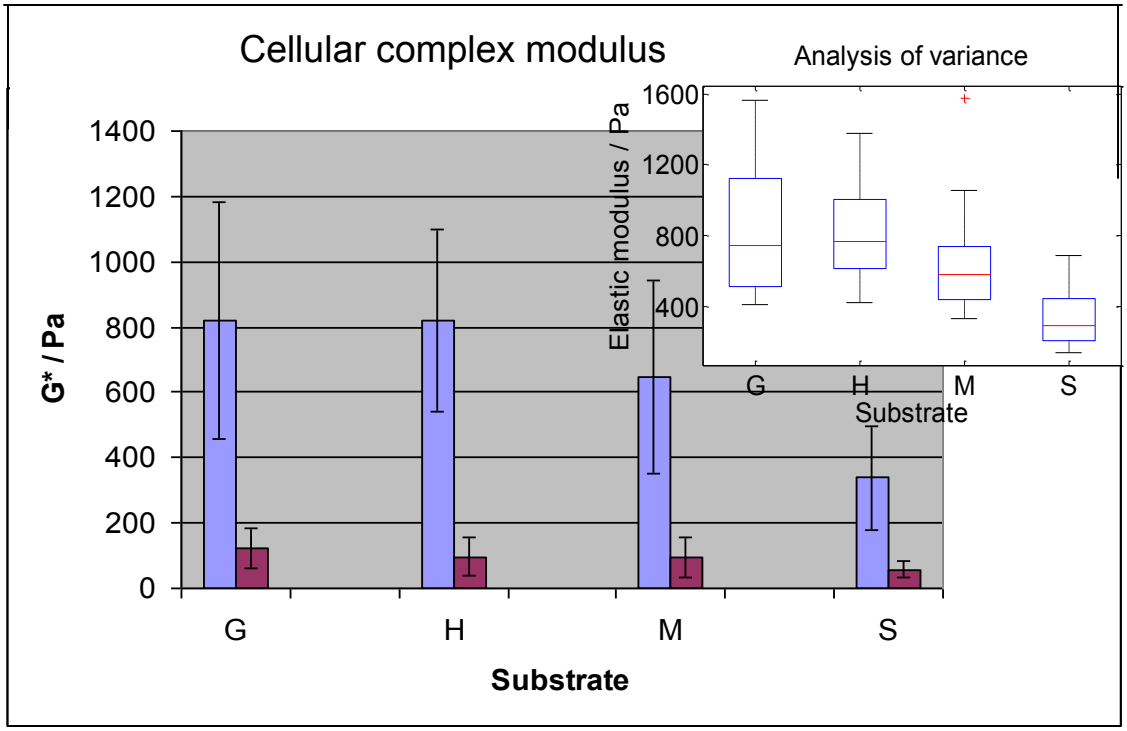

Figure 29: Viscoelasticity of Airway Smooth Muscle Cells as a function of matrix stiffness. The average elastic modulus (G', blue bars) of the cells increases with matrix stiffness to a maximum of ~800 Pa, where it remains the same as the elastic modulus measured on cells plated on glass. The wide error bars (standard deviation) on the medium gel, stiff gel and glass show the broad range in the measured elastic modulus. Cells on the softer gel show a narrower distribution. The loss modulus (G'', purple bars) was low in all cases and with no clear differences. Inset. Analysis of variance (ANOVA) of the elastic modulus of Airway Smooth Muscle Cells. The box plot graph depicts the sample minimum, lower quartile, median, upper quartile, and sample maximum. At 0.05 level of significance, the ANOVA analysis indicates that the mean elastic value of the cells cultured under the four conditions are not all the same. Posterior multiple comparison analysis (both, ANOVA analysis and multiple comparison were performed with the MatLab software), this indicates that the mean of the elastic modulus of the cells cultured on the soft substrate is statistically different from the other groups. No statistical difference of the elastic modulus means was found among the group of cells cultured on medium medium stiffness, hard gel and glass substrates. The number of cells measures was n = 19 for G, glass substrate; n = 16 for H, stiffer gel; n = 19 for M, medium stiffness gel and n = 28 for S, soft gel.

The same analysis revealed that the elastic modulus of cells plated on the soft gel is statistically significantly different at a 0.05 level of significance[4] (or a 95% confidence level) from the elastic modulus of the cells on the other substrates (see Figure 29).

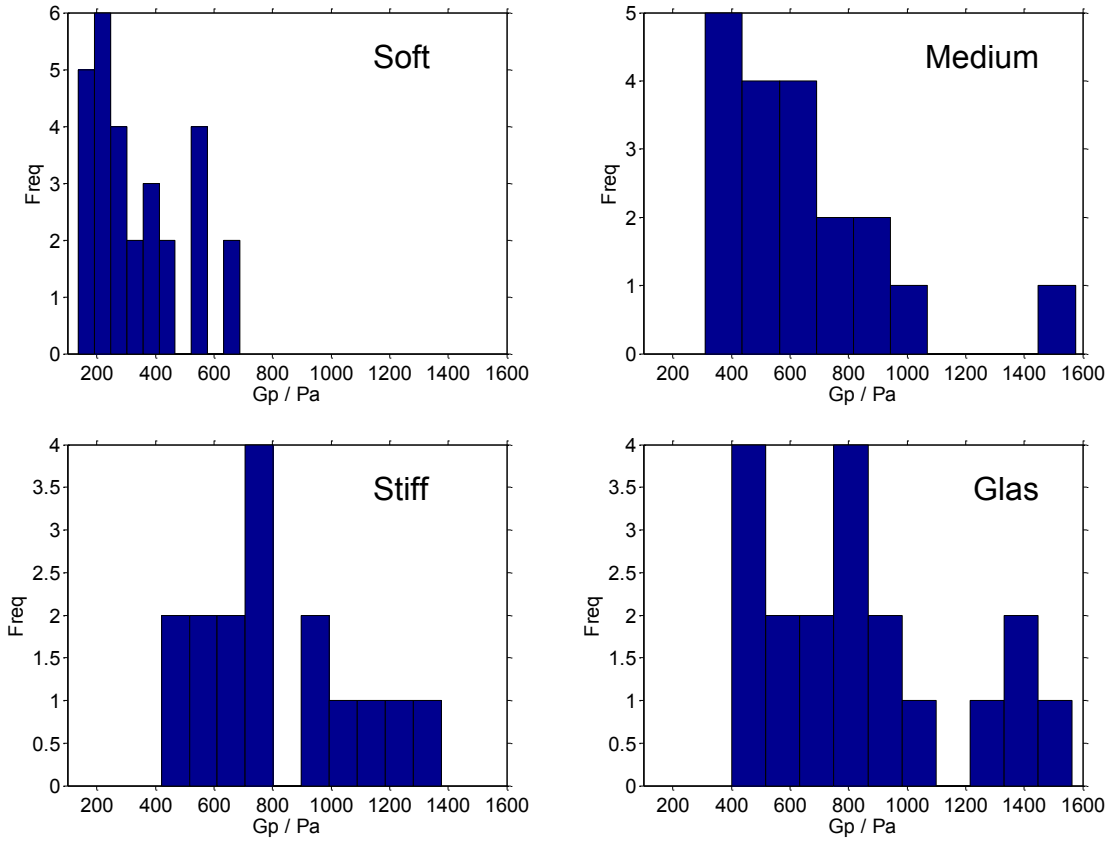

Figure 30: Histogram of the elastic modulus of cells calculated on the soft, medium, and stiff gel substrates and glass.

It is possible that airway smooth muscle cells reach a maximum elastic modulus when plated on even stiffer gels. However, gels with intermediate stiffnesses (between glass and hard gel) would need to be prepared in order to unequivocally prove that larger elastic modulus cannot be reached. In the present thesis, the preparation of stiffer polyacrylamide gels was performed but those gels became opaque which limited the optical observation of the cells and

[4] In this terminology, the level of significance closer to 0 means that there is less probability that the observation occurred by chance. On the contrary, a level of significance closer to 1 means that there is high probability that the observation occurred by chance.

thus made it impossible to determine the contact location where the AFM probe interacted with the cells. Cell culturing and complex modulus measuring on substrates with stiffness between that of the soft and medium gel would be of interest for futures studies that use the methodology presented here.

The loss modulus of the cells appeared more uniform and narrower than the elastic modulus in all the samples. Their estimated averages were 120 ± 60 Pa, 100 ± 60 Pa, 90 ± 60 Pa and 60 ± 30 Pa for the cells growing on the glass, stiff gel, medium stiffness gel and soft gel respectively. These values indicate that the cells are prominently elastic with a low dissipative modulus that essentially remains the same irrespectively of the matrix stiffness. One-way ANOVA did not show any significant difference among the conditions.

An immediate questions is whether or not the variability observed in Figure 29 reflect variations of the complex modulus of cells cultured on different days or from different animals. To address this issue we looked at the elastic modulus (determined by force modulation) of 12 cells. Nine of them (cells cultured on the polyacrylamide substrates) were obtained from the same animal and plated at the same time. The other three cells (cultured on glass substrate) were cultured a different day but they were growing in the same dish which eliminated the variable related to the origin and the incubation conditions of the cells. For each cell measured, only one location on them (between the nucleus and the cell edge) was tested. The data plotted in Figure 31 is the average of three to four indentation modulation cycles (frequency 10 Hz and amplitude 7nm) performed with 15 seconds intervals and in the same location on the cell. In the graph, the error bars are too small to be visible (this error is associated to the uncertainty of the lock-in output signals, refer to Figure 16 and section 2.5.3). The magnitude of this error becomes clearer in Figure 32 where the elastic and loss modulus vs. time is plotted. In the figure, each data point corresponds to the modulus computed for a single indentation modulation cycle at a frequency of 10 Hz and the interval between each indentation cycle was from 15 – 20 s. Each oscillatory cycle lasted for 15 s. Calculation of the error due to the averaging of the loss modulus in time was found to be less than 100 Pa for the elastic

modulus and less than 20 Pa for the loss modulus in cells growing on any other type of gel. Although this result does not exclude the possibility that actin rearrangement under the bead-membrane contact is responsible for the observed variability from cell to cell, it does rule out the possibility that such rearrangement are an important contributor to the variations in the modulus

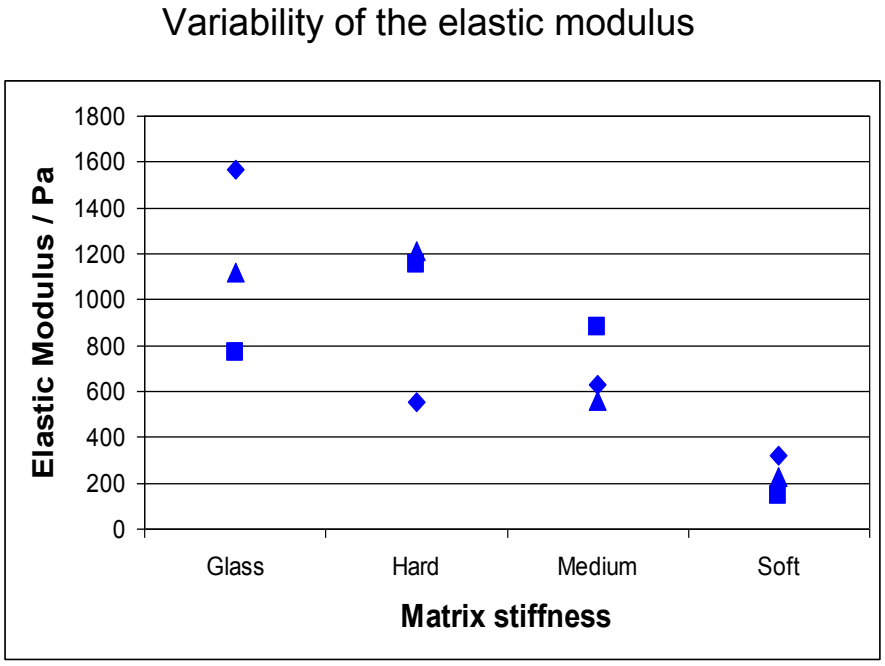

Figure 31: The graph shows the elastic modulus of three cells each measured on different substrates. The cells plated on the polyacrylamide gels were obtained from the same animal and incubated at the same time. However, the cells plated on glass were cultured on a different day. For each condition, the three cells shown were growing on the same culture dish. A single location on the cell was measured. Measurement error bars not shown since they are the same size as the data points. The variability of the results strongly resemble what is observed in Figure 29 and support the conclusion that the variability is not due to cells cultured on different days nor from different animals.

measured for the tested conditions. Only a few cycles (~ 4) were used to measure the complex modulus of the cells presented in Figure 29 and Figure 30. The measurement time was thus short (~ 2 - 3min). Optical observation of the cells during the course of the measurement did not show any changes in morphology or obvious cellular dynamics or migration for any of the tested conditions.

Together, these results strongly suggest that the variability observed in Figure 29 is indeed only a consequence of cell-cell differences and not due to a cell specific response to being probed.To summarize, our results thus suggest that there is a large variability in the elastic modulus even for cells cultured in the same dish. The origin of the variability in Figure 29 does not seem to be due to the origin of the cells (*i.e*. different animal), day of measurement or the (arrested) cell cycle phase. This result, in addition to previous published reports (Smith et al., 2005) that shows that the elastic properties of the cytoplasm region of a

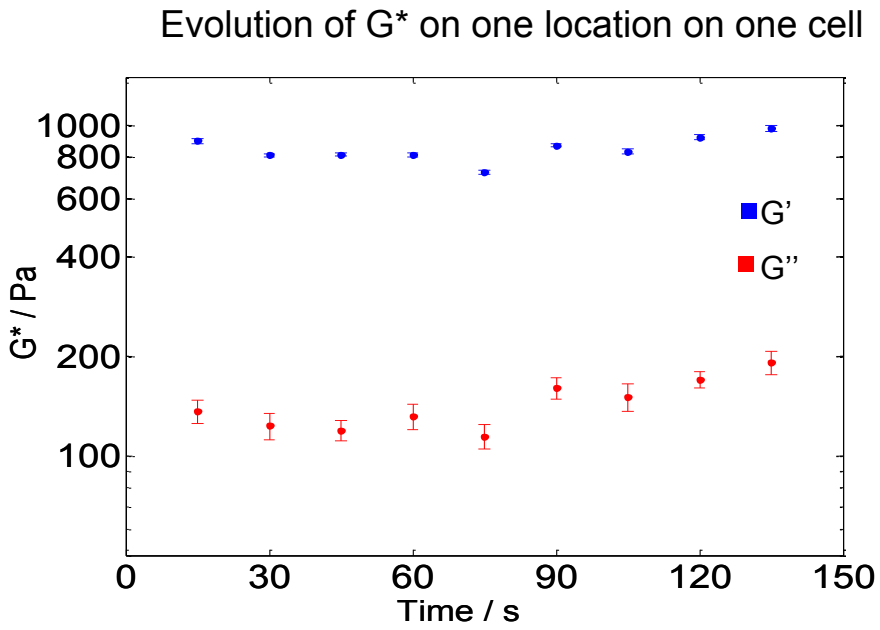

Figure 32: Evolution of the complex modulus for a single cell at a single location in time. For the data showed, the averaged elastic modulus (blue points) was 850 ± 75 Pa while the loss modulus was 140 ± 25 Pa.

single ASMC is not highly variable suggest that the differences in the elastic modulus observed among the substrates is linked to intrinsic differences between the cells. The data above demonstrate that the cells growing on soft substrates with more tissue like mechanical properties are statistically softer and have a lower variability than cells grown on all other substrates. Cells grown on stiffer substrates are similar both in terms of modulus and variability.

5.5 Cell Proliferation.

During the course of the experiments, it was noticed that a different number of cells had to be plated on the gels in order to obtain the same confluence in the same amount of time. This suggested that gel stiffness affected proliferation rate (this has been observed preciously in other cell strands, see Bott et al., 2010; Hadjipanayi et al., 2009). Initial calibration of the number of cells needed to get cell cultures with the same confluence in a certain amount of time showed that 100,000 cells per dish were needed in the soft gel while approximately 40,000 cells per dish were needed in the medium stiffness matrix, 35,000 cells per dish were needed in the hard gel and 25,000 cells per dish were needed in the glass plates. A proliferation assay was then used to quantitatively assess the proliferation rate of Airway Smooth Muscle Cells as a function of the elasticity of the substrate (see Figure 33).

Prior to the experiment, cells were incubated in starvation medium for 24 hour to assure that the cells were in the same phase of the cell cycle at the beginning of the experiment. Addition of the BrdU and subsequent incubation for 18 h allowed the incorporation of the BrdU in the proliferative cells. A proliferation assay with the DNA maker bromodeoxyuridine (BrdU) was performed. The BrdU is incorporated into the DNA strand whenever cells replicate. BrdU is a synthetic nucleoside that is analog to the thymidine[5] and substitutes for it in the DNA strand during replication. Since BrdU is not fluorescent on its own, fluorescent antibodies anti-BrdU are used to detect its incorporation into the newly synthesized DNA.

Proliferation was tested as a function of matrix stiffness as well as serum content in the medium. In our experiments, two serum concentrations were used: 0.5% FBS and 10% FBS. Using Fluorescence Activated Cell Sorting (FACS), significant variation in proliferation was observed among cultures growing on the same matrix but different serum concentration. In general, the softest gel at best

[5] One of the four basic nucleosides that form the DNA (Adenine, Guanine, Thymine and Cytosine)

seems to promote profileration only weakly. Proliferation assays showed that cultures growing in starvation medium (0.5% FBS) have low proliferation rates (less than 10 % of the total population) independent of the mechanical properties of the substrates.

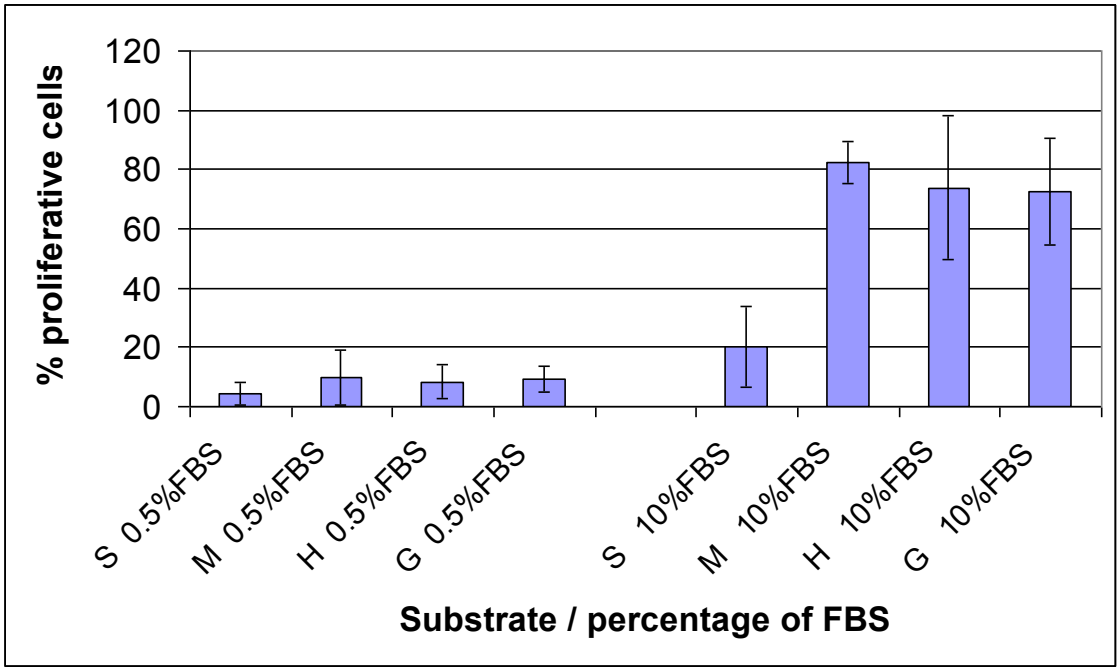

Figure 33: Cellular proliferation assay. Cells cultures in all matrixes tested and in DMEM supplemented with 0.5% FBS show low proliferation rates as compared to cultures supplemented with 10% FBS. The graph shows that soft gels do not promote cell proliferation. However, stiffer gels induce cell proliferation rates of the cell population as high as 82%.

At 10% FBS the proliferation rates were statistically significantly higher with averages ranging from 72% to 82% of proliferation, except for the softest substrate (average of 20%, within one sigma of the 10% observed for 0.5% FBS).

5.6 Genetic expression.

Cellular development is a complex regulated process that involves many steps such as sensing chemical and mechanical cues, triggering signaling cascades that on many occasions start at receptors in the cell membrane and phosphorylation/-dephosphorylation of effector proteins.

To detect any variation in the genetic expression of the airway smooth muscle cells among the tested conditions, Gene Arrays were performed with total RNA. Prior to RNA extraction, the cultures were starved in 0.5% FBS medium for 24 hours to assure that the cells were in the same phase of the cell cycle at the time of the RNA extraction. Three replicates were done per condition. The data was subsequently analyzed by using the software Flexi Array 1.5 obtained from Genome Quebec gene array laboratory.

Determination of the genes that exhibit significant differences among the conditions was done by using One-way Analysis of Variance after the row data was normalized. Of the genes with a level of significance of 0.05 or lower, a selection of genes that are known to be implicated in cytoskeleton arrangement, adhesion and proliferation was used to create the heat map shown in Figure 34. The ontology of the genes was obtained from the Rat Genome Database (http://rgd.mcw.edu/). Generally speaking, it was found that genes related to various cytoskeletal functions are down regulated in cells growing on the softer matrix.

The genes listed in the Figure 34 exhibited significant differences in the means at 0.05 level of significance. Variations in expression among the four tested conditions are represented by different tones of red (higher expression) and green (lower expression). A higher expression of tubulin subunit and tubulin assembly genes (*tubb6, tubg1, tuba4a, tubb2c*) was observed in cells cultured on the soft gels while up-regulation of cytoskeleton rearrangement, force generation, adhesion and proliferation genes (*rhoj, tnnt2, mylpf, myh3, acta1, itgbl1, mfge8, pfn2, pcdh21, krt25*) was found in stiffer gels. Of special interest are the myosin related genes which are involved in force generation. In this case, their expression increases from soft to hard gel and apparently the expression is sustained in cells cultured in glass. An interesting finding, however, is that

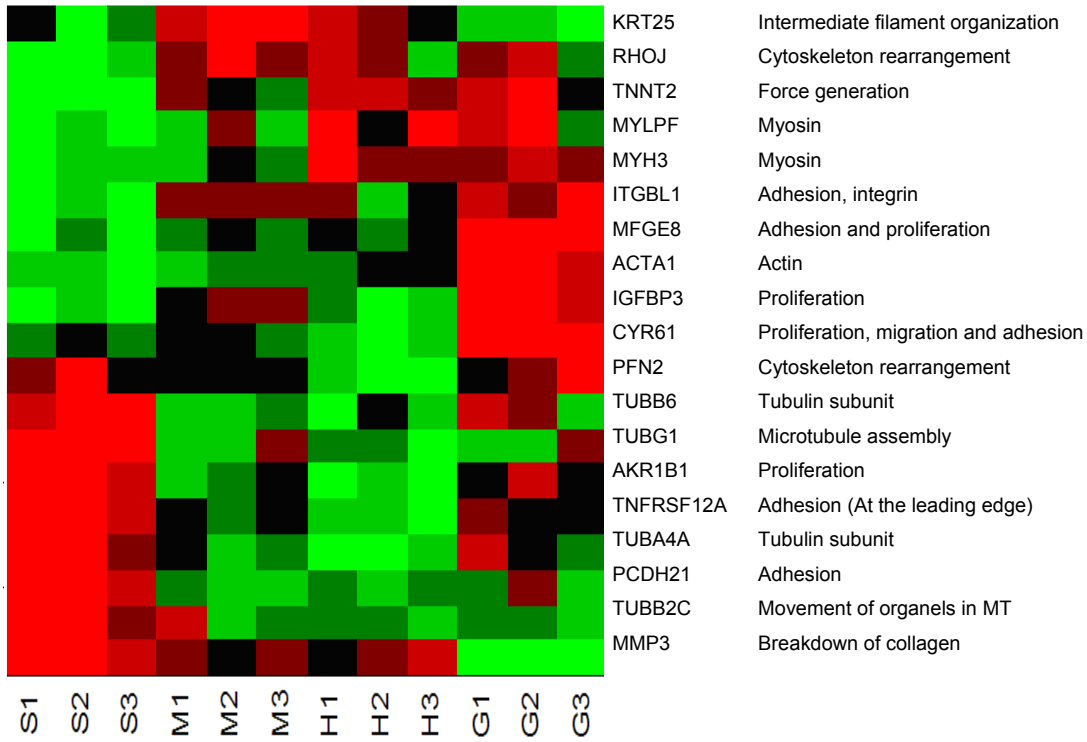

Figure 34: The figure shows the expression of some genes that have been implicated in cytoskeleton, adhesion and proliferation of muscle cells. Bright red and bright green represent high and low expression respectively.

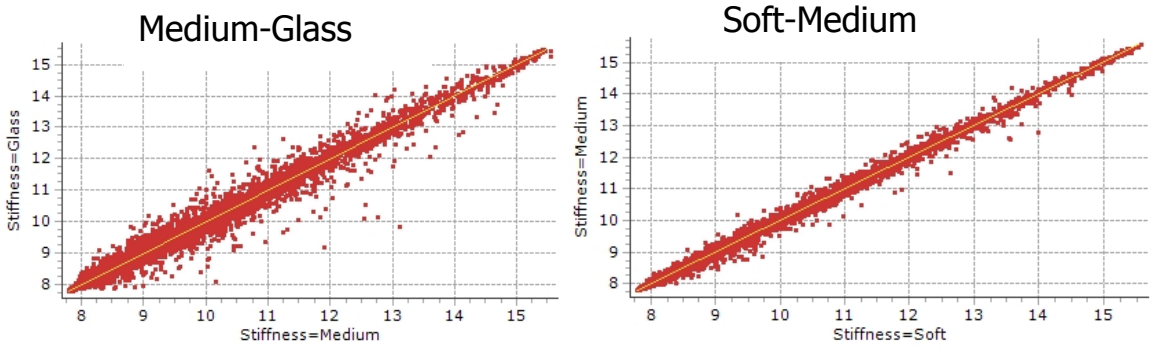

Figure 35: Two scatter plots of expression that show that the larger differences in expression occur between glass and the non-rigid substrates. Each dot represent the expression of a single gene. Genes that located close to the yellow line do not have important differences in expression between the samples while separated dots signify that the expression of the gene have important differences.

generally speaking, the variability of the genetic expression is larger between cells cultivated on glass as compared to any of the gels. (see Figure 35).

5.7 Summary, Conclusions and Discussion

5.7.1 Mechanical properties of the polyacrylamide gel and fibronectin functionalization.

It is well known that chemical cues play an important role in the determination of cell fate, genetic expression, protein content, morphology, functionality, etc. but less is know about the role of mechanical cues on cell behavior. Some of the available knowledge is attributable to Engler et al., (2006a); Saha et al., (2008a). They discovered that variations in matrix stiffness are sufficient to trigger cell differentiation of stem cells. This finding demonstrates that the mechanical properties of the cell surroundings are an important and possibly a determinant factor to trigger several cellular processes. To further study these effects, the AFM was used in the present study as a tool to explore the role of physical cues on the cellular properties such as elasticity, proliferation and gene expression.

In this study, polyacrylamide gels were chosen as substrates for cell cultures because of the simplicity to accomplish the tuning of their stiffness. It can be adjusted by varying the amount of polymer (acrylamide) and cross-linker (BIS-acrylamide). Three polyacrylamide substrates prepared with 10% acrylamide, 0.03% BIS-acrylamide for the softest gel; 10% acrylamide, 0.26% BIS-acrylamide for the medium stiffness gel and 20% acrylamide, 0.50% BIS-acrylamide for the stiff gel were prepared. Additionally, glass substrates were employed to prepare cell cultures. Gels with higher concentrations of acrylamide (30% and 40%) were prepared but they became opaque after polymerization. Since the observation of the cells was performed from underneath by using an inverted optical microscope, the opaqueness of the gels limited the optical localization of the ASMC on the substrates and they were not employed in this thesis (the optical observation of the bead-cell contact is essential to perform the

methodology described in section 2.5). Transparency was not an issue on cell cultures prepared on glass.

One of the objectives of this study was to evaluate the effect of non rigid substrates on cell behavior. Cultures prepared on glass substrates (rigid substrate) were included because it is the most widely used substrate in cell culture preparations. Thus, comparison of cellular behavior on polyacrylamide gels vs. glass substrates is of interest to elucidate how cells react to matrix stiffness. The rigidity of glass (~ 70 GPa, Van Vlack, 1982) is larger than bone (15 – 20 GPa, Hoffmeister et al., 2000; Rho et al., 1993) although both are in the GPa regime. It makes the glass the most rigid substrate employed in this study.

Cell cultures used in the experiments were typically incubated for five days. Therefore, the use of substrates whose mechanical properties are stable for that period of time was necessary. The Young's modulus of the polyacrylamide gels was measured for six consecutive days to keep track of their mechanical stability. The conditions at which the gels were stored during this time were the same than that used when cell cultures were prepared. Force-distance curves at ~ 750 locations on the gels were taken each day. No difference in the Young's modulus was observed in the time indicating that the stiffness of the polyacrylamide gels is not affected by the incubation (see Figure 23). On average, stiffness of the soft, medium and hard gels was 0.9 ± 0.2 kPa, 3.7 ± 0.3 kPa and 6.3 ± 0.5 kPa respectively.

Determination of the Young's modulus of glass with the AFM proved to be unreliable mainly due to the large sensitivity of the Hertz model to small indentations. The curves in Figure 24 shows that the accurate determination of the stiffness of a rigid substrate requires a very precise (precision of nm or lower) estimation of the contact point. Cantilever bending due to movement in liquid might systematically affect the determination of the contact point. Equation 11 predicts that even small uncertainties in the determination of the contact point can affect the calculation of E in stiff materials such as glass and polystyrene.

The use of a much harder indenter (harder than glass) that does not deform is also necessary. This is clearly not the case for polystyrene bead tips

which have a Young's modulus of 2 – 4 GPa depending on the measurement method (Lubarsky et al., 2004; Miyake et al., 2006; Brighton, 1979) and glass (~70 GPa) as the substrate. Hence, it is mainly the indenter which is deformed. Diamond coated tips would need to be used to measure very hard substrates such as glass; their shape is however not well defined, making quantitative analysis of nanoindents challenging.

Finally, the use of very small indentation depths can also contribute to the unreliable determination of the Young's modulus of polystyrene. It is possible that a swelling of the outer layer of the polystyrene leads to measured elastic moduli values much lower than the bulk values reported in the literature. We base this hypothesis on the observation that when old polystyrene beads are imaged in AFM or SEM, they look "fuzzy" which might be an indication of the effect of liquid on the bead surface.

The indentation caused by the beaded cantilever on gels was large (100-350 nm, see Figure 24) and the sensitivity of the Hertz model to the precise determination of the indentation onset thus smaller (see equation 11). The stiffness of the polystyrene, which was three orders of magnitude larger than the stiffness of gels, assured that the deformation occurred only on the substrate. In these situations the Hertz model is thus expected to allow a reliable determination of the mechanical properties of the polyacrylamide gels and cells.

In this study, all the surfaces (polyacrylamide and glass substrates) were coated with fibronectin. There were two reasons to do that: the first is that differences in substrate chemistry can alter cell behavior (Jie Song, 2004) and the second is the simple fact that cells do not adhere to bare polyacrylamide gels. Bare and functionalized glass demonstrated to be a well suited substrate for *in vitro* cultures. In both cases, cells adhere and thrive. However and even though bare and functionalized glass support cell growth, some studies indicate that cells plated on both substrates do not behave equally. Jie Song, 2004 for instance, cultured osteosarcoma TE85 cells on anionic functionalized surfaces as well as bare glass and reported variations in protein content and cell adhesion. This study points out to the necessity of keeping control of the surface chemistry

to avoid variations of cell behavior due to factors other than the variable of interest.

Fibronectin functionalization of the polyacrylamide gels required the use of the linker sulfo-SANPAH which covalently binds to both, the fibronectin protein in one extreme and the polyacrylamide polymer on the other. Passive absorption of the protein into the polyacrylamide gels proved to be ineffective for functionalization.

5.7.2 The use of the AFM to investigate the mechanics of the cells.

There is increasing evidence (Wang and Ingber, 1994; Shyy and Chien, 1997; Jaasma et al., 2007; Gavara et al., 2008; Icard-Arcizet et al., 2008) that the cellular behavior and function are importantly influenced not only by chemical cues, which have been extensively studied for decades, but also respond to the mechanical properties of the surroundings. Although intuitively we expect that the mechanical properties of the substrates (for *in vivo* experiments) or the tissues (living organisms) affect the cellular functions, no detailed studies were reported until recently (*i. e.* Paszek et al., 2005; Discher et al., 2009). However, despite these efforts, many questions still remain unanswered and further studies have to be done to elucidate the fine relation between the mechanical properties of the substrates on the cellular functions and behavior.

A variety of mechanical properties are distinguished in different parts of the organisms, especially in those which have evolved to complex structures with well defined body organization and differentiated tissues. Bone, for example, is a very stiff structure that provides support and resistance to the body of many animals. At the same time, it keeps the bone marrow tissue in its porous, inner structure. Tendons and ligaments are made of connective tissue which contains large numbers of fibroblast and is able to withstand substantial tension when muscle cells shorten or joints are moved. One of the softer tissues in the organism, the brain, is a compact mass of different soft cells. This tissue is very delicate but at the same time highly specialized.

All mammalian cells contain an inner cytoskeleton which is a structure that is composed of microtubules and intermediate filament enclosed by an actin mesh. The cortical actin is located underneath the cell membrane which is the most external part of the cells. It has a typical thickness of from 390 nm to 770 nm (Lang et al., 2000). The thickness of the cell membrane is only ~ 10 nm (McMahon, H. T. and J. L. Gallop, 2005). Given these dimensions and considering the ability of the AFM to produce small loads, indentations and contact radius, this instrument is well suited to study the mechanics of individual cells. Thus, AFM can provide some information to answer questions such as how the elastic properties of tissue is linked to functions and what are these connections? An example of its usefulness is found in a study recently published by our group (Risse et al., 2011) where it was found by AFM force spectroscopy that IL-13 treated cells have an increased response to the stimulation with the contractile agonist histamine. Another example is the observation by AFM force spectroscopy that the ASMC smooth muscle cells contract when exposed to stimuli leading to asthma at the organ level. AFM force spectroscopy can answer questions such as which components of the individual cell reacts and why does this induce a contractile response, as addressed by our group using AFM force spectroscopy of ASCM cells plated on glass cover slips (Smith, 2004). Given the fact that cell phenotype and genotype can differ as a function of substrate properties it is an important question to determine how cell mechanical properties are affected by the substrate.

At the single cell level, recent experiments have indicated a change in elastic properties as a function of the state of the cell. Cancer cells are softer than healthy cells (Sarah and et al., 2008; Suresh, 2007). These empirical observations are not well understood but clearly cell phenotype can in some cases be determined by measurement of the viscoelastic properties of an individual cell.

Small and localized probing forces do not dramatically disturb the cells as a whole and can be applied by an AFM. This is due to the low spring constant of the cantilevers employed in this thesis (0.01 N/m), which allows the application of

picoNewton forces. In this study, small probing forces of 0.3 nN were generally used and produced indentation depths of approximately 200 nm in cells cultured on glass substrates. Indentations produced in cells cultured on the soft polyacrylamide gel were usually larger (~ 400 nm) as a result of their softer nature (see Figure 12). The bead-cell membrane contact radius calculated for the indentation and loading forces mentioned before vary between 0.8 μm and 1 μm (the former for 'stiff' cells, the latter for softer cells). Thus, the use of the beaded cantilever also allowed us to compute the mechanical properties of the samples over an area that averages many individual actin filaments (see Figure 13). Force-volume imaging performed by Smith et al., (2005) on ASMC also evidenced that the use of large contact areas is preferred to average over the elastic properties of a region and be insensitive to punctual cell structures.

5.7.3 Correlation between the substrate stiffness, the viscoelasticity of ASMC and the actin content.

By using the AFM, we found that smooth muscle cells are capable of sensing and adapting to the mechanical properties of their proximate surrounding by adjusting their own mechanical properties, proliferation rate, morphology and genetic expression. The mechanism and feedback loops by which a cell performs this is not understood. Any hypothesis to explain this phenomena can be tested by the AFM method demonstrated in this thesis by knocking-out the relevant genes coding for the structures/proteins suspected and measuring the mechanical properties of cells grown on substrates of different mechanical properties.

The data presented in section 5.4 exhibits a trend that shows an increase in the cell elastic modulus with matrix stiffness. One-way analysis of variance (ANOVA) only found significant difference ($p<0.05$) between cells cultured on the softest substrate and any of the other conditions. The elastic component of the complex modulus increased from 340 ± 160 Pa in cells cultured on the softer substrate to 650 ± 300 Pa in medium stiffness and 820 ± 280 Pa in hard polyacrylamide substrates. Interestingly, the average elastic modulus of cells

cultured on glass (820 ± 360 Pa) did not show a significant difference compared to the storage modulus of cells cultured on the stiffer polyacrylamide gel (see Figure 29). ANOVA performed on the loss modulus of data obtained on cells from the four groups showed no significant differences ($p<0.05$).

A previous study by Smith et al., 2005 has qualitatively shield light on the spatial variation of the elastic modulus of the same cells as used in this study cultivated on glass. Force-volume imaging of confluent cells showed qualitatively that the cell nucleus is softer than the rest of the cell. It was also found that all the cytoplasmic region of the cell have a very similar stiffness when scanning over a large area. Differences in stiffness in the cytoplasm were only evident when probed on a submicron area. We thus conclude that if the nucleus is avoided, relevant and significant measurements of the elastic properties of an individual cell can be performed by a single measurement with a spatial averaging area of at least 1 μm^2. In the experiments presented in this thesis this averaging area was determined to be at least 3 μm^2 from an analysis of the Hertzian contact area.

Exploration of the mechanical properties of cells cultured on stiffnesses larger than 6300 ± 500 Pa and lower than that of glass was not done due to the fact that stiffer polyacrylamide gels turned opaque, limiting the crucial step of cell localization. Future studies, driven by cellular biology inspired hypothesis, might be performed to investigate the transition between soft and medium substrate, as cells grown on the soft substrate are the only ones to show a statistically significant difference in elasticity, shape and profilation as compared to the other cells.

The standard deviation of the measured elastic moduli is substantially larger than experimental errors. Thus a significant variability of the elastic modulus of cells cultured on the same substrate was observed. A larger variability was observed on harder substrates. Currently we do not know where this variability comes from. The cytoskeleton structures beneath the bead-cell contact is relevant, as it might play a critical role in the determination of the mechanical properties as well as in the variability observed within groups. One

could hypothesize that the lower variability observed on cells that belong to soft substrate cultures is in part due to the absence of bundle fibers and more uniform cytoskeleton with only thin interconnected fibers. The observations of the cytoskeleton of identical cells cultured on glass by Smith et al., (2005) leads to the exclusion of this hypothesis, as on an area of 1 μm^2 these cells looked very homogenous outside of the nuclear region. Understanding this variability is an interesting future project that should be driven by a deeper biological understanding.

All the measurement were performed on cell cultures that were starved in DMEM plus 0.5% FBS for 24 h prior to the experiments. This assured that the cells were in the same phase of the cell division cycle and thus the mitotic phase is not responsible for the variability observed. Although not explored in detail, the observed variability is not a consequence of measurements performed on cell cultures prepared on different days since same day measurements already show a large variability (see Figure 31).

The indentation depths used in the experiments are 10 – 20 % of the cell thickness and thus will be insensitive to many cell internal structures. The 10-20% indentation depth maxima was used as this is a criterion known in thin film contact mechanics to lead to the mechanical properties of the thin film being measured and not that of the underneath support), There are other strong indications that the substrate does not directly contribute to the mechanical properties of the measured cells. Bausch et al., 1998, for instance, demonstrated that the penetration of the shear displacement field induced by the movement (*i.e.* torque) of a magnetic bead attached to integrins on the cell membrane is reduced and it does not reach the base of the cell. The result suggests that localized structures are the main responders to localized loads, not the cytoskeleton, and thus the measured mechanical properties. Integrins are connected directly to the cytoskeleton on the inside of the cell membrane, and thus beads used in such experiments are expected to measure a different elastic modulus than beads attached to AFM tips. This difference between magnetic bead, AFM and other measurements is one of the reasons for the on-going

debate regarding the mechanical properties of cells – this is due to the fact, often not recognized, that different methods are sensitive to different structures of a cell. Previous studies performed in our group (Smith et al., 2005) presented evidence implicating actin as the dominant structure responsible for the cell stiffening. Thus, actin dynamic has a prevalent role in near surface mechanics and the AFM data presented in this thesis.

The largest indentations used in our study were lower or at the most equal to the actin cortex thickness reported in the literature (390 nm to 770 nm, Lang et al., 2000). Smith et al., (2005) demonstrated that the mechanical properties of a cell measure by AFM changed dramatically if the cortical actin gel is disrupted with cytochalasin-D. This is similar to the observation of cells treated with a myosin light chain kinase inhibitors (1-(5-iodonaphthalene-1-sulfonyl)-1H-hexahydro-1,4-diazepine hydrochloride, ML-7) Other studies lead by Charras et al., 2005 and Mitchison et al., (2008) have also shown that local pressure variations in the cytoplasm do not distribute instantaneously to the whole cell. This indicates that although the cytoskeleton is a highly connected structure, transduction of forces requires, in addition to the cytoskeletal filaments, cascades of signalization triggered by local mechanical loads. A manuscript published by Ananthakrishnan et al., (2006) reports that although the interior structural elements contribute to the cell shape via their loose coupling to the cortex, it is the outer actin cortical shell that mainly determines the cell's structural response. Taken together, these results suggest that the mechanical properties measured here have a significant contribution from the cortical actin.

In the literature, Podolski and Steck, 1990 have reported that the mesh size of the cortical actin is ~ 0.2 μm. It is formed by thousands of interconnected actin filaments with some thicker actin bundles that extend several micrometers (see Figure 28). Labeling of the fibers with Red-palloidin showed that the distribution of the actin structures differs among cells cultured on the four substrates used. Cells on soft substrates are less extended and display low content of actin bundles while cells cultured on stiffer matrices are generally

larger and display long and clear actin fibers. Node-like structures also appear more frequently on cells from these cultures.

Filopodia-like structures are virtually absent in cell cultured on the softest matrix. However, the length and number of such structures increases in cells cultured on stiff gels and glass substrates. Overall, although slight differences in the actin organization are observed between cells on the stiff matrix and glass, both cell cultures already display a well organized actin structure with long actin filaments and clear filopodia and lamelipodia. Besides actin, integrins are other molecules that might be implicated in the response of the cells to the substrate stiffness (Wilson et al., 1995; von Wichert et al., 2003). Integrins are trans-membrane proteins whose extracellular regions bind to the extracellular matrix while their intracellular part remains connected to the cytoskeleton. Integrins are important elements of the focal adhesion sites where the cell-substrate attachment takes place. In many type of cells, there is an important number of focal adhesion sites (FAS) at the cell edges where lamellipodia extend and locomotion occurs. Pelham and Wang, 1997 suggest that after the cells form an initial adhesion trough the FAS located particularly in the lamellipodia and filopodia, forces exerted on the matrix facilitates locomotion and keep cellular shape at the same time.

Our results thus indicate that cells cultured on soft substrates lack the long and well formed lamellipodia observed on stiffer matrices. On these substrates, the reduced traction (substrates can withstand large deformations before significant resistance arise) might prevent the creation of well formed stress fibers, the maturation of the initial focal adhesion sites, the cell elongation and the signaling cascades triggered by mechanical tensions.

A comprehensive study and description of the biochemical reactions elicited by the cells in response to mechanical stimulation could be performed. Application of local and small, controlled loads with an AFM (or a parallel array of AFMs) on cells cultured on a soft medium and its combination with some of the other techniques described in this thesis might be an effective methodology to shed light into the cellular cascades that are triggered by mechanical stimulus.

The AFM could also be used to effectively simulate different substrate stiffnesses locally on a few cells – allowing for comparison of cells grown under otherwise identical conditions. A first step to understand the sequence of signaling events leading to changes after mechanical contacts is demonstrated in this thesis by observing the formation of a synaptic connection (see section 6).

5.7.4 Cell proliferation rate and genetic expression is influenced by the substrate stiffness.

Initial airway smooth muscle cell cultures show that seeding the same number of cells on the four examined matrices produced cultures which reached confluence at different times. Adjustments in the number of cells plated was necessary to get cell cultures with the same cell density the day on which the experimental procedure was performed. Seeding of 25,000 cell/dish, 35,000 cell/dish, 40,000 cell/dish and 100,000 cell/dish in the glass substrate, the stiff, medium and soft gels respectively produce cultures suitable for AFM measurements after 5 days on incubation. This shows a large disparity of the number of seeded cells (more than two fold) on the soft matrix relative to the other substrates. A proliferation assay was performed to confirm that the differences were indeed due to variations in cell proliferation and not due to variations on the number of cells that initially adhere to the matrix.

The results show that the proliferation rate on soft substrates is ~ 3 fold lower than the proliferation rate in the other conditions when the cultures were incubated with complete medium (DMEM + 10 % FBS). Quiescent cell cultures (0.5% FBS) showed basal proliferation rates lower than 10 % irrespectively of the matrix stiffness (see Figure 33). This finding is an additional piece of information that let us conclude that starvation keeps the cells in the same phase (no proliferative phase) and that it is not a variable that influenced the viscoelastic properties of the cells in the present study.

The molecular mechanism by which the cells sense the matrix stiffness and adapt its behavior (in this case the proliferation rate) is not well understood. However, some studies suggest that integrins and increase myosin light chain

phosphorylation might play a role in that process. For instance, Wilson et al., 1995 reported that when vascular smooth muscle cells cultured in collagen coated surfaces were treated with antibodies that bind the β_3 and $\alpha_v\beta_5$ integrin subunits, the mitogenic response induced by continue oscillatory loads on rat vascular smooth muscle cells was abrogated. A study lead by Cai et al., (1998) demonstrated in fibroblasts that myosin light chain phosphorylation alters signaling pathways that regulate cell growth and division. In other reports (Wang et al., 2006) force induced enhanced expression of alpha-actin (this is an actin isoform that contributes to cell-generated mechanical tension and is normally restricted to smooth muscle) and possible impact in the expression of other genes has been associated to the ability of the actin fiber to serve as mechanotransducer (Wang et al., 2006).

Gene array technology also provides clues regarding the link between cell mechanics, proliferation and gene expression. The data obtained is valuable and exhibits the regulation of genes among the groups cultured on different matrix stiffness. However, as a general trend, the largest differences in genetic expression occurred between the cultures on glass and any of the polyacrylamide gel cultures. This finding does not immediately correlate to our previous observations of cell viscoelasticity (cells plated on soft gels are significantly different from any of the other groups) cytoskeleton organization and proliferation rate (lower in gels cultured on soft gels). However, a plausible explanation arise if we consider that the cells are able to sense the stiffness of the substrate. Thus, the large difference between the stiffness of the glass and the stiffness of the gels could account for some of the observed change in genetic expression. In addition, there are some reports that have found that the actual spatial distribution of the available attachment sites influences the cell behavior (Teixeira et al., 2003; Uttayarat et al., 2005; Ismail et al., 2007; Gadegaard et al., 2008; Yang et al., 2009). Thus, the flatness of the glass substrate in contrast to the porous nature of the gels might impact the genetic profile.

Characterization of the base membrane (Fitton et al., 1998; Abrams et al., 2000; Abrams et al., 2003) has sheld light into the structures that the cell encounters and attaches to *in vivo*. These studies have shown that the base membrane have pore sizes of ~ 100 nm. This is aproximatelly the pore size reported for the stiff polyacrylamide gel (Holmes DL, 1991). This coincidence is an indication that cell cultures prepared on polyacrylamide gels are indeed biologicaly relevant, perhaps even more so than those on glass.

The regulation of gene expression by matrix stiffness is evident when the genes involved in proliferation, cytoskeleton dynamics are compared (see Figure 34). The larger differences encountered in the genetic expression occurred between cultures prepared on gels and glass substrates. Since the cells were kept in an arrested phase of growth before the RNA was collected and the incubation conditions were the same for all the cultures, it is reasonable to assume that any difference among the samples is only due to the substrate stiffness.

Many of the regulated genes appear to be involved in tasks other than the cytoskeleton rearrangement, focal adhesion sites or proliferation. A review of the regulated genes produced a list of genes that have been implicated in cell mechanics (*tnnt2, tubg1, tuba4a, pfn2, krt25, tubb6, mylpf, myh3, rhoj, acta1*; for a brief description of their function refer to Figure 34). Interestingly, the only cytoskeletal proteins that were up-regulated in the soft substrate cultures were the tubulin subunit and tubulin assembly genes (*tubg1, tuba4a, tubb6, tubb2c*). We did not detect changes in intermediate filament genes. An increase in the expression levels of the *acta1* gene in the stiffer substrates was observed (this gene codes for α-actin 1 which is an actin isoform that is normally restricted to cells of smooth muscle; Wang et al., 2006). Genes associated to the production of myosin motors (*mylpf, myh3*) are also regulated. These proteins are regularly associated to the actin bundles and are usually used by the cell to exert mechanical forces and provide support to the cell. The genes *akr1b1*, *igfbp3*, *cyr61*, *tnfrsf12a* gene that regulate cell proliferation also showed differential expression ($p<0.05$, ANOVA analysis). Besides its relation to cell proliferation,

the Tnfrsf12a protein located in the plasma membrane decrease cellular adhesion to the fibronectin and vitronectin extracellular matrix proteins. It reduces cell growth and migration (Meighan-Mantha et al., 1999).

We note that confirmation of the gene expression by PCR was not performed since detailed study of the genes involved in mechanical sensing is beyond the scope of this thesis.

5.7.5 Outlook

The combination of AFM and other well established biological techniques proved to be a useful approach to study mechanical properties of cells as a function of matrix stiffness. The AFM measurements were essential to determine both the mechanical properties of the polyacrylamide gel substrates and the cells cultured on these substrates. The combination of the AFM and the inverted optical microscope allowed us to determine the mechanical properties of single cells at specific locations, something that is challenging to achieve with other available techniques which average the elastic properties of a population of cells. The measurements performed in this thesis were focused on the determination of the complex modulus at regions of the cells between the nucleus and the cell edge. The results show that a large variability mainly in the elastic modulus exists among cells cultured on the same type of substrate and that this is even larger when cells grow on stiffer substrates. Our observations as well as other published results (Smith et al., 2005; Bausch et al., 1998; Charras et al., 2005; Mitchison et al., 2008; Ananthakrishnan et al., 2006) suggest that this might be importantly influenced by the actin distribution just beneath the cell membrane. Paxillin-labeling of the actin fibers showed that the actin arrangement in cells plated on the substrates was distinct, most of the differences were observed between cells cultured on the soft matrix and any of the other substrates, to say, cells on soft substrates lacked the long actin filaments, long lammelipodia and filopodia observed in the other cells. In addition, the spread area was larger on cells cultured on stiffer substrates which suggest a good cell adherence to the substrate and tension of the actin filaments.

Cell proliferation rate was importantly affected by the mechanical properties of the substrate. Cells on the softer matrix exhibited low proliferation rates when cultured in either, complete medium plus 10 % FBS or starvation medium which is another indication of the affectations that the matrix stiffness produce in cell behavior. Gene expression was also importantly affected. Although the overall larger differences in expression were observed between rigid and non-rigid substrates, there are genes importantly related to cell mechanics that exhibit differences among non-rigid substrates.

6 Protein recruitment at presynaptic sites

The central nervous system of mammals is a well specialized tissue that is able to process and store information. It is formed by uncountable neurons interconnected that pass signals to each other and communicate constantly. Its correct function requires the continuous connection and sometimes disconnection of the synapses. Essentially, synapses are responsible for neuronal communication and its strength is of primary importance when long-term learning and memories are formed (Vogt et al., 2005). Synapse formation occurs over the life span but the majority of the connections are set during the embryo period and early postnatal life. During those stages, synapse formation mainly contribute to the establishment of neuronal circuitry. In adults, the formation of new synapses is linked (but not exclusive) to cognitive processes (Waites et al., 2005).

Basically, synapses in the CNS are formed between an axon and a dendrite that connect. Although the axons usually form only one synapse, multiple synapses are found along the dendrites. The initial contact can evolve to a mature synapse or end up as a transient contact that disappear after some time. If the synapse mature, the communications between neurons occur through them. At the synapse, the membrane of an axon (presynaptic site) is in close apposition to the membrane of a dendrite (postsynaptic site). There is a tiny gap between the membranes that serve for the diffusion of the neurotransmitters when neuronal communication occur. Neurotransmitters are storage in vesicles at the presynaptic button during the inactive phase.

At the presynaptic site, an array of molecules are found and serve to different functions such as keeping the membranes linked (adhesion molecules), neurotransmitter receptors, signaling proteins, ion channels and more (Waites et al., 2005, Garner et al., 2002). Ultrastructurally, adjacent to the presynaptic site, the hundreds of vesicles filled with neurotransmitter are visible. Communication starts when a depolarizing action potential cause the vesicles to fuse to the membrane and release their content into the synaptic cleft. The zone where they

fuse is called the active zone and it looks like an electron dense matrix when imaged by electron microscope (see Figure 36). The membrane at the postsynaptic site also look as an electron-dense matrix when imaged but lack the vesicles observed in the presynaptic site. Several receptor, scaffold and other proteins are found there (Phillips et al., 2001; Zhai et al., 2001).

It is noticeable that axons can extend long distances before a successful synapse is formed. This is necessary for communication with cells located far from the CNS such as cells at the extreme of the limbs. During their extension,

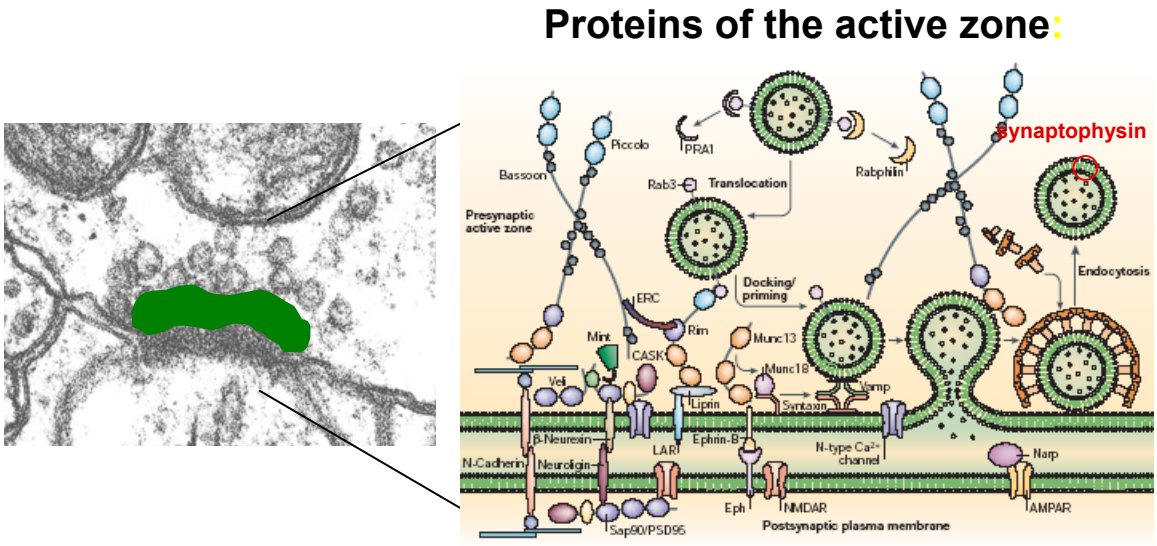

Figure 36: Electron micrograph of a synapse (left). The active zone is enclosed by a green line at the presynaptic site. Neurotransmitter filled vesicles appear rounded and near he active zone. An electron-dense region is also observed at the postsynaptic region. The figure in the right depicts some of the proteins that are located in a mature synapse. Ziv and Garner, 2004

the neurites might encounter several accessible locations to form synapses but these are demoted by the neurites that continue their elongations until they reach a specific target. Research in the field have found some of the molecules that serve as cues for axonal guidance. Netrins, Slits, semaphorins, and ephrinsare some prominent molecules that serve this purpose. Its spatial distribution have proved important to direct the axons, and in particular the growth cone, along specific pathways. The axon find attractive and/or repulsive cues in the extracellular environment and have to respond accordingly. Molecular cues are

not particular for nervous system but also important in inflammatory response. (Dickson, 2002).

Synapses are highly dynamic entities, from their initial creation and pruning to a more consolidated state (Garner et al., 2006). Studies of the initial stages of synaptogenesis are still sparse, in part due to the rarity of synapse creation in culture where single synapses are most conveniently identified and studied in detail (Ziv and Garner, 2004). Even when such events are patiently identified and scrutinized (*e.g.* Ahmari et al., 2000; Friedman et al., 2000; Kaether et al., 2000), the total number of events remains quite low. A method that could reliably induce synaptogenesis at will would therefore be highly desirable.

Another largely unresolved aspect of synaptogenesis is the required identity of synapse-inducing factors. As few specific ligand-receptor triggers have been identified, such as neuroligin/neurexin, SynCAM and/or NGL-2 (Scheiffele et al., 2000; Biederer et al., 2002; Graf et al., 2004; Kim et al., 2006). Studies from the 80's (Burry, 1980, 1982) however indicate that no such specific ligand-receptor interactions are required and that axons are in fact quite promiscuous in their choice of postsynaptic partner. It was found that many (but not all) poly-cationic substances have synaptogenic properties whereas neutral or anionic substances do not.

Our lab has recently shown that presynapses induced by adhesive contact to poly-D-lysine (PDL, an artificial cationic protein) coated beads (as "stand-ins" for dendrites) are functional and share several characteristics with "real" presynapses, such as protein content and presynaptic vesicle recycling ability (Lucido et al., 2009a). In turn, such hemi-synapses are useful in the study of synaptic development. During these studies, we concluded that a method to spatially precisely control the contact between axon and bead would be useful to study the temporal evolution of synaptic development as well as the adhesion between axon and bead. In particular, such a method would enable a systematic study of the recruitment of specific synaptic proteins rather than merely relying on chance encounters between axons and dendrites in culture.

We now introduce a novel method of combining an Atomic Force Microscope and fluorescence microscopy to precisely control a single contact between a hippocampal axon and a protein-coated bead in time and space. We observed the recruitment of Piccolo-Bassoon Transport Vesicles (PTVs) and Synaptic Transport Vesicles (STVs) to the contact site and compare the temporal evolution to the real case (Friedman et al., 2000). In addition, we are in a unique position to observe the initial adhesion between axon and bead. We find that adhesion is immediate and point-like and that unusually long (>50μm) membrane-bounded, protein-containing strings can be elicited from the axon. Furthermore, the adhesion points co-localize with pre-existing or recruited protein puncta, indicating the existence of special, preformed microdomains along an axon.

7 Material and methods (Neurons)

7.1 Primary Cultures of Rat Hippocampal Neurons

Cultures of dissociated rat hippocampal neurons were prepared using a modification of a protocol described in Kaech and Banker, 2006. Hippocampi were dissected from E17/18 embryos, treated with 0.25% trypsin at 37°C followed by Advanced DMEM-10% horse serum, washed 2x with HBSS and mechanically dissociated with a plastic Pasteur pipette. The dissociated neurons were plated at a density of 1.8-2.3 x 10^4 cm^{-2} in, poly-D-lysine (Sigma) coated glass-bottom dishes (MatTek) in serum-free Neurobasal medium supplemented with L-glutamine and B-27. One-third of the medium was replaced every 3-4 days. All culture media purchased from Gibco (Invitrogen). The chosen cell density reflects a compromise between a lower limit that allows for long-term cell survival and a higher limit dictated by the need to locate isolated axons even on *day in vitro* 10 (DIV10).

Transfection was performed on DIV6 using a standard Lipofectamine 2000 (Invitrogen) protocol. Three different plasmids were used (actin-YFP, synaptophysin-GFP and bassoon-GFP). 10-20 neurons were expressing the corresponding fluorescent proteins after 24 hours. High expression levels persisted for up to one week.

Labeling of tubulin in axons was performed with TubulinTracker™ Green (Invitrogen) as described in the product information sheet except that the cell culture was kept in Neurobasal medium during the imaging procedure. The final concentration of TubulinTracker™ Green used was 100mM.

7.2 Time-lapse Protein Recruitment and Adhesion Experiments

Latex beads (7.5µm, Bangs Laboratories) were glued to Atomic Force Microscope (AFM) cantilevers (Veeco, model: MSCT-AUHW) with UV-curable adhesive (Smith et al., 2007b). The beaded cantilevers were incubated in 50µg/ml poly-D-lysine solution overnight at 4°C or used without coating for

control experiments. Gluing the bead onto the cantilever prior to coating rather than *vice versa* prevents drying of the coated bead.

The prepared cantilevers were mounted on a Bioscope AFM (Digital Instruments, Veeco Metrology Group, Santa Barbara, CA) mounted over an inverted optical microscope (Axiovert S100TV, Zeiss) that facilitates bright-field or fluorescence imaging. We used a white-light excitation source sent through a filter cube suitable for GFP imaging. The white-light source was equipped with a mechanical shutter triggered by the image-acquisition program. The shutter was found to be absolutely necessary to avoid bleaching and enable long-term (several hours) image acquisition.

Bead-axon contact was achieved by positioning the cantilever next to a fluorescent axon and moving the cantilever laterally. Before initial contact, it was found to be necessary to leave the cantilever in the sample medium for 30-45 minutes to allow the system to equilibrate thermally, thus minimizing unwanted drift. When the contact occurred (observed with the inverted optical microscope), a movie was acquired with a CCD camera (cascade:1k, photometrics) at a rate of six frames per minute. The temperature of the sample was kept at 37°C by using a heated stage (DH-35 Culture Dish Heater, Warner Instruments) and the pH kept at 7.2 by keeping the sample in a 5% CO_2/air mixture.

7.3 Image analysis and vesicle speed calculation

Movies taken with the CCD camera were processed with the NIH ImageJ software. To calculate the speed of vesicles, a linear region of interest (ROI) was defined along the length of an axon followed by a reslicing of the images along the ROI as a function of time. Horizontal traces indicate localized, immobile vesicles. Diagonal traces represent vesicle movement. Vesicle speed was calculated as the rate of traveled distance (y-axes in Figure 38B and Figure 39B) over the duration of the vesicle movement (x-axes). Calibration of the pixels per unit length for the CCD camera used in the experiments was performed using a silicon sample of known dimensions observed in bright field with the 63x and 100x oil immersion objectives.

8 Applications of the AFM to the study of presynaptic formation (Results)

8.1 Procedure for successful axon/bead contacts

For the experiments described below, we used an instrument that is designed for simultaneous Atomic Force Microscopy (AFM) topography imaging and fluorescence microscopy. We did however not make use of the topography feature but rather used the AFM to contact a cantilever-mounted bead to an axon expressing a synaptic protein of interest with nanometer accuracy. The contacting proceeds as follows:

1. Locate a hippocampal neuron expressing the synaptic protein of interest. Observation of small features (such as “strings,” see below) requires a relatively high expression level.

2. In bright field, find an isolated length of axon.

3. Approach cantilever-mounted bead to surface, making sure to touch down close to, but not onto, the previously identified length of axon.

4. Using AFM controls, move the bead laterally to contact the axon.

We note that the cells expressing fluorescent protein constitute a rather heterogeneous sample, both in terms of expression level and developmental stage of a given cell. This is why before even approaching the bead to the sample, we made sure that the chosen axon had a sufficiently high expression level and that the fluorescent protein was being transported along the length of the axon. As will be shown below, mobile proteins are necessary to induce synapse formation.

Figure 37 shows an example of a contacting procedure (step 4 above) where at the end the bead is seen to slightly perturb the axon; this slight bending

was taken as a sign of a successful bead-neuron contac. Care was taken to avoid perturbing the axon more than necessary, thus limiting potential damage

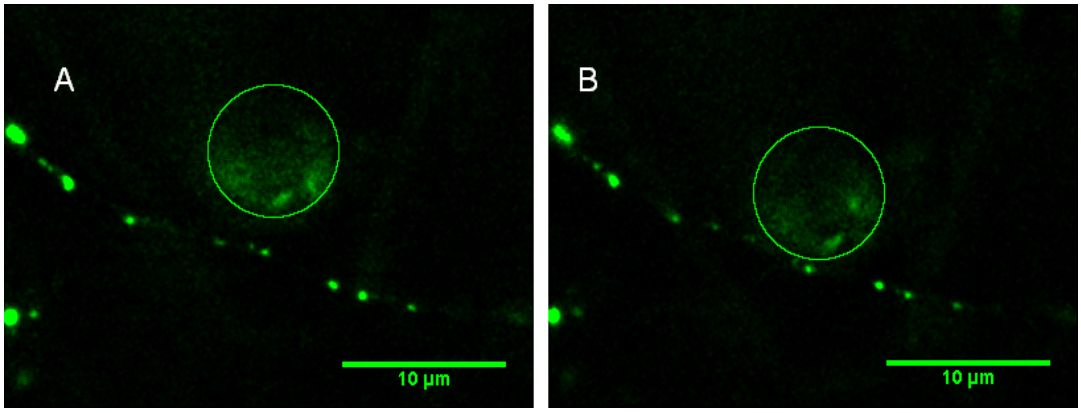

Figure 37: Microbead-axon approach. Precise (nm) control of the bead-axon approach and further contact is achieved by using an AFM. After the bead is brought into contact with the substrate close to a chosen axon (A), it is moved laterally until it gently touches the axon (B). The contact is observed trough an inverted optical microscope. The circle is drawn to indicate the location of the bead attached to the AFM tip.

and/or constriction to the axon.

8.2 Synaptic constituents are transported in vesicles

We observed the PDL-induced recruitment of synaptic constituents bassoon and synaptophysin (see Figure 38 and Figure 39). Bassoon is a scaffolding protein that is actively transported to the synaptic site in so-called Piccolo/Bassoon Transport Vesicles (PTVs) (Zhai et al., 2001; Shapira et al., 2003). Synaptophysin (p38) is a classical presynaptic marker, which is located in the membrane of presynaptic neurotransmitter-containing vesicles and is transported to and from the synapse in a different vesicular carrier named Synaptic Transport Vesicles (STVs).

Consistent with earlier studies (*e.g.* Kaether et al., 2000) we observe bidirectional transport of both bassoon and synaptophysin in PTVs and STVs, respectively. Figure 39B shows the movement of vesicles along a linear ROI as a function of time of a representative time series of synaptophysin transport along an axon. Diagonal tracks are the signatures of moving protein - containing

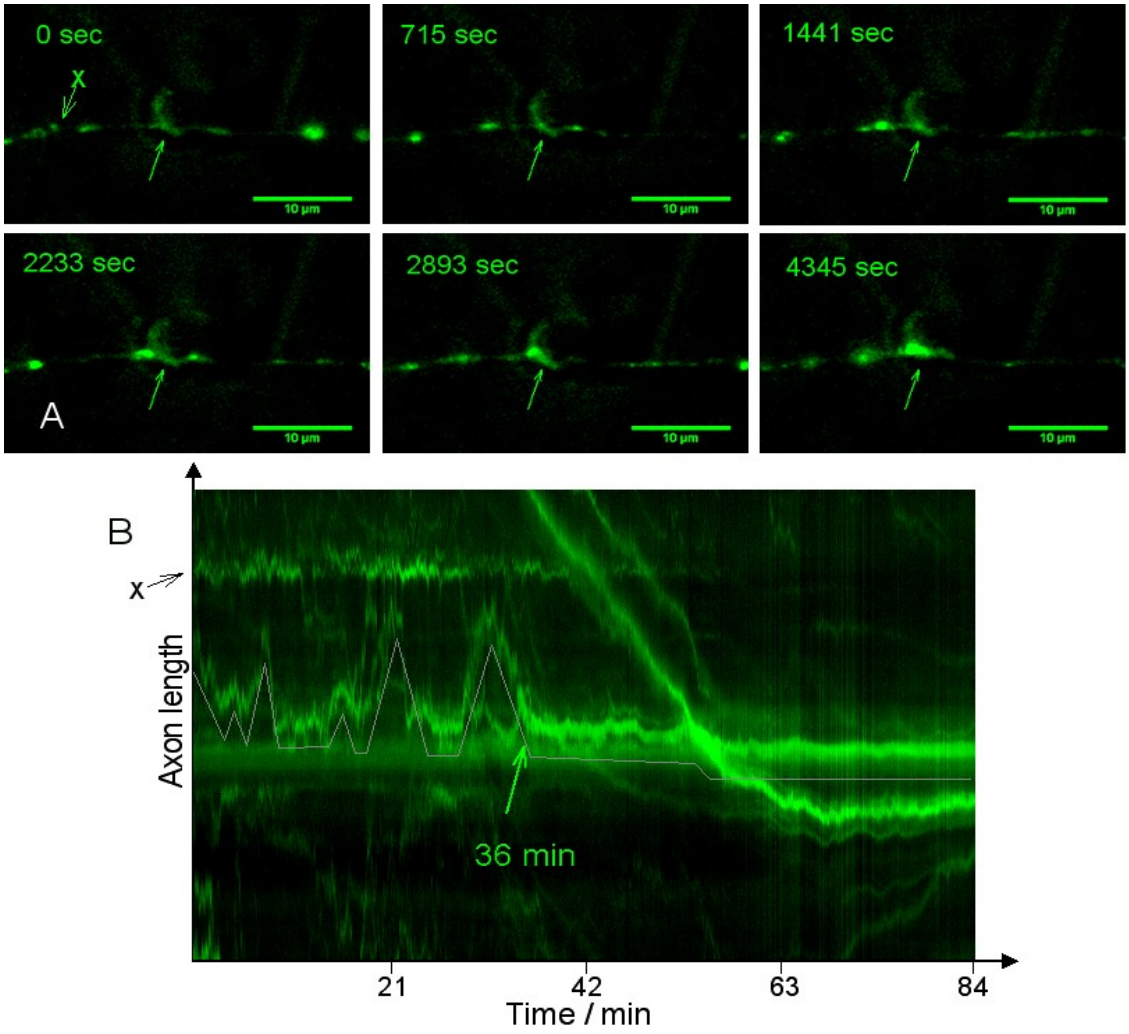

Figure 38: A) Recruitment of Piccolo-Bassoon Transport Vesicles at the bead-axon contact site. The arrow indicates the area of axon-bead contact and hence the position of the recruited bassoon punctum, B) For the analysis of vesicular movement and presynaptic recruitment, a linear region of interest (ROI) was defined along the length of an axon followed by a reslicing of the images along the ROI as a function of time using ImageJ. Effectively, the ROI is plotted as a function of time. Each ROI at a fixed time is a vertical stripe in this image. Localized punctum (mark X in Fig A) show up as horizontal lines in the image (Fig B). Vesicles moving to the right in Fig A correspond to negative slopes (slopes = velocity) in Fig B. Anterograde and retrograde vesicular movement are observed at velocisites in accordance with previous observations. Vesicular recruitment is depicted as an increase in fluorescence intensity at the bead-axon contact site. The highlighted line (white) shows the movement of a vesicle that becomes stable at the bead-axon contact site after 36 min. The average stable recruitment time for 9 experiments was 23±10 min of contact although often vesicles transiently stopped at the bead-axon contact site at earlier times.

vesicles. Note how the diagonal tracks all have the same slope. This is to be expected since the vesicles are being actively transported along microtubules as

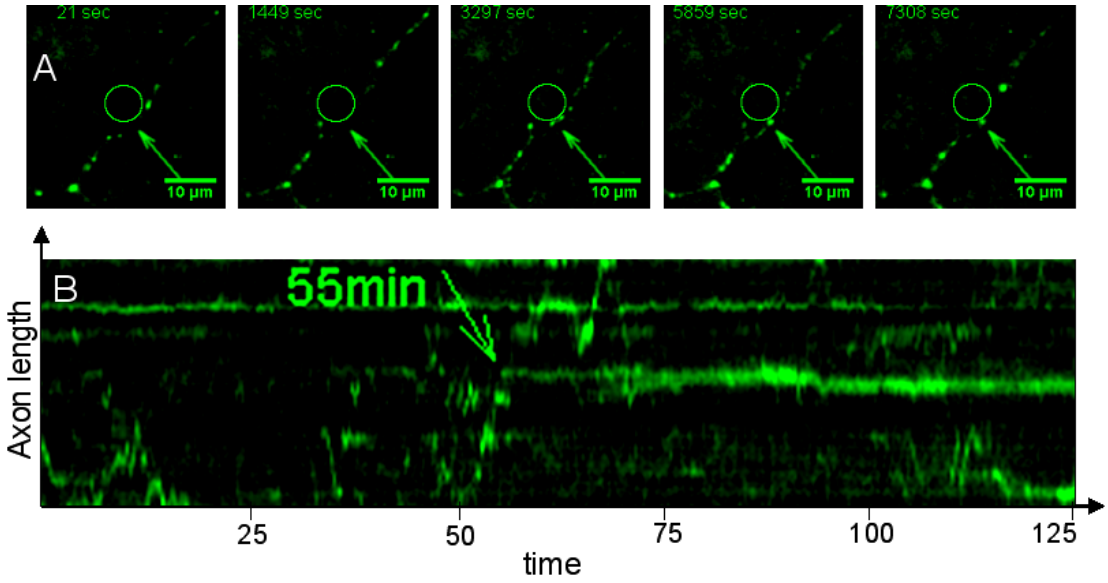

Figure 39: A) Recruitment of Synaptic Transport Vesicles at the bead-axon contact site. The arrow indicates the area of axon-bead contact and hence the position of the recruited synaptophysin punctum B) ROI as a function of time demonstrates anterograde and retrograde vesicular movement as previously observed. In this experiment vesicular recruitment is observed after 55 minutes. On average (8 trials) the recruitment time was observed to be 43 ± 9 min.

the cargo of motor proteins. Calculated speeds computed from the tracks show that the vesicles move at about 0.4 µm/s.

8.3 Bassoon is recruited before synaptophysin

We observed the dynamics of bassoon and synaptophysin recruitment. Figure 39B shows an example of the time course of synaptophysin recruitment. In this case, the observed recruitment time of a stable punctum was 36 minutes. We measured an average recruitment time of 43±9 minutes (see histogram in Figure 40B).

Figure 38G shows an example of the dynamics of bassoon recruitment. We measured an average recruitment time of 23±10 minutes (see histogram in

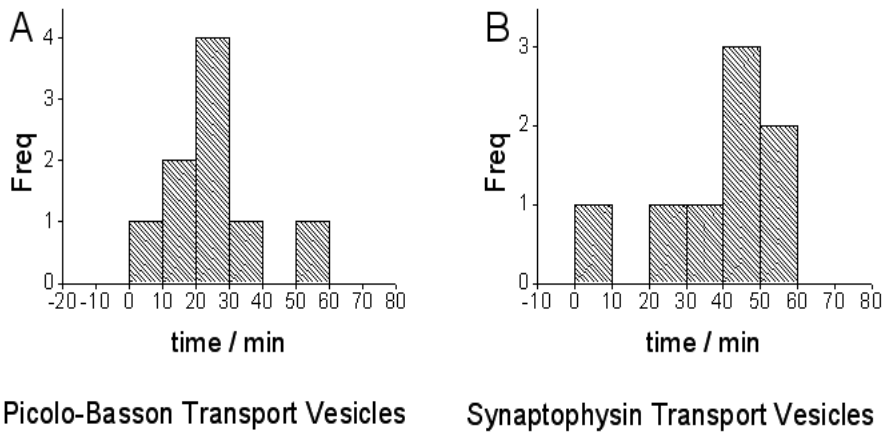

Figure 40: Histograms of recruitment times of (A) Piccolo-Bassoon Transport Vesicles and (B) Synaptic Transport Vesicles. The average bead-axon contact time before vesicular recruitment occurred was 23 min for PTV while that for STV's was 43 min. This difference in recruitment time reflects the order in which proteins are required to assemble to form a presynaptic site.

Figure 40A). PTVs, and thus bassoon is clearly recruited before synaptophysin in STVs.

8.4 Adhesion occurs before protein recruitment

We systematically investigated the onset of adhesion between a PDL-coated bead and an axon simply by laterally contacting an axon, waiting a prescribed time and bringing the bead back to its starting position. The observation that the axon remains attached to the bead was taken as a sign of adhesion. We consistently found that adhesion is almost instantaneous and certainly has already occurred after 5 minutes. With uncoated bead contacts, we routinely found no evidence of adhesion.

The adhesion event does not seem to be correlated (in time) with recruitment although once recruitment has occurred, the focal adhesion point co-localizes with a recruited punctum (Sabo et al., 2006).

8.5 Membrane-bound strings can be pulled out of an axon

Unexpectedly, upon laterally moving a PDL-coated bead away from an axon and consequent detachment from the main axon, we observed the

formation of one or more thin strings between axon and bead (see Figure 41). The strings can be pulled to such great lengths (>50μm) that we reach the maximum dynamic range of our AFM instrument before the strings break. We note in passing that this behavior defeated our original purpose of measuring the adhesion strength between bead and axon based on previously measured elastic parameters (Bernal et al., 2007).

One or two focal adhesion points are observed along the length of the contact area. Adhesion is thus point-like as opposed to along the whole contact area. This behavior is reminiscent of that observed in Sabo et al., 2006 where it is reported that synapses form at “special” sites along the axon where STVs have been observed to pause intermittently. These pause sites are spaced by several μm, the same minimum distance we observe between focal adhesion points.

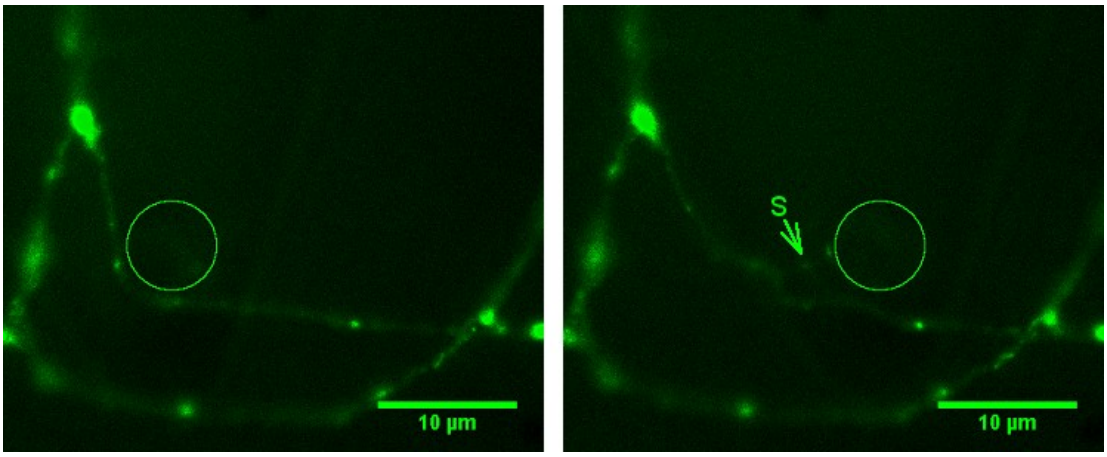

Figure 41: String formation observed upon pulling an adhesive bead away from an axon. The movie shows the axon of a cell expressing synaptophysin-GFP. A long thin fluorescent string (S in fig B) was formed between the site of protein recruitment in the axon and the adhesion point in the bead. After stretching the string, it tends to minimize its length by displacing its initial point of contact along the axon. We have observed strings as long as 50um, limited by the AFM scan range. In separate experiments, we demonstrated that such strings contain tubulin, bassoon and actin as well as synaptophysin.

Another curious observation is the fact that when moving a bead-attached string parallel to an axon, the string initially stretches further but then quickly slides along the axon in order to minimize string length.

8.6 *Properties of axon strings*

We observe that focal adhesion points coincide with synaptic protein puncta. Recruited protein can stay at the axon or follow the bead; in both cases, the focal adhesion points co-localize with the protein punctum. The co-localization of adhesion points and protein puncta, be it those from preformed synapses or new synapses induced by the contacting of a PDL-coated bead, suggests that only some parts, presumably preformed compartments, of the axon have the ability to form synapses.

We created strings from axons in which were expressed three different fluorescent proteins, one at a time: synaptophysin-GFP, bassoon-GFP and actin-YFP; as well as in axons where tubulin was fluorescently labeled with the dye Tubulin Tracker™ Green (Invitrogen). In all four cases, we readily observed the strings to fluoresce. Hence, at least these four proteins must be present in the

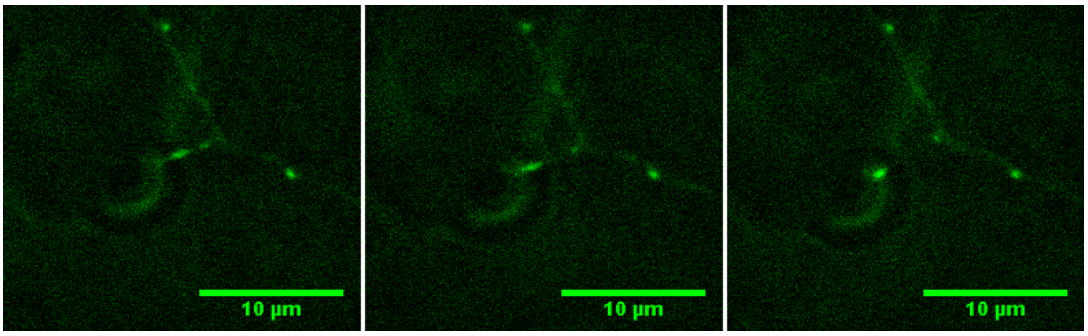

Figure 42: Proteins moving along string, still images separated by ~1 s. The observation of vesicles moving along a formed string was a rare event. When observed, it resembled the usual movement of vesicles along the axons. This is not surprising given the detection of actin and tubulin, two important components of the transport apparatus, in the strings.

strings. Whether the protein inside the strings is structured in a functional way similar to than of true axons is uncertain but we did occasionally observe the motion of a proteinaceous punctum along a string (see Figure 42). We cannot readily distinguish between F- and G-actin but when pulling a string, we are effectively creating a large membrane fluctuation.

8.7 Discussion

The second system used to explore the potential of AFM to apply small forces and controlled interactions were neuronal cultures. A number of techniques to study the protein content at synaptic sites has been available to researches in the past (Garner et al., 2000; Kennedy, 2000; Scannevin and Huganir, 2000; Dresbach et al., 2001; Murthy and Camilli, 2003; Benson and Tanaka, 1998; Ichtchenko et al., 1996; Dieck et al., 1998). Many of those techniques are widely used in biological studies. However, time lapse studies of protein recruitment at presynapses are scarce in part due to the lack of a technique capable of inducing the presynaptic array at will. The few studies that have addressed the issue relied upon random dendrite-axon encounters where no control of either the contact site or contact time were possible (Ahmari et al., 2000; Friedman et al., 2000; Kaether et al., 2000).

In this study, we successfully induced the formation of presynaptic sites that have several characteristics of presynapses formed at axon-dendrite contacts (Lucido et al., 2009b). We made use of the AFM to put a poly-D-lysine coated bead in contact with an axon. The advantages of using the AFM include a nanometric precision in the positioning of the bead relative to the axon as well as a good control of the time and duration of the bead-axon contact. To increase the likelihood of observing the recruitment of proteins, we chose axons with relatively high fluorescent intensity and observable vesicle movement in the axon shaft (Qiang et al., 2010). Measurements of the recruitment times for synaptophysin, and bassoon at the contact site showed that synaptophysin is recruited after bassoon. This marks a natural time course where bassoon, a known scaffolding protein, is recruited first, presumably to stabilize the framework needed to tether presynaptic vesicles (here marked by synaptophysin) at the synaptic site. We observe the same recruitment timing of these two particular protein-containing vesicles as happens upon natural axon/dendrite contact (Friedman et al., 2000). This demonstrates that the inductive signals from the PDL-coated beads to the axon have the same effects as the signals from a contacting dendrite.

Reslicing of a linear ROI (see Figure 38B and Figure 39B) defined along the length of the axon allows the observation of vesicle movement in anterograde and retrograde directions in accordance with previous reports (Kaether et al., 2000). This allows transport speed to be measured.

Although two proteins were studied in this work, the technique presented here would allow time lapse studies of the recruitment of any other protein in the presynaptic site, the only requirement would be to get neurons expressing the fluorescently tagged protein of interest. One could even study cooperative effects by labeling with different colors.

Bead-axon adhesion of poly-D-lysine coated beads occurs shortly after contact and definitively before recruitment. The type of interaction that occurs is believed to happen between the positively charged surface of the bead and the negatively charged motives of heparan sulfate proteoglycan (HSPG) transmembrane proteins (Lucido et al., 2009b). Besides, it has been shown that the cytoskeleton is rearranged at the presynaptic site in mature synapses (Garner et al., 2002) thus the mere redistribution of the underlying cytoskeleton (which has a net negative charge, Janmey et al., 1998) due to simple charge interaction with the poly-D-lysine molecules on the bead could be a potential contributor to the formation of presynapses (Liu et al., 2006).

Surprisingly, bead-axon adhesion of poly-D-lysine coated beads was observed to be strong enough to pull membrane strings from the main axon. We determined that those strings contained actin, synaptophysin, piccolo-bassoon and tubulin. In few cases, we observed movement of protein punctum along the formed strings which could signify that the strings are indeed functional axon branches.

Recent results support this idea. Yang et al., (2009) and Lan and Papoian, (2008) have shown that membrane fluctuation can facilitate the formation of filopodia by creating “empty” space between the membrane and the tip of the actin filaments where actin polymerization and elongation occur (Bray and Chapman, 1985). The mechanical stress exerted on the cytoskeleton when the bead is pulled could severe some microtubule fibers generating free microtubule

ends. Qiang et al., (2010) showed that the appearance of an increased number of interstitial branches in axons is related to the generation of free microtubule ends in the axon shaft. Subsequent organization and filling of the strings with cytoskeleton, vesicles and other internal components of the axon directed by either active transport (newly formed microtubule filaments) or Brownian motion could end up in a functional axon branch (Goldberg and Burmeister, 1986).

8.8 Conclusion

The AFM is constantly increasing its presence in biological sciences. Their uses enclose an increasingly extending set of methods to study some relevant questions. In this part, we believed we have introduced a new use for the AFM in biology. The remarkable spatial precision and time resolution that can be achieved with the AFM has let us to study the recruitment time of the proteins that are present at the presynapse site. The induction of the protein recruitment with the poly-D-lysin coated bead cantilever allowed to determine that bassoon is recruited first than synaptophysin to the presynaptic site. We demonstrated that this developed technique gives information that is in good agreement with previously established recruitment times for these proteins (Friedman et al., 2000). Besides, this technique demonstrated to be suitable to study recruitment times of almost any other protein that is located at the presynatic site. The only change to the method would be to transfect the neurons with a vector carrying the sequence to synthesize the protein of interest. It is even possible to do two color microscopy to determine the recruitment times for more than one protein at the same time.

In addition, the use of the AFM in this study allowed to pull long treads (> 50 µm) from the axon shaft that are apparently functional if we look at the movies that show what appears like a vesicle moving along one of the treads. Further assessing of the proteins contained in the treads demonstrated that actin, synaptophisin, bassoon and tubulin are present which is other indication of the functionality of the treads. Concluding experiments to demonstrate their functionality and capacity to produce synapses have yet to be developed by

neuroscientists with the available techniques to observe vesicle fusion to the membrane after an action potential arises. If this is demonstrated, the AFM would become an important tool to study the synapses by “artificially” connecting axons and dendrites.

9 General Conclusion

In science and other fields, new hypothesis are often proposed and new questions arise. Most of the time, a proper description of the subject is possible with the available techniques but there are some times where suitable techniques to test a hypothesis or uncover an answer are limited or not available. This has happened in several fields many times in history but can be exemplified by the well-known Leonardo da Vinci's drawings of several apparatus and flying machines that remained as an idea for many years and even centuries due to the limitations in technology at that time. The most recent construction of gigantic colliders obey the necessity of new apparatus capable of unveil and detect particles that have been proposed by theoretical physicists. Something similar might be happening to the study of the behavior of individual cells. Techniques to study and collect information from hundreds or thousands of cells have been available for many years but only recently, new tools to study single cell behavior have been developed. One of such techniques is the AFM which is gaining ground in biology research.

It has been shown in many studies that the AFM is a valuable tool in biology. Particularly, in this thesis the AFM was employed to measure mechanical properties of cells and to control the poly-D-lysin coated bead-axon contact, which induces protein recruitment at the presynaptic site. These two examples show the flexibility of the AFM and demonstrate its potential to contribute to biology in areas other than its well known ability to produce topographic images of samples. Furthermore, it has been demonstrated that the use of the AFM and other biology techniques are highly valuable to study the response of the biological material to some stimulus. Biology is complex, so many methods need to be combined to achieve a detailed understanding. In our case, the stimulus employed to study cell behavior comprise the use of non-rigid materials and the contact of axons with poly-D-lysin coated beads. The combination of the AFM and the inverted optical microscope was essential for many purposes in this study since the optical view of the cells (either bright field

or fluorescence microscopy) allowed the location and latter precise positioning of the cell beneath the AFM cantilever.

The calculation of the mechanical properties and analysis of the force-distance curves revealed that although the theory behind the calculation of the properties is valid for both soft or very hard substrates, the experimental data (force spectroscopy curves) obtained with the AFM using soft cantilevers is more suitable to measure the mechanical properties of less rigid substrates. This is mainly because the Hertz model is extremely sensitive to the (small) contact point error for very stiff materials.

We have demonstrated the biological potential of the inherent spatial and temporal control of the AFM. Determination of the contact as a function of time allowed measurement of protein recruitment in synapse formation.

This study also allowed to determine some AFM system related factors whose improvement is desirable. Phase contrast microscopy allows the easy, high contrast observation of cells. It was not available on the microscope system used in the present study. However the new AFM (Asylum) acquired by our group is equipped with this type of optical microscope. It simplifies the observation of the cell regions (nucleus, cytoplasm, edges) without the necessity of dyes. It is always preferred to perform experiments on cells with no dyes, as these might interfere with cellular processes.

In the future, some experiments to complement the results presented here should be performed. For instance, one should determine the mechanical properties of transfected cell cultures to identify the dynamic response of structures underneath the contact area, the effect of the inhibition of myosin motors on the mechanical properties of the cells, and investigate the genetic expression with a more sensitive technique (PCR) to quantify in detail the expression level of genes. Characterization of the fibronectin mesh size and arrangement on the different substrates should be performed. A method to prepare polyacrylamide gels with gradient stiffness should be developed.

Regarding the neuron study in this thesis, one can measure the time arrival of other proteins present at the synapse using the same methodology to

convert the presently known static information of which proteins are involved to a complete dynamic picture of events. Furthermore, it would be interesting to study the effect of other positively charger molecules in the formation of presynaptic sites. Determination of the functionality of the pulled strings and the exploration of the possibility to create artificial neuronal networks with these strings is an exciting and open field that begs be investigated.

10 Appendix 1

The main piece of code used in the calculation of the Young's modulus was the follow. However, some helper functions were required. They are found at the end of the main code.

```
function FVAnalysis
%%Force volume file must be exported as row data instead of nm
%%The text file to be analyzed must not have any space between the image data
%%and the f-v data. The first line also must be deleted. Only numerical
%%data must be included in the text file.
clc;
clear;
%Create and then hide the GUI.
f = figure('Visible','off','Position',[360,500,600,300]);
%GUI components.
htextspringcte = uicontrol('Style','text',...
   'String','Spring Constant (N/m)',...
   'Position',[10,180,120,15]);              %[left bottom width height]
hspringcte = uicontrol('Style','edit',...
   'String','0.01',...
   'Position',[10,150,70,25],...
   'Callback',{@springcte_Callback});
htextdefsensit = uicontrol('Style','text',...
   'String','Deflection Sensitivity (nm/V)',...
   'Position',[10,110,140,15]);
hdefsensit = uicontrol('Style','edit',...
   'String','134.2383',...
   'Position',[10,80,70,25]);
htextramp = uicontrol('Style','text',...
```

```
    'String','Ramp size (nm)',...
    'Position',[10,40,120,15]);
hramp = uicontrol('Style','edit',...
    'String','1000',...
    'Position',[10,10,70,25]);
htextbeadradius = uicontrol('Style','text',...
    'String','Bead Radius (nm)',...
    'Position',[160,180,120,15]);              %[left bottom width height]
hbeadradius = uicontrol('Style','edit',...
    'String','2250',...
    'Position',[160,150,70,25]);
htextdate = uicontrol('Style','text',...
    'String','Date exp done',...
    'Position',[160,40,70,15]);
hdate = uicontrol('Style','edit',...
    'String','000000',...
    'Position',[160,10,70,25]);
htextpiezosensit = uicontrol('Style','text',...
    'String','Piezo sensit (nm/V)',...
    'Position',[160,110,110,15]);              %[left bottom width height]
hpiezosensit = uicontrol('Style','edit',...
    'String','9.825793',...
    'Position',[160,80,70,25]);
htextImZScale = uicontrol('Style','text',...
    'String',{'\*Ciao image list';'\@2:Z scale (V/LSB)'},...
    'Position',[310,180,120,30]);              %[left bottom width height]
hImZScale = uicontrol('Style','edit',...
    'String','0.006713765',...
    'Position',[310,150,90,25]);
htextFTTD = uicontrol('Style','text',...
    'String',{'\*Ciao force list';'\@4:Trig threshold Deflection (V/LSB)'},...
```

```
    'Position',[310,90,120,45]);              %[left bottom width height]
hFTTD = uicontrol('Style','edit',...
    'String','0.0000381470',...
    'Position',[310,60,90,25]);
htextpixel = uicontrol('Style','text',...
    'String','pixels per side',...
    'Position',[460,180,120,15]);         %[left bottom width height]
hpixel = uicontrol('Style','edit',...
    'String','16',...
    'Position',[460,150,70,25]);
htextScanSize = uicontrol('Style','text',...
    'String','Scan Size (um)',...
    'Position',[460,110,120,15]);         %[left bottom width height]
hScanSize = uicontrol('Style','edit',...
    'String','30',...
    'Position',[460,70,70,25]);
htextcomment = uicontrol('Style','text',...
    'String',{'This program uses a .txt';'file exported from Nanoscope in row
data units without header. All text must be deleted from the file as well as any
space between the Image data and the F-d curves data. Number of columns
must be 256 if 16x16 image or 512 if 32x32 image. For semi-automatic fitting,
chose an initial interval to fit in line 273 of the program and also let
semiautomatic fitting to run in the same line.'},...
    'Position',[10,220,580,70]);
 hopenfile = uicontrol('Style','pushbutton',...
    'String','Open file and run',...
    'Position',[310,20,100,25],...
    'Callback',{@openfile_Callback},...
    'UserData','FileName');
 %Align GUI components
align([htextspringcte,hspringcte,htextdefsensit,hdefsensit,htextramp,...
```

```
            hramp],'Center','None');
        align([htextbeadradius,hbeadradius,htextdate,hdate,htextpiezosensit,...
            hpiezosensit],'Center','None');
        align([htextImZScale,hImZScale,htextFTTD,hFTTD,hopenfile],'Center','No
ne');
        align([htextcomment],'Center','None');
        %Initialize the GUI. Change units to normalized so components resize
        %automatically.
        set([f,htextspringcte,hspringcte,htextdefsensit,hdefsensit,htextramp,...
            hramp,htextbeadradius,hbeadradius,htextdate,hdate,...
            htextpiezosensit,hpiezosensit,htextcomment,...

htextImZScale,hImZScale,htextFTTD,hFTTD,hopenfile],'Units','normalized');
        %Assign the GUI a name to appear in the window title.
        set(f,'Name','Force Volume')
        %Move the GUI to the center of the screen.
        movegui(f,'center')
        %Make the GUI visible.
        set(f,'Visible','on');
            %Callback for simple_gui. These callback automatically
            %have access to component handles, initialized data
            %and calculate Young's Modulus.
            function [FVData] = openfile_Callback(source,eventdata)
                %Displays the open file window
                [FileName,PathName,FilterIndex] = uigetfile('*.txt','FilterSpec',...
                    'DialogTitle','Location',[1 2]);
                %File location
                Location = [PathName,FileName];
                %Import the .txt files that contains both the Image and the F-d
                %curves of the force volume file and storage the data in the
                %variable called "FVData"
```

```
        FVData = importdata(Location);
        save('FVData','FVData')        %For debug
        %Pick data that corresponde to the thopographyc image and storage
        %it in the matrix "DataIm". Still raw data
        NumColFVData = size(FVData,2);
        DataIm = FVData(1:NumColFVData,:);
        save('DataIm','DataIm')       %For debug
        %Pick data that correspond to the F-d curves. Both fordware and
        %backward curves. Still raw data
        DataFd = FVData(NumColFVData+1:end,:);
        save('DataFd','DataFd')       %For debug
        %Loop to generate a 16x16 or 32x32 cell with the values
        %that will be used to plot the hight image
        format long
        NumPixelsPerSide                =                str2num(get(hpixel,'String'));
    %NumPixelsPerSide take values 16 or 32
        PointsPerPixel = NumColFVData/NumPixelsPerSide;
        for y = 1:1:NumPixelsPerSide
           for x = 1:1:NumPixelsPerSide
              box    =    DataIm(1+(y-1)*PointsPerPixel:y*PointsPerPixel,1+(x-
    1)*PointsPerPixel:x*PointsPerPixel);
             pixelImAv(y,x)                                                    =
    mean(mean(box))*str2num(get(hImZScale,'String'))*str2num(get(hpiezose
    nsit,'String'));
             %Since pixelImAv is in row data (bits), we must multiply it by the
    volt/LSB
              %to get the voltage applied to the piezo and then multiply it by z
sensit
              %to get the number in nm
              %\*Ciao image list
```

```
                %\@2:Z scale: V [Sens. Zscan] (0.006713765 V/LSB) 200.9027
V

%http://www.physics.arizona.edu/~smanne/DI/software/v43header.html
                end
            end
            save('pixelImAv','pixelImAv')       %For debug
            %Generates and saves the image(topographic) figure
            XYStep = str2num(get(hScanSize,'String'))/NumPixelsPerSide;
            DataImX = [0:XYStep:XYStep*(NumPixelsPerSide)];
            temparr = zeros(1,NumPixelsPerSide);
            pixelImAv = [pixelImAv;temparr]; clear temparr;
            temparr = zeros(NumPixelsPerSide+1,1);
            pixelImAv = [pixelImAv,temparr]; clear temparr;
            DataImY = DataImX';
            fig2 = figure('name', 'Hight Image');
            figImAv = surf(DataImX,DataImX,pixelImAv);
            title('Hight');
            xlabel('um');
            ylabel('um');
            zlabel('nm');
            colorbar
            saveas(figImAv,'Hight_Image_Cte_Force.fig')
            %Array with the number of f-d curves in the .txt file
            for k = 1:NumPixelsPerSide*NumPixelsPerSide
                pixel{k} = (k);
            end
            save('pixel','pixel')       %For debug
            %Array with the coordenate of the f-d curves. Read left to
            %right and top to bottom
            r = 0;
```

```
for k = 1:NumPixelsPerSide
   for q = 1:NumPixelsPerSide
      r = r+1;
      coordenate{r} = [k,q];
   end
end
save('coord','coordenate')       %For debug
%Array with the hight of the surface at each f-d curve
r = 0;
for k = 1:NumPixelsPerSide
   for q = 1:NumPixelsPerSide
      r = r+1;
      hight{r} = pixelImAv(k,q);
   end
end
save('hight','hight')       %For debug
%Pick the approach and withdraw curves and storage them in
%different arrays
defsens = str2num(get(hdefsensit,'String'));
k = size(DataFd);
NumPointsFd = k(1,1)*k(1,2)/((NumPixelsPerSide^2)*2);
DataFdCollumn = reshape(DataFd',[],1);
save('DataFdCollumn','DataFdCollumn')       %For debug
for k = 1:NumPixelsPerSide^2
   approach{k}      =      DataFdCollumn(1+(k-1)*2*NumPointsFd:(2*k-
1)*NumPointsFd,1)*str2num(get(hFTTD,'String'))*defsens;
   %\*Ciao force list
   %\@4:Trig threshold Deflection: V [Sens. Deflection]
   %(0.0000381470 V/LSB) 0.4166667 V

%http://www.physics.arizona.edu/~smanne/DI/software/v43header.html
```

```
        end
        save('approach','approach')       %For debug
        %Create a structure array with the properties of the f-d curves
        for k = 1:NumPixelsPerSide*NumPixelsPerSide;
        Xaxes{k}                                                                    =
    [0:str2num(get(hramp,'String'))/NumPointsFd:str2num(get(hramp,'String'))-
    str2num(get(hramp,'String'))/NumPointsFd]';
        end
        save('Xaxes','Xaxes')   %For debug
        s = struct('Pixel', pixel','Coordenate', coordenate','Hight', hight',...
           'Xaxes',  Xaxes','Approach',  approach','Young_Mod',  [1],'Rsquare',
[1]);
        %Rearrange the fd so that the lowest data point is zero
        q = size(s);
        for k = 1:q(1,1)
           minimA = find(s(k,1).Approach == min(s(k,1).Approach));
           s(k,1).Approach = s(k,1).Approach - s(k,1).Approach(minimA(1,1));
        end
        %Flip Approach and reverse so that the bending apears at the
        %right of the f-d
        q = size(s);
        for k = 1:q(1,1)
              s(k,1).Approach = flipdim(s(k,1).Approach,1);
        end

        save('s','s')       %For debug

        %Fit to Hertz model
        beadradius= str2num(get(hbeadradius,'String'));
        date = get(hdate,'String');
        for k = 1:q(1,1)
```

```
k
%110423NewStart
[xm, ym] = IndentCorrection(s(k,1).Xaxes, s(k,1).Approach);
for ww = 1:numel(xm)-1;
   if xm(ww) < xm(ww + 1);
      CanFit(ww) = 0;
   else
      CanFit(ww) = 1;
   end
end
ToFit = sum(CanFit);
if ToFit == 0;
   s(k,1).Xaxes = xm';
   s(k,1).Approach = ym';
%else
   %s(k,1).Xaxes = xm';
   %s(k,1).Approach = ym';
end

save('s','s'); save('xm','xm')      %For debug
%110423NewEnd

[M,F] = mode(s(k,1).Approach,1);
if F < 200
   %Semi automatic
   RT = s(k,1).Xaxes(309,1);
   RC = s(k,1).Xaxes(510,1);
   [E,                inic,                r2]                =
dualfitting2(s(k,1).Xaxes,s(k,1).Approach*str2num(get(hspringcte,'String')),
...
```

```
            beadradius,k,date,[RT 0 RC 0]);%[6.015625000000000e+02 0
9.941406250000000e+02 0]);

            s(k,1).Young_Mod(1) = E;
            s(k,1).Rsquare(1) = r2; %%
            s(k,1).Hight(1)  =  s(k,1).Hight(1)+(str2num(get(hramp,'String'))-
inic); %%
            save('s','s')      %For debug
          else
            s(k,1).Young_Mod(1) = 1;
            save('s','s')      %For debug
          end
        end
        %Plot Young_Mod
        %Loop to generate a 16x16 or 32x32 cell 'pixel' with the values that
will be used to
        %plot the Young_Mod image and the Real Hight Image
        r = 1;
        pixelFd = zeros(NumPixelsPerSide,NumPixelsPerSide);
        pixelRealHight = zeros(NumPixelsPerSide,NumPixelsPerSide); %%
        for y = 1:1:NumPixelsPerSide
          for x = 1:1:NumPixelsPerSide
            pixelFd(y,x) = s(r,1).Young_Mod;
            pixelRealHight(y,x) = s(r,1).Hight; %%
            r = r +1;
          end
        end
        %pixelFd = flipdim(pixelFd,1);
        save('pixelFd','pixelFd')          %For Debug
        save('pixelRealHight','pixelRealHight')          %For Debug %%
        %Creates the plot of the Young_Mod and the Real Hight image
```

```
        DataImY = DataImX';
        fig4 = figure('name', 'Young Mod');
        temparr = zeros(1,NumPixelsPerSide);
        pixelFd = [pixelFd;temparr]; clear temparr;
        temparr = zeros(NumPixelsPerSide+1,1);
        pixelFd = [pixelFd,temparr]; clear temparr;
        figFd = surf(DataImX,DataImY,pixelFd);
        title('Young Mod');
        xlabel('um');
        ylabel('um');
        zlabel('Pa');
        colorbar
        saveas(figFd,'Young_Mod.fig')
        fig5 = figure('name', 'Contact Hight'); %%
        temparr = zeros(1,NumPixelsPerSide);
        pixelRealHight = [pixelRealHight;temparr]; clear temparr;
        temparr = zeros(NumPixelsPerSide+1,1);
        pixelRealHight = [pixelRealHight,temparr]; clear temparr;
        figRH = surf(DataImX,DataImY,pixelRealHight); %%
        title('Topography Contact'); %%
        xlabel('um'); %%
        ylabel('um'); %%
        zlabel('nm'); %%
        colorbar %%
        saveas(figRH,'Contact_Hight.fig') %%
    end
end
```

Function 1: Dualfitting2,

```
function [ENm2, inic, r2] = dualfitting1(x,y,beadradius,m,date,val)
```

```
fullscreen = get(0,'ScreenSize');
fig3 = figure('name', 'Choose the interval to fit',...
   'Position',[0 70 fullscreen(3) fullscreen(4)-150]);    %Create the
figure where a point is going to be chosen
plot(x,y);                %in order to start the fit
axis tight
hold on
%dualcursor
val;                          %val = [x1 y1 x2 y2]
valX1 = find(x == val(1,1));
valX2 = find(x == val(1,3));
datastep = 2;
rsquares = zeros(round((valX2-valX1)/datastep)-2,1);
for k = 1:round((valX2-valX1)/datastep)-2;
   PXaxes = x(valX1+datastep*k:valX2)-x(valX1+datastep*k);
   PApproach = y(valX1+datastep*k:valX2)-y(valX1+datastep*k);
   [ci,gof,a,b] = Hertz(PXaxes,PApproach);
   rsquares(k,1) = gof.rsquare;
end
s1=fitoptions('Method','NonlinearLeastSquares',...
'Lower', [-inf, -inf],...
'Upper', [inf, inf],...
'Startpoint', [1, 1]);
f1=fittype('a*x+b','options',s1);
%110423NewStart
firstpoint = 150;
%110423NewEnd
[ci1,gof1]=fit(x(firstpoint:valX1),y(firstpoint:valX1),f1);
yst = y(firstpoint:valX1)+ci1(x(firstpoint:valX1));
sd = 2*std(yst)
figure(fig3)
```

```
                plot(ci1);
                maxci11 = max(rsquares);
                maxci11X = round(find(rsquares == maxci11));
                k = maxci11X;
                if y(valX1+datastep*k) >= ci1(x(valX1+datastep*k))+sd
                   while y(valX1+datastep*k) >= ci1(x(valX1+datastep*k))+sd
                   k = k - datastep;
                   end
                end
                PXaxes = x(valX1+datastep*k:valX2)-x(valX1+datastep*k);
                PApproach = y(valX1+datastep*k:valX2)-y(valX1+datastep*k);
                [ci,gof,a,b] = Hertz(PXaxes,PApproach);
                r2 = gof.rsquare;
                figure(fig3)
                yy = a*PXaxes.^(3/2)+b;
                hplot1                                                    =
plot(PXaxes+x(valX1+datastep*k),yy+y(valX1+datastep*k),'r');
                xlabel('z / nm')
                ylabel('Force / nN')
                temp = PXaxes+x(valX1+datastep*k);
                [sizetempY,sizetempX] = size(temp);
                inic = temp(1,1);
                fina = temp(sizetempY,1);
                E=a*3*(1-0.5^2)/(4*beadradius^0.5);
                ENm2=E*1e9;
                ht1=text(10,100,['E=',num2str(ENm2)], 'units', 'pixels');
                ht2=text(10,120,['r2=',num2str(gof.rsquare)], 'units', 'pixels');
                saveas(fig3,[date 'fig' num2str(m)]);
                close(fig3)
        end
```

Function 2: Hertz

```
function [ci,gof,aHertz,bHertz]=Hertz(x,y)
s=fitoptions('Method','NonlinearLeastSquares',...
'Lower', [-inf, 0],...
'Upper', [inf, inf],...
'Startpoint', [1, 0]);
f=fittype('a*x^(3/2)+b','options',s);
[ci,gof]=fit(x,y,f);
ContactCoeff=coeffvalues(ci);
aHertz=ContactCoeff(1);
bHertz=ContactCoeff(2);
end
```

11 Appendix 2

In the one-way analysis of variance methodology, the numerator of the variance (also called total sum of squares or Total SS) which is given by,

$$\sum_{ij}(y_{ij}-\bar{y})^2 = \sum_{ij} y_{ij}^{\ 2} - (\sum_{ij} y_{ij})^2 / n$$

Is partitioned into two components (in the above equation, *j* is an observation for the treatment *i*),

Total SS = SST + SSE

$$\sum_{ij}(y_{ij}-\bar{y})^2 = \sum_{i} n_i(\bar{y}_i-\bar{y})^2 + \sum_{ij}(y_{ij}-\bar{y}_i)^2$$

where n_i is the number of observations for treatment *i*. In the above identity, the total variation in the data is split into a portions due to changes in the values of the independent variable and a portion due to random error.

The mean squares due to the treatment and due to error are written as;

MST = SST / DFT

MET = SSE / DFE

Where DFT is the degree of freedom for treatment (= no. of treatments - 1) and DFE the degrees of freedom for error (= total number of observations - no. of treatments)

One-way ANOVA methodology predicts that;

F = MST/MSE

Thus, the F distribution is used to determine whether the means are significantly different or not.

An example follows,

Data used for the calculations,

Glass / Pa	Hard / Pa	Medium / Pa	Soft / Pa
512	779	746	227
401	672	483	283
774	556	311	379
409	1156	1053	528

704	1212	388	403
613	967	353	292
523	420	613	200
1564	438	579	553
768	755	631	409
808	784	880	547
930	693	562	439
714	555	680	206
1395	986	713	560
870	719	421	442
985	1018	563	263
1340	1377	1575	322
1221		862	146
822		499	229
401		377	352
			156
			688
			265
			205
			138
			213
			186
			639
			184

1st step. Compute the total SS, SST and SSE,

SS_{total} = 9287150 Pa^2

SST = 3702850 Pa^2

SSE = 5584300 Pa^2

2nd step. Compute MST, MSE and their ratio, *F*.

MST = 3702850 Pa^2 / (4 - 1) = 1234280 Pa^2

MSE = 5584300 Pa^2 / (78 - 4) = 71590 Pa^2

F = 17

Now, looking at an F-distribution table (this table can be consulted in many references)

F(DFT, DFE) = F(3,74) = 2.73.

One-way ANOVA predicts that if the calculated F is larger than F(DFT, DFE), there is difference among the means.

Combination of this result with multiple compassion analysis performed in MatLab programming software allowed to determine that the mean that is different from the others is the one that correspond to cell cultured on soft gels.

12 Bibliography

Abrams G, Murphy C, Wang Z-Y, Nealey P, Bjorling D (2003) "Ultrastructural basement membrane topography of the bladder epithelium" Urological Research 31:341-346-346.

Abrams GA, Goodman SL, Nealey PF, Franco M, Murphy CJ (2000) "Nanoscale topography of the basement membrane underlying the corneal epithelium of the rhesus macaque" Cell and Tissue Research 299:39-46-46.

Afrin R, Arakawa H, Osada T, Ikai A (2003) "Extraction of membrane proteins from a living cell surface using the atomic force microscope and covalent crosslinkers" Cell Biochemistry and Biophysics 39:101-117.

Afrin R, Ikai A (2006) "Force profiles of protein pulling with or without cytoskeletal links studied by AFM" Biochemical and Biophysical Research Communications 348:238-244.

Afrin R, Zohora US, Uehara H, Watanabe-Nakayama T, Ikai A (2009) "Atomic force microscopy for cellular level manipulation: imaging intracellular structures and DNA delivery through a membrane hole" Journal of Molecular Recognition 22:363-372.

Ahmari SE, Buchanan J, Smith SJ (2000) "Assembly of presynaptic active zones from cytoplasmic transport packets" Nature Neuroscience 3:445-451.

Alcaraz J, Buscemi L, Grabulosa M, Trepat X, Fabry B, Farré R, Navajas D (2003) "Microrheology of Human Lung Epithelial Cells Measured by Atomic Force Microscopy" 84:2071-2079.

Alcaraz J, Buscemi L, Puig-de-Morales M, Colchero J, Baró A, Navajas D (2002) "Correction of Microrheological Measurements of Soft Samples with Atomic Force Microscopy for the Hydrodynamic Drag on the Cantilever" Langmuir 18:716-721.

Ananthakrishnan R, Guck J, Wottawah F, Schinkinger S, Lincoln B, Romeyke M, Moon T, Käs J (2006) "Quantifying the contribution of actin networks to the elastic strength of fibroblasts" Journal of Theoretical Biology 242:502-516.

Ando T, Kodera N, Takai E, Maruyama D, Saito K, Toda A (2001) "A high-speed atomic force microscope for studying biological macromolecules" Proceedings of the National Academy of Sciences of the United States of America 98:12468-12472.

Andrew Yacoot LK (2008) "Aspects of scanning force microscope probes and their effects on dimensional measurement" Journal of Physics D: Applied Physics 10:103001.

Ashkenazi A, Dixit VM (1998) "Death Receptors: Signaling and Modulation" Science 281:1305-1308.

Bailly M, Macaluso F, Cammer M, Chan A, Segall JE, Condeelis JS (1999) "Relationship between Arp2/3 Complex and the Barbed Ends of Actin Filaments at the Leading Edge of Carcinoma Cells after Epidermal Growth Factor Stimulation" The Journal of Cell Biology 145:331-345.

Bausch AR, Ziemann F, Boulbitch AA, Jacobson K, Sackmann E (1998) "Local Measurements of Viscoelastic Parameters of Adherent Cell Surfaces by Magnetic Bead Microrheometry" Biophysical Journal 75:2038-2049.

Benson DL, Tanaka H (1998) "N-Cadherin Redistribution during Synaptogenesis in Hippocampal Neurons" J Neurosci 18:6892-6904.
Bernal R, Pullarkat PA, Melo F (2007) "Mechanical Properties of Axons" Physical review letters 99:018301-018304.
Biederer T, Sara Y, Mozhayeva M, Atasoy D, Liu X, Kavalali ET, Sudhof TC (2002) "SynCAM, a Synaptic Adhesion Molecule That Drives Synapse Assembly" Science 297:1525-1531.
Binnig G, Quate CF, Gerber C (1986) "Atomic Force Microscope" Physical Review Letters 56:930.
Bott K, Upton Z, Schrobback K, Ehrbar M, Hubbell JA, Lutolf MP, Rizzi SC (2010) "The effect of matrix characteristics on fibroblast proliferation in 3D gels" Biomaterials 31:8454-8464.
Brangwynne CP, MacKintosh FC, Kumar S, Geisse NA, Talbot J, Mahadevan L, Parker KK, Ingber DE, Weitz DA (2006) "Microtubules can bear enhanced compressive loads in living cells because of lateral reinforcement" The Journal of Cell Biology 173:733-741.
Bray D, Chapman K (1985) "Analysis of microspike movements on the neuronal growth cone" Journal of Neuroscience 5:3204-3213.
Brighton CA, G. Pritchard and G. A. Skinner (ed.) (1979) Styrene polymers: Technology and environmental aspects. London: Applied Science Publishers.
Burnham NA, Chen X, Hodges CS, Matei GA, Thoreson EJ, Roberts CJ, Davies MC, Tendler SJB (2003) "Comparison of calibration methods for atomic-force microscopy cantilevers" Nanotechnology 14:1-6.
Burry RW (1980) "Formation of apparent presynaptic elements in response to poly-basic compounds" Brain Research 184:85-98.
Burry RW (1982) "Development of apparent presynaptic elements formed in response to polylysine coated surfaces" Brain Research 247:1-16.
Cai S, Pestic-Dragovich L, O'Donnell ME, Wang N, Ingber D, Elson E, De Lanerolle P (1998) "Regulation of cytoskeletal mechanics and cell growth by myosin light chain phosphorylation" American Journal of Physiology - Cell Physiology 275:C1349-C1356.
Carlier M-F (1990) "Actin polymerization and ATP hydrolysis" Advances in Biophysics 26:51-73.
Casuso I, Kodera N, Le Grimellec C, Ando T, Scheuring S (2009) "Contact-Mode High-Resolution High-Speed Atomic Force Microscopy Movies of the Purple Membrane" Biophysical Journal 97:1354-1361.
Cavalcante FSA, Ito S, Brewer K, Sakai H, Alencar AM, Almeida MP, Andrade JS, Majumdar A, Ingenito EP, Suki B (2005) "Mechanical interactions between collagen and proteoglycans: implications for the stability of lung tissue" Journal of Applied Physiology 98:672-679.
Charras GT, Yarrow JC, Horton MA, Mahadevan L, Mitchison TJ (2005) "Non-equilibration of hydrostatic pressure in blebbing cells" Nature 435:365-369.
Cheng C-M, Steward Jr RL, LeDuc PR (2009a) "Probing cell structure by controlling the mechanical environment with cell-substrate interactions" Journal of Biomechanics 42:187-192.

Cheng G, Tse J, Jain RK, Munn LL (2009b) "Micro-Environmental Mechanical Stress Controls Tumor Spheroid Size and Morphology by Suppressing Proliferation and Inducing Apoptosis in Cancer Cells" PLoS ONE 4:e4632.

Chiquet M (1999) "Regulation of extracellular matrix gene expression by mechanical stress" Matrix Biology 18:417-426.

Chiquet M, Renedo AS, Huber F, Flück M (2003) "How do fibroblasts translate mechanical signals into changes in extracellular matrix production?" Matrix Biology 22:73-80.

Cleveland JP, Manne S, Bocek D, Hansma PK (1993) "A nondestructive method for determining the spring constant of cantilevers for scanning force microscopy" Review of Scientific Instruments 64:403-405.

Derjaguin BV, Muller VM, Toporov YP (1975) "Effect of contact deformations on the adhesion of particles" Journal of Colloid and Interface Science 53:314-326.

Desai A, Mitchison TJ (2003) "Microtubule polymerization dynamics" Annual Review of Cell and Developmental Biology 13:83-117.

Dickson BJ (2002) "Molecular Mechanisms of Axon Guidance" Science 298:1959-1964.

Dieck S, Sanmarti-Vila L, Langnaese K, Richter K, Kindler S, Soyke A, Wex H, Smalla K-H, Kampf U, Franzer J-T, Stumm M, Garner CC, Gundelfinger ED (1998) "Bassoon, a Novel Zinc-finger CAG/Glutamine-repeat Protein Selectively Localized at the Active Zone of Presynaptic Nerve Terminals" J Cell Biol 142:499-509.

Dimitriadis EK, Horkay F, Maresca J, Kachar B, Chadwick RS (2002) "Determination of Elastic Moduli of Thin Layers of Soft Material Using the Atomic Force Microscope" 82:2798-2810.

Disanza A, Mantoani S, Hertzog M, Gerboth S, Frittoli E, Steffen A, Berhoerster K, Kreienkamp H-J, Milanesi F, Fiore PPD, Ciliberto A, Stradal TEB, Scita G (2006) "Regulation of cell shape by Cdc42 is mediated by the synergic actin-bundling activity of the Eps8-IRSp53 complex" Nat Cell Biol 8:1337-1347.

Discher DE, Mooney DJ, Zandstra PW (2009) "Growth Factors, Matrices, and Forces Combine and Control Stem Cells" Science 324:1673-1677.

Dresbach T, Qualmann B, Kessels MM, Garner CC, Gundelfinger * ED (2001) "The presynaptic cytomatrix of brain synapses" Cellular and Molecular Life Sciences 58:94-116.

Durisic N, Wiseman PW, Grütter P, Heyes CD (2009) "A Common Mechanism Underlies the Dark Fraction Formation and Fluorescence Blinking of Quantum Dots" ACS Nano 3:1167-1175.

Dvorak JA, Nagao E (1998) "Kinetic Analysis of the Mitotic Cycle of Living Vertebrate Cells by Atomic Force Microscopy" Experimental Cell Research 242:69-74.

Eckel R, Walhorn V, Pelargus C, Martini J, Nann T, Anselmetti D, Ros R (2006) Combined TIRF-AFM setup: controlled quenching of individual quantum dots. vol. 6092 (Enderlein, J. and Gryczynski, Z. K., eds), pp 609209-609208 San Jose, CA, USA: SPIE.

Engler AJ, Sen S, Sweeney HL, Discher DE (2006a) "Matrix Elasticity Directs Stem Cell Lineage Specification" Cell 126:677-689.

Engler AJ, Sen S, Sweeney HL, Discher DE (2006b) "Matrix Elasticity Directs Stem Cell Lineage Specification" 126:677-689.

Espenel C, Giocondi M-C, Seantier B, Dosset P, Milhiet P-E, Le Grimellec C (2008) "Temperature-dependent imaging of living cells by AFM" Ultramicroscopy 108:1174-1180.
Fabry B, Maksym GN, Butler JP, Glogauer M, Navajas D, Fredberg JJ (2001) "Scaling the Microrheology of Living Cells" Physical Review Letters 87:148102.
Farshid G (2000) "The deformation behavior and viscoelastic properties of chondrocytes in articular cartilage" Biorheology 37:27-44.
Findley W, J. Lai, and K. Onaran (1976) Creep and Relaxation of Nonlinear Viscoelastic Materials. New York: Dover Publications, Inc.
Fischer-Cripps AC (1999) "The Hertzian contact surface" Journal of Materials Science 34:129-137.
Fitton JH, Dalton BA, Beumer G, Johnson G, Griesser HJ, Steele JG (1998) "Surface topography can interfere with epithelial tissue migration" Journal of Biomedical Materials Research 42:245-257.
Fletcher DA, Mullins RD (2010) "Cell mechanics and the cytoskeleton" Nature 463:485-492.
Footer MJ, Kerssemakers JWJ, Theriot JA, Dogterom M (2007) "Direct measurement of force generation by actin filament polymerization using an optical trap" Proceedings of the National Academy of Sciences 104:2181-2186.
Friedman HV, Bresler T, Garner CC, Ziv NE (2000) "Assembly of new individual excitatory synapses: Time course and temporal order of synaptic molecule recruitment" Neuron 27:57-69.
García R, Pérez R (2002) "Dynamic atomic force microscopy methods" Surface Science Reports 47:197-301.
Garner C, Waites C, Ziv N (2006) "Synapse development: still looking for the forest, still lost in the trees" Cell and Tissue Research 326:249-262.
Garner CC, Nash J, Huganir RL (2000) "PDZ domains in synapse assembly and signalling" Trends in Cell Biology 10:274-280.
Garner CC, Zhai RG, Gundelfinger ED, Ziv NE (2002) "Molecular mechanisms of CNS synaptogenesis" Trends in Neurosciences 25:243-250.
Gavara N, Roca-Cusachs P, Sunyer R, Farré R, Navajas D (2008) "Mapping Cell-Matrix Stresses during Stretch Reveals Inelastic Reorganization of the Cytoskeleton" Biophysical Journal 95:464-471.
Goldberg DJ, Burmeister DW (1986) "Stages in axon formation: observations of growth of Aplysia axons in culture using video-enhanced contrast-differential interference contrast microscopy" J Cell Biol 103:1921-1931.
Graf ER, Zhang X, Jin S-X, Linhoff MW, Craig AM (2004) "Neurexins Induce Differentiation of GABA and Glutamate Postsynaptic Specializations via Neuroligins" Cell 119:1013-1026.
Hadjipanayi E, Mudera V, Brown RA (2009) "Close dependence of fibroblast proliferation on collagen scaffold matrix stiffness" Journal of Tissue Engineering and Regenerative Medicine 3:77-84.
Hamon L, Pastré D, Dupaigne P, Breton CL, Cam EL, Piétrement O (2007) "High-resolution AFM imaging of single-stranded DNA-binding (SSB) protein—DNA complexes" Nucleic Acids Research 35:e58.

Han SW, Nakamura C, Obataya I, Nakamura N, Miyake J (2005) "A molecular delivery system by using AFM and nanoneedle" Biosensors and Bioelectronics 20:2120-2125.

Hansma PK, Cleveland JP, Radmacher M, Walters DA, Hillner PE, Bezanilla M, Fritz M, Vie D, Hansma HG, Prater CB, Massie J, Fukunaga L, Gurley J, Elings V (1994) "Tapping mode atomic force microscopy in liquids" Applied Physics Letters 64:1738-1740.

Hansma PK, Schitter G, Fantner GE, Prater C (2006) "High-Speed Atomic Force Microscopy" Science 314:601-602.

Hassan E, Heinz WF, Antonik MD, D'Costa NP, Nageswaran S, Schoenenberger CA, Hoh JH (1998) "Relative microelastic mapping of living cells by atomic force microscopy" Biophys J 74:1564-1578.

Heinz WF, Hoh JH (1999) "Spatially resolved force spectroscopy of biological surfaces using the atomic force microscope" Trends in Biotechnology 17:143-150.

Herrmann H, Bar H, Kreplak L, Strelkov SV, Aebi U (2007) "Intermediate filaments: from cell architecture to nanomechanics" Nat Rev Mol Cell Biol 8:562-573.

Hertz H (1882) "Über den Berührung fester elastischer Körper" J Reine Angew Mathematik 92:156-171.

Hoffmeister B, Smith S, Handley S, Rho J (2000) "Anisotropy of Young's modulus of human tibial cortical bone" Medical and Biological Engineering and Computing 38:333-338.

Hofmann UG, Rotsch C, Parak WJ, Radmacher M (1997) "Investigating the Cytoskeleton of Chicken Cardiocytes with the Atomic Force Microscope" Journal of Structural Biology 119:84-91.

Holbery JD, Eden VL, Sarikaya M, Fisher RM (2000) "Experimental determination of scanning probe microscope cantilever spring constants utilizing a nanoindentation apparatus" Review of Scientific Instruments 71:3769-3776.

Holmes DL SN (1991) "Estimation of polyacrylamide gel pore size from Ferguson plots of linear DNA fragments. II. Comparison of gels with different crosslinker concentrations, added agarose and added linear polyacrylamide." Electrophoresis 12:612-619.

Holzapfel GA, Sommer G, Regitnig P (2004) "Anisotropic Mechanical Properties of Tissue Components in Human Atherosclerotic Plaques" Journal of Biomechanical Engineering 126:657-665.

Humphris ADL, Miles MJ, Hobbs JK (2005) "A mechanical microscope: High-speed atomic force microscopy" Applied Physics Letters 86:034106.

Hutter JL, Bechhoefer J (1993) "Calibration of atomic-force microscope tips" Review of Scientific Instruments 64:1868-1873.

Icard-Arcizet D, Cardoso O, Richert A, Hénon S (2008) "Cell Stiffening in Response to External Stress is Correlated to Actin Recruitment" Biophysical Journal 94:2906-2913.

Ichtchenko K, Nguyen T, Südhof TC (1996) "Structures, Alternative Splicing, and Neurexin Binding of Multiple Neuroligins" Journal of Biological Chemistry 271:2676-2682.

Ingber DE (2002) "Mechanical Signaling and the Cellular Response to Extracellular Matrix in Angiogenesis and Cardiovascular Physiology" Circ Res 91:877-887.

Isambert H, Venier P, Maggs A, Fattoum A, Kassab R, Pantaloni D, Carlier M (1995) "Flexibility of actin filaments derived from thermal fluctuations. Effect of bound nucleotide, phalloidin, and muscle regulatory proteins" Journal of Biological Chemistry 270:11437-11444.

Jaasma MJ, Jackson WM, Tang RY, Keaveny TM (2007) "Adaptation of cellular mechanical behavior to mechanical loading for osteoblastic cells" Journal of Biomechanics 40:1938-1945.

Janmey PA, Käs J, Shah JV, Allen PG, Tang JX (1998) "Cytoskeletal Networks and Filament Bundles: Regulation by Proteins and Polycations" Biological Bulletin 194:334-336.

Janmey PA, McCulloch CA (2007) "Cell Mechanics: Integrating Cell Responses to Mechanical Stimuli" Annual Review of Biomedical Engineering 9:1-34.

Jie Song JC, Catherine M. Klapperich, Vincent Eng and Carolyn R. Bertozzi (2004) "Functional glass slides for in vitro evaluation of interactions between osteosarcoma TE85 cells and mineral-binding ligands" J Mater Chem 14:2643-2648.

Johnson KL (1987) Contact mechanics. Cambridge: Cambridge University Press.

Johnson KL, Kendall K, Roberts AD (1971) "Surface Energy and the Contact of Elastic Solids" Proceedings of the Royal Society of London A Mathematical and Physical Sciences 324:301-313.

Jonas O, Duschl C (2010) "Force propagation and force generation in cells" Cytoskeleton 67:555-563.

Kaech S, Banker G (2006) "Culturing hippocampal neurons" Nat Protoc 1:2406-2415.

Kaether C, Skehel P, Dotti CG (2000) "Axonal Membrane Proteins Are Transported in Distinct Carriers: A Two-Color Video Microscopy Study in Cultured Hippocampal Neurons" Mol Biol Cell 11:1213-1224.

Kataoka N, Iwaki K, Hashimoto K, Mochizuki S, Ogasawara Y, Sato M, Tsujioka K, Kajiya F (2002) "Measurements of endothelial cell-to-cell and cell-to-substrate gaps and micromechanical properties of endothelial cells during monocyte adhesion" Proceedings of the National Academy of Sciences of the United States of America 99:15638-15643.

Kennedy MB (2000) "Signal-Processing Machines at the Postsynaptic Density" Science 290:750-754.

Kienberger F, Zhu R, Moser R, Blaas D, Hinterdorfer P (2004) "Monitoring RNA Release from Human Rhinovirus by Dynamic Force Microscopy" J Virol 78:3203-3209.

Kim H, Uehara H, Afrin R, Arakawa H, Sekiguchi H, Osada T, Ikai A (2008) Application of Atomic Force Microscopy to the Study of Expressed Molecules in or on a Single Living Cell. In: Applied Scanning Probe Methods IX(Tomitori, M. et al., eds), pp 149-175: Springer Berlin Heidelberg.

Kim S, Burette A, Chung HS, Kwon SK, Woo J, Lee HW, Kim K, Kim H, Weinberg RJ, Kim E (2006) "NGL family PSD-95-interacting adhesion molecules regulate excitatory synapse formation" Nat Neurosci 9:1294-1301.

Kodera N, Yamamoto D, Ishikawa R, Ando T (2010) "Video imaging of walking myosin V by high-speed atomic force microscopy" Nature 468:72-76.

Kopp-Marsaudon S, Leclère P, Dubourg F, Lazzaroni R, Aimé JP (2000) "Quantitative Measurement of the Mechanical Contribution to Tapping-Mode Atomic Force Microscopy Images of Soft Materials" Langmuir 16:8432-8437.

Kreplak L, Bär H, Leterrier JF, Herrmann H, Aebi U (2005) "Exploring the Mechanical Behavior of Single Intermediate Filaments" Journal of Molecular Biology 354:569-577.

Kreplak L, Fudge D (2007) "Biomechanical properties of intermediate filaments: from tissues to single filaments and back" BioEssays 29:26-35.

Lan Y, Papoian GA (2008) "The stochastic dynamics of filopodial growth" Biophys J 94:3839-3852.

Landau LD, and E. M. Lifshitz. (1986) Theory of Elasticity. Oxford: Pergamon Press.

Lang T, Wacker I, Wunderlich I, Rohrbach A, Giese G, Soldati T, Almers W (2000) "Role of Actin Cortex in the Subplasmalemmal Transport of Secretory Granules in PC-12 Cells" Biophysical Journal 78:2863-2877.

Lantz MA, Hug HJ, Hoffmann R, van Schendel PJA, Kappenberger P, Martin S, Baratoff A, Güntherodt H-J (2001) "Quantitative Measurement of Short-Range Chemical Bonding Forces" Science 291:2580-2583.

Laurent VM, Kasas S, Yersin A, Schäffer TE, Catsicas S, Dietler G, Verkhovsky AB, Meister J-J (2005) "Gradient of Rigidity in the Lamellipodia of Migrating Cells Revealed by Atomic Force Microscopy" 89:667-675.

Le Grimellec C, Lesniewska E, Giocondi M-C, Finot E, Vié V, Goudonnet J-P (1998) "Imaging of the Surface of Living Cells by Low-Force Contact-Mode Atomic Force Microscopy" Biophysical Journal 75:695-703.

Liu BF, Ma J, Xu QY, Cui FZ (2006) "Regulation of charged groups and laminin patterns for selective neuronal adhesion" Colloids and Surfaces B: Biointerfaces 53:175-178.

Liu C-X, et al. (2005) "Measurement of Breaking Force of Fluorescence Labelled Microtubules with Optical Tweezers" Chinese Physics Letters 22:1278.

Lo C-M, Wang H-B, Dembo M, Wang Y-l (2000) "Cell Movement Is Guided by the Rigidity of the Substrate" Biophysical Journal 79:144-152.

Lubarsky GV, Davidson MR, Bradley RH (2004) "Elastic modulus, oxidation depth and adhesion force of surface modified polystyrene studied by AFM and XPS" Surface Science 558:135-144.

Lucido AL, Sanchez FS, Thostrup P, Kwiatkowski AV, Ortiz SL, Gopalakrishnan G, Liazoghli D, Belkaid W, Lennox RB, Grutter P, Garner CC, Colman DR (2009a) "Rapid assembly of functional presynaptic boutons triggered by adhesive contacts" Journal of Neuroscience submitted.

Lucido AL, Suarez Sanchez F, Thostrup P, Kwiatkowski AV, Leal-Ortiz S, Gopalakrishnan G, Liazoghli D, Belkaid W, Lennox RB, Grutter P, Garner CC, Colman DR (2009b) "Rapid Assembly of Functional Presynaptic Boutons Triggered by Adhesive Contacts" J Neurosci 29:12449-12466.

Lulevich V, Zink T, Chen H-Y, Liu F-T, Liu G-y (2006) "Cell Mechanics Using Atomic Force Microscopy-Based Single-Cell Compression" Langmuir 22:8151-8155.

Ma X, Sun P, He P, Han P, Wang J, Qiao S, Li D (2010) "Development of monoclonal antibodies and a competitive ELISA detection method for glycinin, an allergen in soybean" Food Chemistry 121:546-551.

Makishima A, Mackenzie JD (1973) "Direct calculation of Young's moidulus of glass" Journal of Non-Crystalline Solids 12:35-45.
Makishima A, Mackenzie JD (1975) "Calculation of bulk modulus, shear modulus and Poisson's ratio of glass" Journal of Non-Crystalline Solids 17:147-157.
Meadows PY, Bemis JE, Walker GC (2003) "Single-Molecule Force Spectroscopy of Isolated and Aggregated Fibronectin Proteins on Negatively Charged Surfaces in Aqueous Liquids" Langmuir 19:9566-9572.
Meighan-Mantha RL, Hsu DKW, Guo Y, Brown SAN, Feng S-LY, Peifley KA, Alberts GF, Copeland NG, Gilbert DJ, Jenkins NA, Richards CM, Winkles JA (1999) "The Mitogen-inducible Fn14 Gene Encodes a Type I Transmembrane Protein that Modulates Fibroblast Adhesion and Migration" Journal of Biological Chemistry 274:33166-33176.
Mitchison TJ, Charras GT, Mahadevan L (2008) "Implications of a poroelastic cytoplasm for the dynamics of animal cell shape" Seminars in Cell & Developmental Biology 19:215-223.
Miyake K, Satomi N, Sasaki S (2006) "Elastic modulus of polystyrene film from near surface to bulk measured by nanoindentation using atomic force microscopy" Applied Physics Letters 89:031925-031923.
Mogilner A, Rubinstein B (2010) "Actin disassembly 'clock' and membrane tension determine cell shape and turning: a mathematical model" Journal of Physics: Condensed Matter 22:194118.
Moldovan N, Keun-Ho K, Espinosa HD (2006) "Design and fabrication of a novel microfluidic nanoprobe" Microelectromechanical Systems, Journal of 15:204-213.
Möller C, Allen M, Elings V, Engel A, Müller DJ (1999) "Tapping-Mode Atomic Force Microscopy Produces Faithful High-Resolution Images of Protein Surfaces" 77:1150-1158.
Mücke N, Kirmse R, Wedig T, Leterrier JF, Kreplak L (2005) "Investigation of the morphology of intermediate filaments adsorbed to different solid supports" Journal of Structural Biology 150:268-276.
Mücke N, Kreplak L, Kirmse R, Wedig T, Herrmann H, Aebi U, Langowski J (2004) "Assessing the Flexibility of Intermediate Filaments by Atomic Force Microscopy" Journal of Molecular Biology 335:1241-1250.
Muller DJ, Engel A, Carrascosa JL, Velez M (1997) "The bacteriophage [phgr]29 head-tail connector imaged at high resolution with the atomic force microscope in buffer solution" EMBO J 16:2547-2553.
Muller VM, Derjaguin BV, Toporov YP (1983) "On two methods of calculation of the force of sticking of an elastic sphere to a rigid plane" Colloids and Surfaces 7:251-259.
Murthy VN, Camilli PD (2003) "CELL BIOLOGY OF THE PRESYNAPTIC TERMINAL" Annual Review of Neuroscience 26:701-728.
Nash G, Johnson C, Meiselman H (1984) "Mechanical properties of oxygenated red blood cells in sickle cell (HbSS) disease" Blood 63:73-82.
Nathalie C, Olivier T, Yanik T, Jean-Jacques M (2002) "Contribution of the nucleus to the mechanical properties of endothelial cells" Journal of Biomechanics 35:177-187.

Nix JJVaWD (1992) "A new bulge test technique for the determination of Young's modulus and Poisson's ratio of thin films." Journal of Materials Research pp 3242-3249

Nogales E (2003) "Structural insights into microtubule function" Annual Review of Biochemistry 69:277-302.

Olson EN, Nordheim A (2010) "Linking actin dynamics and gene transcription to drive cellular motile functions" Nat Rev Mol Cell Biol 11:353-365.

Oyabu N, Custance, Oacute, scar, Yi I, Sugawara Y, Morita S (2003) "Mechanical Vertical Manipulation of Selected Single Atoms by Soft Nanoindentation Using Near Contact Atomic Force Microscopy" Physical Review Letters 90:176102.

Pasternak C, Wong S, Elson EL (1995) "Mechanical function of dystrophin in muscle cells" The Journal of Cell Biology 128:355-361.

Paszek MJ, Zahir N, Johnson KR, Lakins JN, Rozenberg GI, Gefen A, Reinhart-King CA, Margulies SS, Dembo M, Boettiger D, Hammer DA, Weaver VM (2005) "Tensional homeostasis and the malignant phenotype" Cancer Cell 8:241-254.

Pelham RJ, Wang Y-l (1997) "Cell locomotion and focal adhesions are regulated by substrate flexibility" Proceedings of the National Academy of Sciences of the United States of America 94:13661-13665.

Perez R, Scarontich I, Payne MC, Terakura K (1998) "Surface-tip interactions in noncontact atomic-force microscopy on reactive surfaces: Si(111)" Physical Review B 58:10835.

Petroll WM, Cavanagh HD, Jester JV (2004) "Dynamic three-dimensional visualization of collagen matrix remodeling and cytoskeletal organization in living corneal fibroblasts" Scanning 26:1-10.

Pfaendtner J, Lyman E, Pollard TD, Voth GA (2010) "Structure and Dynamics of the Actin Filament" Journal of Molecular Biology 396:252-263.

Phillips GR, Huang JK, Wang Y, Tanaka H, Shapiro L, Zhang W, Shan W-S, Arndt K, Frank M, Gordon RE (2001) "The Presynaptic Particle Web: Ultrastructure, Composition, Dissolution, and Reconstitution" Neuron 32:63-77.

Pierobon P, Achouri S, Courty S, Dunn AR, Spudich JA, Dahan M, Cappello G (2009) "Velocity, Processivity, and Individual Steps of Single Myosin V Molecules in Live Cells" 96:4268-4275.

Piner RD, Zhu J, Xu F, Hong S, Mirkin CA (1999) ""Dip-Pen" Nanolithography" Science 283:661-663.

Podolski JL, Steck TL (1990) "Length distribution of F-actin in Dictyostelium discoideum" Journal of Biological Chemistry 265:1312-1318.

Pollard TD, Blanchoin L, Mullins RD (2000) "Molecular mechanisms controlling actin filament dynamics in nonmuscle cells" Annual Review of Biophysics and Biomolecular Structure 29:545-576.

Pollard TD, Cooper JA (2009) "Actin, a Central Player in Cell Shape and Movement" Science 326:1208-1212.

Putman CAJ, Werf KOVd, Grooth BGD, Hulst NFV, Greve J (1994) "Tapping mode atomic force microscopy in liquid" Applied Physics Letters 64:2454-2456.

Qiang L, Yu W, Liu M, Solowska JM, Baas PW (2010) "Basic fibroblast growth factor elicits formation of interstitial axonal branches via enhanced severing of microtubules" Mol Biol Cell 21:334-344.

Reiter G, Castelein G, Hoerner P, Riess G, Sommer J-U, Floudas G (2000) "Morphologies of diblock copolymer thin films before and after crystallization" Eur Phys J E 2:319-334.
Rho JY, Ashman RB, Turner CH (1993) "Young's modulus of trabecular and cortical bone material: Ultrasonic and microtensile measurements" Journal of Biomechanics 26:111-119.
Risse P-A, Jo T, Suarez F, Hirota N, Tolloczko B, Ferraro P, Grütter P, Martin JG (2011) "Interleukin-13 inhibits proliferation and enhances contractility of human airway smooth muscle cells without change in contractile phenotype" American Journal of Physiology - Lung Cellular and Molecular Physiology.
Robert A. Robergs RL (2002) "The surprising history of the "HRmax=220-age" equation" Journal of Exercise Physiology 5.
Rosenblatt N, Hu S, Chen J, Wang N, Stamenovic D (2004) "Distending stress of the cytoskeleton is a key determinant of cell rheological behavior" Biochemical and Biophysical Research Communications 321:617-622.
Rotsch C, Braet F, Wisse E, Radmacher M (1997) "AFM IMAGING AND ELASTICITY MEASUREMENTS ON LIVING RAT LIVER MACROPHAGES" Cell Biology International 21:685-696.
Rotsch C, Jacobson K, Radmacher M (1999) "Dimensional and mechanical dynamics of active and stable edges in motile fibroblasts investigated by using atomic force microscopy" Proceedings of the National Academy of Sciences of the United States of America 96:921-926.
Rugar D, Mamin HJ, Guethner P (1989) "Improved fiber-optic interferometer for atomic force microscopy" Applied Physics Letters 55:2588-2590.
Sabo SL, Gomes RA, McAllister AK (2006) "Formation of Presynaptic Terminals at Predefined Sites along Axons" J Neurosci 26:10813-10825.
Sader JE (1995) "Parallel beam approximation for V-shaped atomic force microscope cantilevers" Review of Scientific Instruments 66:4583-4587.
Sader JE (ed.) (2002) Calibration of atomic force microscopy cantilevers: Marcel Dekker Inc.
Sader JE, Larson I, Mulvaney P, White LR (1995) "Method for the calibration of atomic force microscope cantilevers" Review of Scientific Instruments 66:3789-3798.
Saha K, Keung AJ, Irwin EF, Li Y, Little L, Schaffer DV, Healy KE (2008a) "Substrate Modulus Directs Neural Stem Cell Behavior" Biophysical Journal 95:4426-4438.
Saha K, Keung AJ, Irwin EF, Li Y, Little L, Schaffer DV, Healy KE (2008b) "Substrate Modulus Directs Neural Stem Cell Behavior" 95:4426-4438.
San Paulo A, García R (2000) "High-Resolution Imaging of Antibodies by Tapping-Mode Atomic Force Microscopy: Attractive and Repulsive Tip-Sample Interaction Regimes" Biophysical Journal 78:1599-1605.
Santacroce M, Orsini F, Perego C, Lenardi C, Castagna M, Mari SA, Sacchi VF, Poletti G (2006) "Atomic force microscopy imaging of actin cortical cytoskeleton of Xenopus laevis oocyte" Journal of Microscopy 223:57-65.
Sarah EC, et al. (2008) "AFM-based analysis of human metastatic cancer cells" Nanotechnology 19:384003.

Sato M, Nagayama K, Kataoka N, Sasaki M, Hane K (2000) "Local mechanical properties measured by atomic force microscopy for cultured bovine endothelial cells exposed to shear stress" Journal of Biomechanics 33:127-135.

Scannevin RH, Huganir RL (2000) "Postsynaptic organisation and regulation of excitatory synapses" Nat Rev Neurosci 1:133-141.

Schaffer TE, Cleveland JP, Ohnesorge F, Walters DA, Hansma PK (1996) "Studies of vibrating atomic force microscope cantilevers in liquid" Journal of Applied Physics 80:3622-3627.

Scheiffele P, Fan J, Choih J, Fetter R, Serafini T (2000) "Neuroligin Expressed in Nonneuronal Cells Triggers Presynaptic Development in Contacting Axons" Cell 101:657-669.

Schneider SW, Yano Y, Sumpio BE, Jena BP, Geibel JP, Gekle M, Oberleithner H (1997) "Rapid aldosterone-induced cell volume increase of endothelial cells measured by the atomic force microscope" Cell Biology International 21:759-768.

Shapira M, Zhai RG, Dresbach T, Bresler T, Torres VI, Gundelfinger ED, Ziv NE, Garner CC (2003) "Unitary Assembly of Presynaptic Active Zones from Piccolo-Bassoon Transport Vesicles" Neuron 38:237-252.

Shore SA (2004) "Airway Smooth Muscle in Asthma — Not Just More of the Same" New England Journal of Medicine 351:531-532.

Shyy JYJ, Chien S (1997) "Role of integrins in cellular responses to mechanical stress and adhesion" Current Opinion in Cell Biology 9:707-713.

Simmons RM, Finer JT, Warrick HM, Kralik B, Chu S, Spudich JA. (1993) "Force on single actin filaments in a motility assay measured with an optical trap" Adv Exp Med Biol 331-337.

Smith B (2004) "Cellular Biomechanics Investigated by Atomic Force Microscopy (Thesis)".

Smith BA, Roy H, De Koninck P, Grütter P, De Koninck Y (2007a) "Dendritic Spine Viscoelasticity and Soft-Glassy Nature: Balancing Dynamic Remodeling with Structural Stability" Biophysical Journal 92:1419-1430.

Smith BA, Roy H, De Koninck P, Grutter P, De Koninck Y (2007b) "Dendritic spine viscoelasticity and soft-glassy nature: balancing dynamic remodeling with structural stability" Biophys J 92:1419-1430.

Smith BA, Tolloczko B, Martin JG, Grütter P (2005) "Probing the Viscoelastic Behavior of Cultured Airway Smooth Muscle Cells with Atomic Force Microscopy: Stiffening Induced by Contractile Agonist" Biophysical Journal 88:2994-3007.

Sokolov I (2007) Atomic force microscopy in cancer cell research. Valencia, CA: merican Scientific Publishers.

Stark RW, Drobek T, Heckl WM (2001) "Thermomechanical noise of a free v-shaped cantilever for atomic-force microscopy" Ultramicroscopy 86:207-215.

Sugimoto Y, Jelinek P, Pou P, Abe M, Morita S, Perez R, Custance O (2007) "Mechanism for Room-Temperature Single-Atom Lateral Manipulations on Semiconductors using Dynamic Force Microscopy" Physical Review Letters 98:106104.

Sun Y, Arakawa H, Osada T, Ikai A (2002) "Tapping and contact mode imaging of native chromosomes and extraction of genomic DNA using AFM tips" Applied Surface Science 188:499-505.

Suresh S (2007) "Nanomedicine: Elastic clues in cancer detection" Nat Nano 2:748-749.
Svitkina TM, Borisy GG (1999) "Arp2/3 Complex and Actin Depolymerizing Factor/Cofilin in Dendritic Organization and Treadmilling of Actin Filament Array in Lamellipodia" The Journal of Cell Biology 145:1009-1026.
Tamara KB, et al. (2005) "Human epithelial cells increase their rigidity with ageing in vitro : direct measurements" Physics in Medicine and Biology 50:81.
Tanaka EM, Kirschner MW (1991) "Microtubule behavior in the growth cones of living neurons during axon elongation" The Journal of Cell Biology 115:345-363.
Tolloczko B, Jia YL, Martin JG (1995) "Serotonin-evoked calcium transients in airway smooth muscle cells" Am J Physiol 269:L234-240.
Tortora JP, N. P. Anagnostakos (1990) Principles of Anatomy and Physiology. New York: Harper-Collins.
Van Vlack LH (1982) Materials for Engineering. Reading, MA: Addison-Wesley Publishing Company.
Vogt AK, Wrobel G, Meyer W, Knoll W, Offenhausser A (2005) "Synaptic plasticity in micropatterned neuronal networks" Biomaterials 26:2549-2557.
von Wichert G, Jiang G, Kostic A, De Vos K, Sap J, Sheetz MP (2003) "RPTP-α acts as a transducer of mechanical force on αv/β3-integrin–cytoskeleton linkages" The Journal of Cell Biology 161:143-153.
Waites CL, Craig AM, Garner CC (2005) "Mechanisms of vertebrate synaptogenesis" Annu Rev Neurosci 28:251-274.
Wang J, Zohar R, McCulloch CA (2006) "Multiple roles of [alpha]-smooth muscle actin in mechanotransduction" Experimental Cell Research 312:205-214.
Wang N, Ingber DE (1994) "Control of cytoskeletal mechanics by extracellular matrix, cell shape, and mechanical tension" Biophysical Journal 66:2181-2189.
Wang N, Tytell JD, Ingber DE (2009) "Mechanotransduction at a distance: mechanically coupling the extracellular matrix with the nucleus" Nat Rev Mol Cell Biol 10:75-82.
Wang YL, Pelham RJ, Jr. (1998) "Preparation of a flexible, porous polyacrylamide substrate for mechanical studies of cultured cells" Methods Enzymol 298:489-496.
Wilson E, Sudhir K, Ives HE (1995) "Mechanical strain of rat vascular smooth muscle cells is sensed by specific extracellular matrix/integrin interactions" The Journal of Clinical Investigation 96:2364-2372.
Wirtz D (2009) "Particle-Tracking Microrheology of Living Cells: Principles and Applications" Annual Review of Biophysics 38:301-326.
Yamane Y, Shiga H, Haga H, Kawabata K, Abe K, Ito E (2000) "Quantitative analyses of topography and elasticity of living and fixed astrocytes" Journal of Electron Microscopy 49:463-471.
Yang C, Hoelzle M, Disanza A, Scita G, Svitkina T (2009) "Coordination of membrane and actin cytoskeleton dynamics during filopodia protrusion" PLoS One 4:e5678.
You HX, Lau JM, Zhang S, Yu L (2000) "Atomic force microscopy imaging of living cells: a preliminary study of the disruptive effect of the cantilever tip on cell morphology" Ultramicroscopy 82:297-305.

Yuan H, Kononov S, Cavalcante FSA, Lutchen KR, Ingenito EP, Suki B (2000) "Effects of collagenase and elastase on the mechanical properties of lung tissue strips" Journal of Applied Physiology 89:3-14.

Zhai RG, Vardinon-Friedman H, Cases-Langhoff C, Becker B, Gundelfinger ED, Ziv NE, Garner CC (2001) "Assembling the presynaptic active zone: a characterization of an active one precursor vesicle" Neuron 29:131-143.

Zigler J, Lepe-Zuniga J, Vistica B, Gery I (1985) "Analysis of the cytotoxic effects of light-exposed hepes-containing culture medium" In Vitro Cellular & Developmental Biology - Plant 21:282-287.

Ziv NE, Garner CC (2004) "Cellular and molecular mechanisms of presynaptic assembly" Nature Reviews Neuroscience 5:385-399.